UNIVERSIDADE D
COIMBRA

Gonçalo da Costa Rodrigues Ferreira

Effect of blueberry juice supplementation in a rat model of prediabetes: control diets and molecular mechanisms

Dissertação no âmbito do Mestrado em Farmacologia Aplicada, sob orientação científica do Professor Doutor António Pedro de Barros Gomes e da Professora Doutora Isabel Vitória Neves de Figueiredo Santos Pereira apresentada à Faculdade de Farmácia da Universidade de Coimbra

Fevereiro de 2022

Faculdade de Farmácia da Universidade de Coimbra

Effect of blueberry juice supplementation in a rat model of prediabetes: control diets and molecular mechanisms

Gonçalo da Costa Rodrigues Ferreira

Dissertação no âmbito do Mestrado em Farmacologia Aplicada, sob orientação científica do Professor Doutor António Pedro de Barros Gomes e da Professora Doutora Isabel Vitória Neves de Figueiredo Santos Pereira apresentada à Faculdade de Farmácia da Universidade de Coimbra

Fevereiro de 2022

UNIVERSIDADE D
COIMBRA

This work was funded in part by funds from the European Regional Development Fund (ERDF) through the Center 2020 Regional Operational Program (project CENTRO-01-0145-ERDF- 000012-HealthyAging2020), COMPETE 2020 - Operational Competitiveness and Internationalization Program and Portuguese national funds through the Foundation for Science and Technology (FCT): PTDC / SAU-NUT / 31712/2017, POCI-01-0145-FEDER- 031712 and POCI-01-0145-FEDER-007440, strategic projects UID/NEU/04539/2013 (CNC.IBILI Consortium: IBILI + CNC) and UID/NEU/04539/2019 and UID/NEU/04539/2020 (CIBB Consortium: iCBR + CNC). We thank to the Mangualde Farmers Cooperative (Cooperativa Agropecuária dos Agricultores de Mangualde - COAPE) for their partnership in this project through the supply of blueberries.

“He who has a why to live for can bear almost any how.”
Friedrich Nietzsche

Agradecimentos

Esta foi uma longa jornada, repleta de desafios, tropeções e superações, mas acima de tudo, uma experiência extraordinariamente enriquecedora que me tornou mais e melhor. Este importante marco na minha vida não ficaria concluído sem primeiro expressar o meu agradecimento a todos os que contribuíram para que conseguisse ultrapassar todos os obstáculos e alcançasse os meus objetivos. É a eles que dedico esta tese.

Ao meu orientador **Doutor Pedro Gomes**, agradeço toda a disponibilidade, paciência e acompanhamento ao longo de todos os passos desta etapa. Agradeço todos os conselhos, sugestões e todos os conhecimentos e ensinamentos técnico-científicos transmitidos que foram uma mais valia tanto para a realização desta tese como certamente serão para futuros projetos que a este se seguirão.

À **Doutora Isabel Vitória**, pelo entusiasmo e interesse que as suas aulas me proporcionaram e que serviram de alicerces para os meus primeiros passos neste projeto. Agradeço também a disponibilidade para a orientação deste trabalho. Obrigado pela singular recetividade e empatia.

Ao **Doutor Flávio Reis** por me ter acolhido de braços abertos na sua fantástica equipa. Agradeço a disponibilidade e interesse demonstrado por este trabalho assim como todo o apoio e encorajamento ao longo de todo o processo. Obrigado pela sempre presença e profissionalismo.

A toda a **BB Team**, pela excelente, calorosa e simpática forma como me integraram na equipa. À **Doutora Sofia Viana** pela boa disposição, disponibilidade e encorajamento demonstrado. Ao **Pedro Vieira**, à **Inês Preguiça**, ao **André Alves**, à **Beatriz Ormonde**, à **Carolina Ferreira** e ao novo membro da BB team, **Gonçalo Ferreira**. Agradeço-vos todo o apoio, aconselhamento, paciência e motivação que foram sem dúvida muito importantes para mim. Um muito obrigado também pelo companheirismo, pelos momentos de descontração e todas as produtivas discussões científicas nas pausas do café. Um agradecimento especial à **Sara Nunes**, por se ter preocupado e interessado por este projeto desde o primeiro dia. Pelos sábios conselhos, ensinamentos e orientação. Por ter sido um pilar na fase final deste projeto. Por ouvir todos os desabafos, mas acima de tudo pela amizade.

A todos os amigos que Coimbra me deu, estou muito grato pelos nossos caminhos se terem cruzado. À minha **"maninha" Rosa** e à **Catí** por me motivarem nos piores momentos e impedirem que parasse de seguir em frente independentemente de tudo o que se passava à minha volta. À **Jéssica**, pela ajuda nos momentos mais stressantes, pelos esclarecimentos, disponibilidade e desabafos em tantos cafés. À **Báá**, **Andreia**, **Margs** e **Mafalda** por serem

o meu porto seguro em Coimbra. Por me darem um teto quando não tinha, por todas as refeições com legumes que aprendi a gostar, todas as noitadas, tanto a bater chinelo como a trabalhar, todas as experiências e tudo o que passamos juntos.

A"*Os Meus*", ***Gang 115***, "Na amizade a matemática faz sempre sentido, o teu problema é o meu problema por isso a gente divide." Obrigado a todos por comprovarem a veracidade do lema ao longo dos anos, principalmente neste último.

Ao **Rafa**, um amigo para a vida. Obrigado pelos conselhos e apoio ao longo dos momentos mais difíceis, pelas opiniões sinceras, por seres um verdadeiro amigo tanto para mim como para a minha família, mas acima de tudo pela tua lealdade, crença e confiança em mim.

E por último, e mais importante, à minha família.

Ao homem do bigode (**'Vô**), às **tias** doidas e às **primas** desnaturadas que tanto amo. Agradeço-vos por me darem sempre força e constituírem o lar para onde posso sempre voltar. Sem vocês nada no meu percurso teria sentido.

Às três estrelas que tenho lá em cima. Gostava que presenciassem este momento comigo.

Ao meu pai, à minha mãe e a minha irmã por todo o apoio incansável, todas as oportunidades e por nunca terem desistido de mim. À minha irmã **Catarina**, pela paciência, pela amizade e cumplicidade, por todas as chamadas, pelos conselhos nos assuntos mais importantes. Foi o teu apoio que me deu força e confiança na hora de tomar as decisões mais difíceis. À minha ***mamacita***, por todo o carinho, educação, preocupações, tupperwares a transbordar de amor (e comida). Sou muito grato por te ter e é para mim um privilégio poder chamar-te "Mãe". Ao meu **pai**, obrigado por seres um exemplo de luta, sacrifício, persistência e bondade. Por me provares que com trabalho, tudo é possível. Por todas as longas conversas e ensinamentos que guardo comigo para a vida. Espero um dia conseguir ser metade do homem que és. Dedico-vos todas as minhas vitórias porque tudo o que sou e que algum dia serei, devo-o a vocês. Espero poder tomar tão bem conta de vocês como vocês tomaram e tomam de mim. São a parte mais importante da minha vida.

A todos aqueles que me tiraram do sítio mais escuro, me fizeram crescer e perceber que é a responsabilidade voluntariamente aceite, que dá sentido à vida. Obrigado!

"Super Sumo"

- G.F

Table of Contents

Abbreviations

Ab	Antibody
ADA	American Diabetes Association
AGEs	Advanced glycation end products
ALPs	Autophagy-lysosomal pathways
ALT	Alanine aminotransferase
ANOVA	One-way analysis of variance
AST	Aspartate aminotransferase
ATF4	Activating transcription factor 4
ATF6α	Activating transcription factor 6
Atgs	Autophagy-related genes
ATP	Adenosine triphosphate
BAT	Brown adipose tissue
BCA	Bicinchoninic acid
Bcl-2	B-cell lymphoma 2
BiP	Immunoglobulin heavy chain binding protein
BJ	Blueberry juice
BSA	Bovine serum albumin
BW	Body weight
CAPS	N-cyclohexyl-3-aminopropanesulfonic acid
CD	Chow diet
CHOP	C/EBP homologous protein
COAPE	Cooperativa Agropecuária dos Agricultores de Mangualde
CRP	C-reactive protein
DTT	Dithiothreitol
ECL	Enhanced chemiluminescence substrate
EDTA	Ethylenediaminetetraacetic acid
eIF2α	Eukaryotic initiation factor 2-α
ER	Endoplasmic reticulum
ERAD	Endoplasmic-reticulum-associated protein degradation
eWAT	Epididymal white adipose tissue
FFA	Free fatty acids
FPG	Fasting plasma glucose
GADD34	Growth arrest and DNA damage protein 34
GAPDH	Glyceraldehyde 3-phosphate dehydrogenase
GRP78	78-kDa glucose-regulated protein
GTT	Glucose tolerance test
H&E	Hematoxylin and eosin
HbA1c	Glycated hemoglobin
HDL	High-density lipoproteins
HFD	High-fat diet
HFHS	High-fat high-sucrose diet
HSD	High-sugar diet
iBAT	Interscapular brown adipose tissue
iCBR	Coimbra Institute for Clinical and Biomedical Research
IFG	Impaired fasting glucose

IGT	Impaired glucose tolerance
IL-6	Interleukin 6
IRE-1	Inositol-requiring enzyme 1
IRS-1	Insulin receptor substrate 1
JAK-STAT	Janus kinases signal transducer and activator of transcription
JNK	c-Jun N-terminal kinase
LC3-II	Microtubule-associated protein 1 light chain 3-II
LD	Lipid droplet
LDL	Low-density lipoproteins
LDR	Linear dynamic range
LFD	Low fat diet
MAPK	Mitogen-activated protein kinase
mTOR	Mammalian target of rapamycin
MWM	Molecular weight marker
NAFLD	Nonalcoholic fatty liver disease
NASH	Nonalcoholic steatohepatitis
NF-kB	Nuclear factor kappa B
OGTT	Oral glucose tolerance test
OLETF	Otsuka Long-Evans Tokushima Fatty rats
ORBEA	*Órgão Responsável pelo Bem-Estar dos Animais* (Organ Responsible for Animal Welfare)
p.m.w.	Predicted molecular weight
p62/SQSTM1	Protein p62/sequestosome-1
PAI-1	Plasminogen activator inhibitor-1
PERK	Protein kinase-like ER kinase
PGC-1α	Peroxisome proliferator-activated receptor-gamma coactivator-1alpha
PI3K	Phosphatidylinositol 3-kinase
PKC	Protein kinase C
PMSF	Phenylmethylsulfonyl fluoride
PVDF	Polyvinylidene difluoride
RIPA	Radioimmunoprecipitation assay
ROS	Reactive oxygen species
SAT	Subcutaneous adipose tissues
SDS	Sodium dodecyl sulphate
SEM	Standard errors of the mean
T1DM	Type 1 diabetes mellitus
T2DM	Type 2 diabetes mellitus
TBS-T	Tris-buffered saline and tween-20
TG	Triglyceride
TLR-4	Toll like receptor-4
TNF-α	Tumor necrosis factor-alpha
TRAF2	TNF receptor-associated factor 2
UCP-1	Uncoupling protein-1
ULK	Unc51 like kinase
UPR	Unfolded protein response
VAT	Visceral adipose tissue
VLDL	Very low-density lipoproteins

WAT	White adipose tissue
WB	Western blot
WHO	World Health Organization
XBP-1	X-box binding protein-1

List of Figures

List of Tables

Resumo

A pré-diabetes é um estado intermédio entre a tolerância normal à glucose e a diabetes *mellitus* tipo 2 (DMT2), tem a obesidade como um dos principais fatores de risco e está associada a diversas complicações, incluindo a esteatose hepática. A progressão da esteatose hepática tem sido associada à disfunção da resposta ao *stress* do retículo endoplasmático (RE) e da autofagia. O estudo da pré-diabetes é dificultado pela escassez de modelos animais, sendo a maioria destes induzidos por dietas refinadas com um elevado teor de lípidos e/ou de hidratos de carbono. Estas dietas refinadas são geralmente comparadas com dietas controlo não refinadas; contudo, estas diferem marcadamente na composição nutricional, especialmente no conteúdo de fibras e fitoestrógenio, o que pode levar a diferenças fenotípicas inesperadas e a interpretações erróneas dos resultados. Embora as intervenções farmacológicas sejam indispensáveis para a controlo da DMT2, na pré-diabetes - um estádio em que a doença ainda não está totalmente estabelecida - as modificações do estilo de vida são recomendadas como intervenções de primeira linha. Os frutos vermelhos, incluindo o mirtilo, têm sido associados a efeitos benéficos em diversas condições, incluindo em doenças metabólicas e cardiovasculares, em função dos seus efeitos antioxidantes, anti-inflamatórios, hipolipemiantes e sensibilizadores da insulina, entre outros. Considerando que a resistência à insulina, a dislipidemia, o *stress* oxidativo e a inflamação são os principais promotores da progressão da pré-diabetes e do desenvolvimento das suas complicações, a utilização do mirtilo pode ser uma intervenção nutracêutica valiosa nesta fase precoce da doença. No entanto, o potencial do mirtilo na prevenção da pré-diabetes em condições relevantes para a patogénese humana, bem como os mecanismos moleculares envolvidos permanecem em grande parte inexplorados.

Este projeto tem como principais objetivos: 1) avaliar as alterações metabólicas, histológicas e moleculares num modelo animal de pré-diabetes induzidas por uma dieta rica em gordura e sacarose (HFHS), em comparação com dois tipos de dietas controlo e 2) identificar os mecanismos moleculares responsáveis pelos potenciais efeitos protetores da suplementação de sumo de mirtilo (BJ) contra a progressão da pré-diabetes.

Ratos Wistar machos foram alimentados durante 24 semanas com uma dieta refinada HFHS indutora de pré-diabetes, uma dieta refinada (equiparada em nutrientes) com baixo teor em gordura (LFD) e uma dieta controlo-padrão não refinada (CD). Um quarto grupo foi alimentado com uma dieta HFHS suplementada com BJ (HFHS + BJ) a partir da 16ª semana, momento em que o fenótipo pré-diabético foi alcançado. O peso

corporal foi monitorizado ao longo de todo o estudo. Após o sacrifício, o fígado e os depósitos de tecido adiposo branco epididimal (TABe) e castanho interescapular (TACi) foram recolhidos e utilizados para análise histológica. O sangue foi utilizado para análise bioquímica. Marcadores de termogénese, *stress* do RE e de autofagia foram avaliados no TACi e no fígado, respetivamente, através da quantificação da expressão de algumas proteínas por Western blot.

Os animais alimentados com HFHS apresentaram características de pré-diabetes, incluindo aumento da adiposidade e do peso corporal, hiperinsulinemia pós-prandial, intolerância à glicose e esteatose hepática, em paralelo com um aumento dos marcadores de termogénese UCP-1 e PGC-1α no TACi. Surpreendentemente, quando comparados com a CD, os animais alimentados com LFD apresentaram anomalias metabólicas consideráveis, tais como o aumento da massa de TABe, hiperinsulinemia pós-prandial, intolerância à glicose e esteatose hepática. A desregulação da resposta ao *stress* do RE e da autofagia foram também observadas nos grupos HFHS e LFD, quando comparados com o grupo CD. O consumo de BJ não afetou o ganho de peso corporal e adiposidade, porém atenuou a intolerância à glicose e inibiu as alterações induzidas pela dieta nos marcadores de termogénese, de *stress* do RE e autofágicos. Paralelamente, o BJ agravou o conteúdo sérico e hepático de triglicéridos.

Em conjunto, os nossos resultados demonstraram que 24 semanas de dieta HFHS promovem um estado de pré-diabetes em ratos e que a gravidade das alterações metabólicas depende da composição nutricional da dieta controlo, salientando a importância da sua seleção cuidadosa na interpretação dos estudos metabólicos. Para além disso, combinada com uma dieta HFHS, a suplementação com mirtilo pode agravar o metabolismo lipídico num modelo de pré-diabetes em roedor; assim o consumo de mirtilo deverá ser devidamente ponderado nesta fase precoce da doença.

Palavras-chave: Pré-diabetes, Modelos animais induzidos por dieta, Dietas controlo, Sumo de mirtilo, Intervenção nutracêutica, Autofagia, Resposta ao *stress* do retículo endoplasmático, Esteatose hepática.

Abstract

Prediabetes is an intermediate state between normal glucose tolerance and type 2 diabetes (T2DM), with obesity as a major risk factor and associated with many complications such as hepatic steatosis. The progression of hepatic steatosis has been associated with impaired endoplasmic reticulum (ER) stress response and autophagy. The study of prediabetes has been hampered by the scarcity of animal models, most of which are induced by refined diets with a high fat and/or sugar content. These refined diets are usually compared to unrefined control diets ("chow diet"); however, they markedly differ in nutritional composition, especially fiber and phytoestrogen content, which may lead to unanticipated phenotypic differences and erroneous interpretations of results. Although pharmacological interventions are indispensable for the management of T2DM, in prediabetes—a stage where the disease is not yet fully established—lifestyle modifications are instead recommended as first-line interventions. Red fruits, including blueberries, have been associated with beneficial effects in a variety of conditions, including metabolic and cardiovascular diseases, due to their antioxidant, anti-inflammatory, hypolipemic, and insulin sensitizing effects, among others. Considering that insulin resistance, dyslipidemia, oxidative stress and inflammation are the main drivers of prediabetes progression and the development of its complications, blueberry may be a valuable nutraceutical intervention in this early stage of the disease. Nonetheless, the blueberry potential to protect against prediabetes under conditions relevant for human pathogenesis and the molecular mechanisms involved remain largely unexplored.

This project aims to: 1) evaluate metabolic, histological and molecular changes in an animal model of prediabetes induced by a high-fat high-sucrose (HFHS) diet compared to two types of control diets, and to 2) identify molecular mechanisms responsible for the putative protective effects of blueberry juice (BJ) supplementation against prediabetes progression.

Male Wistar rats were fed for 24 weeks with a prediabetes-inducing refined HFHS diet, a nutrient-matched refined low-fat diet (LFD) and a standard unrefined control diet (CD). A fourth group was fed a HFHS diet supplemented with BJ (HFHS+BJ) starting at week 16, the point when the prediabetic phenotype was achieved. Body weight was monitored throughout the study. After sacrifice, liver and epididymal white (eWAT) and interscapular brown (iBAT) adipose tissue depots were collected and used for histological

analysis. Blood was used for biochemical analysis. Thermogenesis, ER stress and autophagy markers were assessed in the iBAT and liver, respectively, by Western blot analysis.

HFHS-fed animals presented features of prediabetes, including increased body weight and adiposity, postprandial hyperinsulinemia, glucose intolerance and hepatic steatosis, in parallel with an increase in thermogenic markers UCP-1 and PGC-1α in iBAT. Surprisingly, when compared to CD, LFD-fed animals presented considerable metabolic abnormalities, such as increased eWAT mass, postprandial hyperinsulinemia, glucose intolerance and hepatic steatosis. Impaired ER stress response and autophagy were also observed in both the HFHS and LFD groups, when compared to the CD group. BJ consumption was devoid of effect on body weight gain and adiposity, but attenuated glucose intolerance and decreased the diet-induced alterations in thermogenic, ER stress and autophagic markers. In parallel, BJ aggravated serum and hepatic triglyceride content.

Together, our findings demonstrate that 24 weeks of HFHS diet models prediabetes in rats and that the severity of metabolic alterations depends on the nutrient composition of the control diet, highlighting the importance of its careful selection in interpreting metabolic studies. Furthermore, whole blueberry supplementation worsened lipid metabolism in a prediabetic rat model; thus, the blueberry consumption at this early state of the disease should be carefully considered.

Keywords: Prediabetes, Diet-induced animal models, Control diets, Blueberry juice, Nutraceutical intervention, Autophagy, Endoplasmic reticulum stress response, Hepatic steatosis.

Chapter I

Introduction

1.1. Prediabetes

1.1.1. Definition and diagnostic criteria

Prediabetes is an intermediate stage between normal glucose tolerance and the establishment of type 2 diabetes mellitus (T2DM), representing a high-risk state for diabetes development. It is typically defined as blood glucose levels above normal but below diabetes diagnostic thresholds (Hostalek, 2019; Tabák *et al.*, 2012). Prediabetes is manifested by the presence of impaired fasting glucose (IFG), impaired glucose tolerance (IGT) or both, *(Edwards e Cusi, 2016)* and is simultaneously associated with insulin resistance and β-cell dysfunction *(Tabák et al., 2012)*.

There is currently a lack of consensus in the terminology of this condition as the term prediabetes has been criticized because that not all prediabetic patients will develop diabetes and that this term may imply that no intervention is necessary as no disease is present *(Edwards e Cusi, 2016)*. As a consequence, in addition to prediabetes, alternative terms have been used to refer to this metabolic state, namely IFG, IGT, non-diabetic hyperglycaemia, and intermediate hyperglycaemia *(International Diabetes Federation, 2019*). For instance, an International Expert Committee assembled by the American Diabetes Association (ADA) suggested the use of "high-risk state of developing diabetes" while the term "intermediate hyperglycaemia" is preferred by the World Health Organization (WHO) and by the *Direção Geral da Saúde* (DGS) (*Direção-Geral da Saúde, 2011; Tabák et al., 2012*).

The diagnostic criteria for prediabetes have evolved over time and, just like the terminology, are not uniform across organizations (Bansal, 2015; Tabák *et al.*, 2012). The two most commonly used diagnostic criteria for prediabetes are from the WHO and from the ADA. Both definitions are based on fasting plasma glucose (FPG) concentrations, two-hour plasma glucose concentrations during an oral glucose tolerance test (OGTT) and/or hemoglobin A1c (HbA1c) concentrations, having this last parameter been included recently *(Beulens et al., 2019)*.

To the WHO, high risk for developing diabetes relates to two distinct states, IFG defined as FPG of 6.1–6.9 mmol/L (in the absence of IGT) and IGT defined as postload plasma glucose of 7.8–11.0 mmol/L based on 2h OGTT or a combination of both *(Tabák*

et al., 2012). To the DGS, the definition of intermediate hyperglycaemia is based on the application of the same thresholds for IGT and IGF as the ones defined by the WHO *(Diagnosis and classification of diabetes mellitus., 2011)*. The ADA, Although applying the same thresholds for IGT, ADA uses a lower cut-off value for IFG (FPG 5.6–6.9 mmol/L) and has additionally introduced HbA1c of 5.7–6.4% as a new category of high diabetes risk (Table 1) *(Tabák et al., 2012)*.

Table 1 – Comparison of prediabetes diagnosis criteria according to WHO, ADA and DGS Norm.

Criteria/ Organization	IGT (2-h PG during 75g OGTT)	IFG (FPG)	HbA1c
WHO	7.8-11.0 mmol/L (140-190 mg/dL)	6.1-6.9 mmol/L (110-125 mg/dL)	ND
ADA	7.8-11.0 mmol/L (140-190 mg/dL)	5.6-6.9 mmol/L (100-125 mg/dL)	5.7-6.4% (39-47 mmol/L)
DGS	7.8-11.0 mmol/L (140-190 mg/dL)	6.1-6.9 mmol/L (110-125 mg/dL)	ND

ADA - American Diabetes Association; DGS - *Direção Geral de Saúde*; FPG - Fasting plasma glucose; IGT - Impaired glucose tolerance; IFG - Impaired fasting glucose; HBA1c - Glycated hemoglobin; ND - Not defined; PG - Plasma glucose; OGTT - Oral glucose tolerance; WHO - World Health Organization.

1.1.2. Epidemiology of Prediabetes

Based on 62 studies from 49 countries, the IDF estimated that the number of adults (20-79 years) with prediabetes worldwide in 2019 was 373.9 million (1 in 13 adults or 7.5% of the world population in this age group) and projected to rise to 453.8 million (8.0%) by 2030 and 548.4 million (8.6%) by 2045 *(International Diabetes Federation, 2019*).

In Europe, it was estimated that the number of adults with prediabetes in 2019 was 36.6 million (5.5% of the regional adults in this age) and projected to rise to 39.7 million (5.9%) by 2030 and 40.3 million (6.1%) by 2045 *(International Diabetes Federation, 2019)*.

According to *(Raposo, 2020)* in 2018, 2.1 million adults (20-79 years) had prediabetes, representing 28.0% of the total Portuguese population and 41.6% of the population in this age group (Figure 1) *(Raposo, 2020)*.

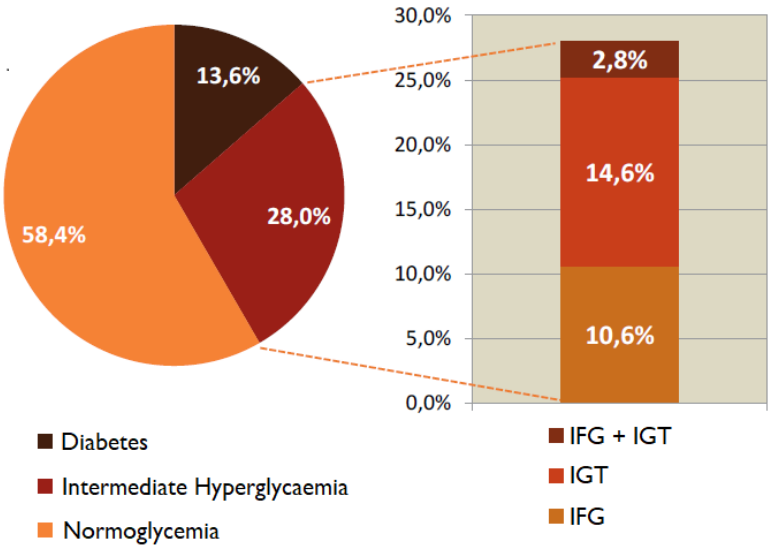

Figure 1 – Prevalence estimates of diabetes and intermediate hyperglycemia (prediabetes) in Portugal in 2018. IFG - Impaired fasting glucose; IGT - Impaired glucose tolerance. Taken from Annual Report of the Portuguese National Diabetes Observatory, Edition 2019 (Raposo, 2020) - Diabetologia, S.P.D., Diabetes: Factos e Números - O Ano de 2016, 2017 e 2018 - Relatório Anual do Observatório Nacional da Diabetes. 2019.

1.1.3. Pathophysiological mechanisms of Prediabetes

The progression from prediabetes to diabetes is a complex and continuous process characterized by several pathophysiological alterations, in particular the dysregulation of fasting glucose and postload glucose homeostasis due to defects in insulin sensitivity and secretion (*Tabák et al., 2012*). This progression is mainly driven by the impairment of pancreatic β-cell function and insulin resistance, along with low-grade inflammation, oxidative stress, steatosis, lipotoxicity and glucotoxicity (*Ferrannini, Gastaldelli e Iozzo, 2011; Flier, 2000; Rocha et al., 2020*).

Even though genetic variants can predispose to an impaired β-cell function, elevated levels of free fatty acids (FFA) (lipotoxicity), hyperglycemia (glucotoxicity), low-grade inflammation and oxidative stress can worsen this scenario *(Prato, Del, 2009)*.

1.1.3.1. Insulin resistance and β-cell dysfunction

Insulin resistance is characterized by the inability of insulin to (1) stimulate glucose uptake in skeletal muscle and adipose tissue, (2) inhibit adipose tissue lipolysis and (3) inhibit liver gluconeogenesis, resulting in the inability of cells to respond adequately to changes in glucose levels (*Czech, 2020; Flier, 2000; Rocha et al., 2020*). Insulin resistance is

already present in prediabetes, along with changes in β-cell mass and increased rates of insulin secretion, as shown in a study where insulin sensitivity was reduced and insulin secretion elevated 13 years before the onset of diabetes (*Tabák et al., 2012*). Nonetheless, insulin resistance appears to be the earliest metabolic abnormality that leads to prediabetes progression (*Edwards e Cusi, 2016*). During this period, insulin production increases (compensatory hyperinsulinemia) to compensate for insulin resistance and maintain glucose levels within normal range. Over time, different levels of genetic susceptibility allied with the increased workload lead to impaired β-cell function and insufficient insulin secretion. As a consequence, glucose levels increase rapidly and a hyperglycemic environment is established (*Tabák et al., 2012*). Long-term exposure to high glucose levels causes glucotoxicity, which promotes β-cell dysfunction and a decrease in insulin synthesis and secretion, as well as insulin resistance. In turn, insulin resistance and β-cell dysfunction promote hyperglycemia, leading to a vicious cycle with continuous β-cell deterioration and the progression of prediabetes. Thus, insulin resistance and β-cell dysfunction promote each other and are the main drivers of prediabetes progression (*Cernea e Dobreanu, 2013; Czech, 2020*).

In addition, insulin resistance and β-cell dysfunction have been associated with several distinct mechanisms of lipotoxicity such as (1) increased fatty acid oxidation and esterification (2) accelerated ceramide synthesis (3) accumulation of malonyl–CoA and long-chain fatty-acyl-CoA and (4) fatty acid-induced apoptosis and activation of endoplasmic reticulum (ER) stress *(Prato, Del, 2009*).

Although the main molecular pathways of insulin resistance are not completely clarified, lipid accumulation in adipose and non-adipose tissues (liver and muscle) contributes to a chronic inflammatory state that plays a fundamental role in insulin resistance *(León-Pedroza et al., 2015; Sokolowska e Blachnio-Zabielska, 2019*). Furthermore, FFAs also play an important role in insulin resistance development, since increased FFA accumulation in hepatocytes leads to the inhibition of insulin-mediated suppression of glycogenolysis, thus promoting hyperglycemia (*Boden, 2003*). Additionally, elevated TG levels are correlated with the detrimental actions of FFAs on the insulin gene expression (*Hagman et al., 2005*).

While under fasting conditions the majority of glucose consumption occurs in noninsulin-dependent tissues such as the brain and the nervous system, under abundant nutrient/ postprandial conditions, the majority of glucose is consumed by insulin-

dependent tissues such as the muscle, adipose tissue and liver, as a result of nutrient-stimulated insulin secretion (*Prato, Del, 2009; Stumvoll, Goldstein e Haeften, 2005)*. The endogenous glucose production occurs mainly in the liver (85%) and, to a minor extent, in the kidneys (15%) (*DeFronzo, 2004*). The increase in plasma levels inhibits hepatic glucose production via glycogenolysis and gluconeogenesis, promoting skeletal muscle glucose uptake and inhibiting the release of FFAs by the adipose tissue (Figure 2) (*DeFronzo, 2004; Stumvoll, Goldstein e Haeften, 2005*).

Insulin resistance in the adipose tissue increases lipolysis, which promotes the release of FFAs. The increase in FFA levels can induce gluconeogenesis, which in turn results in the increase of glucose levels leading to chronic hyperglycemia (*Guilherme et al., 2008; Lambadiari, Triantafyllou e Dimitriadis, 2015; Moreno-Indias e Tinahones, 2015*). Furthermore, elevated levels of FFAs can result in lipotoxicity, as lipid deposition as TGs occurs in other tissues than adipose tissue, which have direct consequences. Fat accumulation in pancreas is a major determinant of β-cell dysfunction and the ectopic fat in the liver (hepatic steatosis), is the major determinant of decreased hepatic insulin sensitivity resulting in fasting hyperglycemia, which is already present in prediabetic state and associated with T2DM progression (*Tsalamandris et al., 2019*).

In prediabetes and T2DM, characterized by the impairment of insulin secretion and action, insulin-mediated processes like peripheral glucose uptake and VLDL-TG secretion from hepatocytes, are compromised in both fasting and fed state *(Kim et al., 2010; Kumar et al., 2019; Smith et al., 1999*). As a result, a vicious cycle responsible for both the maintenance and worsening of the diabetic state is established, where insulin resistance in peripheral tissues leads to a hyperglycemic state that leads to an increase in circulating FFAs, which in turn worsen insulin secretion and insulin resistance *(Prato e Tiengo, 2001; Stumvoll, Goldstein e Haeften, 2005*).

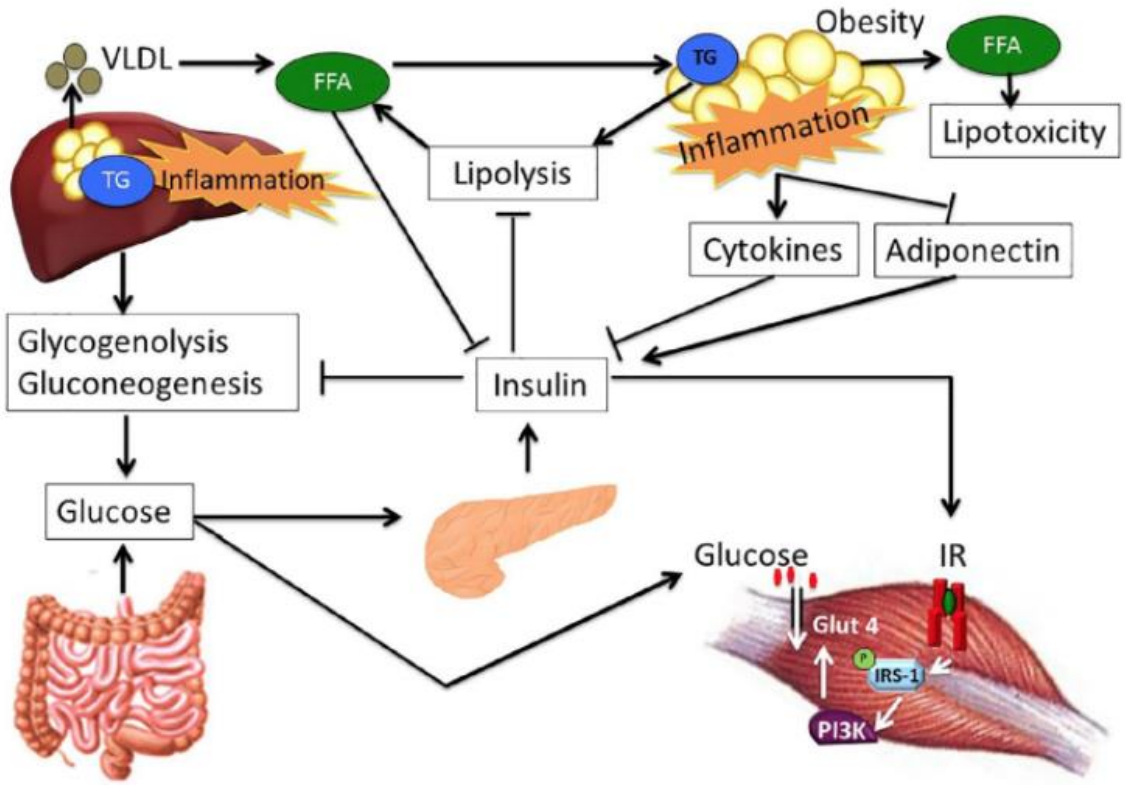

Figure 2 – Skeletal muscle, liver adipose tissue, and cross talk in insulin resistance and obesity. VLDL - Very-low density lipoproteins; FFA - Free fatty acids; TG - Triglycerides; IR - Insulin resistance; Taken from: *K. Albracht-Schulte et al. / Journal of Nutritional Biochemistry 58 (2018) 1-16 (Albracht-Schulte et al., 2018).*

1.1.3.2. Oxidative stress and low-grade inflammation

The functional state of β-cells correlates with the state of the disease status and its reversibility (*DeFronzo, 2004; DeFronzo e Abdul-Ghani, 2011)*. β-cell growth and survival can be affected by multiple mechanisms such as oxidative stress, inflammation, mitochondrial dysfunction, and endoplasmic reticulum (ER) stress (*Donath et al., 2008; Gloyn et al., 2008; Lenzen, 2008; Muoio e Newgard, 2008)*.

Oxidative stress is defined as an imbalance between (1) the production and accumulation in cells and tissues of reactive oxygen species (ROS) - chemical species that result in activation or reduction of molecular oxygen or its reduction byproducts – and (2) the inability to detoxify these reactive products by a biological system *(Nunes S, Soares, Pereira F, 2012; Pizzino et al., 2017*). Oxidative stress may result from long-term exposure to high glucose levels , which increases the metabolic flux into the mitochondria promoting excessive production (*Cernea e Dobreanu, 2013*). The increase in mitochondrial ROS production occurs through multiple pathways including increased

formation of advanced glycation end products (AGEs) from glucose auto-oxidation, the activation of classic isoforms of protein kinase C (PKC), and the increased activation of polyol and hexosamine pathways (Figure 3). The activation of these pathways also increases glucotoxicity, which can cause cellular injury (*Nunes S, Soares, Pereira F, 2012*).

In hyperglycemic states, excessive ROS production can directly impair insulin synthesis and secretion by activating stress response pathways that damage β-cells *(Cernea e Dobreanu, 2013; Luc et al., 2019*). Moreover, oxidative stress disrupts the function and integrity of proteins, lipids and DNA (e.g., impair receptors and enzymes, induces lipid peroxidation, degrades polyunsaturated fatty acids of the membranes, damages pyrimidine and purine bases and induces aminoacids oxidation) (*Cernea e Dobreanu, 2013)*.

The close relationship between oxidative stress and prediabetes is well established, as hyperglycemia can lead to oxidative stress and, in turn, oxidative stress leads to impaired insulin secretion from β-cells and impaired glucose uptake in fat cells and muscle (*Luc et al., 2019)*.

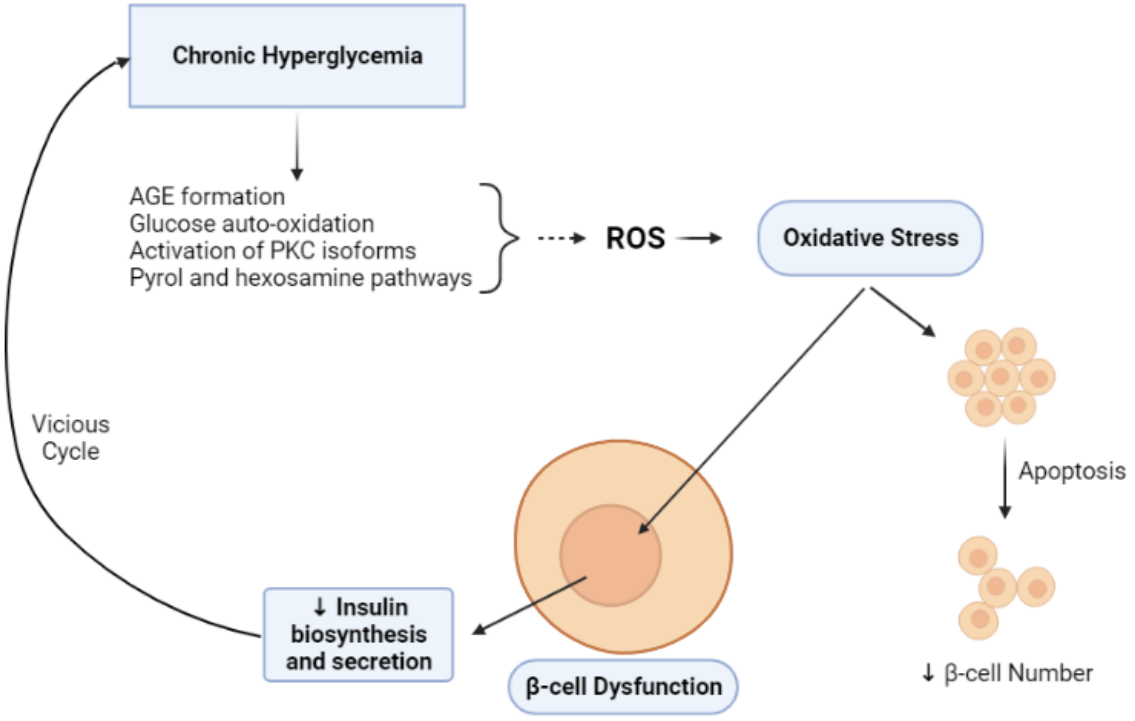

Figure 3 – The vicious cycle between oxidative stress and hyperglycemia. AGE - Advanced glycation end-products; ROS - Reactive oxygen species; PKC - Protein kinase C; Original image adapted from *(Kaneto* et al*., 2005; Robertson* et al*., 2003).*

Low-grade inflammation also plays a significant role in the pathophysiology of prediabetes, being this state associated with high levels of numerous inflammatory markers and cytokines such as interleukin 6 (IL-6), C-reactive protein (CRP) and tumor necrosis factor-alpha (TNF-α). These important pro-inflammatory cytokines are involved in the development of insulin resistance in adipocytes and peripheral tissues through the phosphorylation of insulin receptor substrate-1 (IRS-1) and the enhancement of adipocyte lipolysis *(Akash, Rehman e Liaqat, 2018; Luc et al., 2019; Wang et al., 2016*). Moreover, the levels of some of these inflammatory markers vary along with the progression of the glycemic status *(Luc et al., 2019*).

Hyperglycemia *per se* can lead to a state of systemic inflammation (*León-Pedroza et al., 2015)* and can induce chronic inflammation through various mechanisms by promoting upregulation of chemokines and cytokines and by modulating various pathways that converge towards nuclear factor kappa B (NF-kB) signaling (*Luc et al., 2019*).

Proinflammatory cytokines (e.g., TNF-α, IL-6) promote the activation of three major inflammation-associated signaling pathways, the mitogen-activated protein kinase (MAPK) pathway, the NF-kB pathway, and the Janus kinase signal transducer and activator of transcription (JAK-STAT) pathway. TNF-α stimulates JNK and NF-kB pathways and IL-6 activates JAK-STAT pathway (*Chen et al., 2015*). These pathways promote systemic inflammation that affects the liver, pancreas, muscle, and mainly the adipose tissue. As a consequence, the recruitment and infiltration of macrophages in these tissues occurs, particularly in the adipose tissue, which releases ROS, proinflammatory cytokines (e.g., TNF-α) and chemokines that perpetuate a local and systemic low-grade inflammation and establish a vicious cycle leading to pathophysiological processes such as insulin resistance (*León-Pedroza et al., 2015*). This chronic low-grade inflammation is a major cause of insulin resistance, making obesity the major risk factor for insulin resistance-related diseases such as prediabetes and T2DM (*Chen et al., 2015; Clemente-Postigo et al., 2020)*.

In addition to the effects of hyperglycemia on inflammation, the increase in FFA levels also contributes to inflammation by enhancing NF-KB signaling and the expression of TNF-α and IL-6 through the activation of toll-like receptors (e.g. TLR-4) in macrophages and adipocytes (*Luc et al., 2019*).

1.1.4. Risk factors and complications of Diabetes

The progression of prediabetes to overt T2DM is influenced by several genetic and environmental factors. Although some risk factors are unmodifiable, such as age, sex, ethnicity and family history of T2DM, others can be modified by changing unhealthy lifestyle habits, such as alcohol and tobacco consumption, hypercaloric dietary regimens and sedentary lifestyle that lead to overweight and obesity (*Beulens et al., 2019; Ntzani e Kavvoura, 2012; Tabák et al., 2012; Wu et al., 2020*). Since unhealthy dietary patterns and sedentary lifestyle are major causes of diabetes, the implementation of healthy dietary habits plays a major role in the prevention of overt T2DM *(Tsalamandris et al., 2019).*

Diabetic subjects develop multiple long-term complications. One of the main pathophysiological complications of prediabetes is nonalcoholic fatty liver disease (NAFLD), a condition characterized by excess lipid accumulation in hepatocytes (hepatic steatosis), its hallmark feature *(Donnelly et al., 2005).* Furthermore, diabetic patients have a higher incidence of both microvascular complications, such as nephropathy, peripheral neuropathy and retinopathy, and macrovascular complications, such as cerebrovascular disease, vascular cerebral accident, arterial coronary disease, peripheral vascular disease, or acute myocardial infarction (*Tsalamandris et al., 2019*).

1.1.5. Obesity as a major risk factor for Prediabetes progression

Obesity is defined by the WHO as abnormal or excessive fat accumulation that may impair health. The WHO considers obesity an "issue that has grown to epidemic proportions", estimating that the worldwide prevalence of obesity nearly tripled between 1975 and 2016 and that in 2016, about 13% of the world's adult population (11% of men and 15% of women) were obese (*World Health Organization, 2021*).

Obesity is a major risk factor for prediabetes progression, since obesity can induce and exacerbate hyperglycemia and insulin resistance promoting the progression from prediabetes to overt T2DM (*Flier, 2000).* The major modifiable risk factors that underlie obesity are sedentary lifestyles, associated with decreased energy expenditure, and unhealthy hypercaloric diets, associated with increased energy intake. Obesity is a state of positive energy imbalance, with energy intake exceeding energy expenditure, resulting

in an increase in body mass *(Ailshul, 1975)*. It is well accepted that a positive energy balance leads to the initial fat accumulation in subcutaneous tissues and later in other tissue compartments (visceral tissues), accumulating in key organs such as the muscle, heart, pancreas, and liver. This fat deposition is also designated as ectopic lipid deposition (*Tsalamandris et al., 2019*).

1.1.5.1. Adipose tissue overview

The adipose tissue is a heterogeneous, complex structure composed mostly by adipocytes and other cell types, including endothelial cells, mesenchymal cells, fibroblasts, immune cells and preadipocytes (*Suganami* e *Ogawa, 2010*). Adipose tissue plays a crucial role in the regulation of energy homeostasis, by controlling both energy storage and expenditure, and also exerts important functions as an endocrine organ through the production and release of a vast number of metabolically active molecules, termed adipokines, that play a key role in crosstalk with other metabolic organs such as the brain, liver, muscle and pancreas. These mediators include leptin, adiponectin, resistin, TNF-α, IL-6, plasminogen activator inhibitor 1 (PAI-1), fatty acids, sex steroids and numerous growth factors, which are involved in inflammatory pathways and perform numerous functions at cardiovascular, endocrine, immunologic and metabolic level (*Klaus, 2005; Tsalamandris et al., 2019*). Metabolic disorders are often associated with insufficient or excessive adipose tissue mass. For example, the production and secretion of resistin, adipsin and leptin increases with obesity and are associated with insulin resistance, inflammation and an increased risk of other pathological conditions (*Gustafson et al., 2009*).

Anatomically, adipose tissues can be classified according to their distribution or depot localization as subcutaneous adipose tissues (SAT) or visceral adipose tissue (VAT). While SAT is localized beneath the skin, VAT, also known as intrabdominal fat, is present mainly in the mesentery and omentum, surrounding the viscera in abdominal cavity and drains through the portal circulation to the liver (*Mittal Balraj, 2019; Suganami* e *Ogawa, 2010*). This physical classification entails important functional implications. VAT produces a large amount of pro-inflammatory factors and harbors a large amount of inflammatory cells (macrophages and monocytes). Furthermore, VAT adipocytes are more metabolically active, more insulin-resistant and have a greater lipolytic activity than SAT adipocytes. On the other hand, SAT is the major source of leptin and adiponectin production, and only when SAT accumulation capacity is exceeded or impaired does this

energy accumulate in the VAT. *(Suganami e Ogawa, 2010; Yamamoto et al., 2020*). Visceral obesity is strongly correlated with the development and progression of diabetes and cardiovascular diseases as it contributes to systemic inflammation and oxidative stress that lead to insulin resistance. Furthermore, epidemiological studies showed that VAT accumulation is associated with increased metabolic risk and overall mortality while SAT expansion decreases the risk of T2DM development and ameliorates insulin sensitivity *(Klaus, 2005; Luc et al., 2019; Mittal Balraj, 2019*).

Adipose tissues can also be broadly classified as white adipose tissue (WAT), brown adipose tissue (BAT), and beige adipose tissue (an intermediate phenotype between WAT and BAT). BAT is much less abundant than WAT and they differ in terms of localization and functions (*Betz e Enerbäck, 2018; Suganami e Ogawa, 2010*). In rodents, brown adipocytes are found in discrete areas such as interscapular, perirenal, intercostal, and cervical depots (Sanchez-Gurmaches, Hung e Guertin, 2016). Brown adipocytes are found in clusters scattered within WAT areas (*Kaisanlahti e Glumoff, 2019)* and derive from white adipocyte precursors, the beige adipocytes, by a transdifferentiation process known as WAT browning (*Park, 2014*). Beige adipocytes are localized within BAT and WAT (*Montanari, Pošćić e Colitti, 2017*) (Figure 4).

The differentiation of BAT is regulated by multiple molecules. One of the most important is the peroxisome proliferator-activated receptor-gamma coactivator 1α (PGC-1α), which regulates oxidative metabolism and mitochondrial biogenesis. Its genetic ablation results in impaired cold-induced adaptive thermogenesis due to the absence of adrenergic stimulus response via cAMP. Thus, PGC-1α is a crucial factor in thermogenesis regulation (*Seale, 2010*).

BAT and beige adipose tissue are thermogenic tissues, playing a crucial role in energy expenditure, as they convert chemical energy stored in the form of triglycerides in lipid droplets into heat through mitochondrial activity, in a process called non-shivering adaptive thermogenesis. This process is facilitated by a mitochondrial carrier protein – thermogenin or uncoupling protein 1 (UCP-1), which is located on the inner membrane of mitochondria and is highly expressed in BAT (*Betz e Enerbäck, 2018)*. High UCP-1 expression is a defense mechanism against hypothermia and obesity. Cold exposure induces thermogenic activation, which promotes lipolysis. In turn, fatty acids derived from lipolysis induce UCP1-dependent heat production in activated beige and brown adipocytes. This way, thermogenesis promotes energy expenditure and fat loss as the

triglycerides in lipid droplets are converted into heat (*Betz e Enerbäck, 2018; Ikeda e Yamada, 2020; Montanari, Pošćić e Colitti, 2017; Torres et al., 2019*). Therefore, thermogenesis without ATP production (i.e., non-shivering thermogenesis) is an effective way of promoting energy dissipation and creating a negative energy balance. Thus, brown and beige adipocytes have sparked interest in the scientific community given their ability to positively modulate multiple metabolic conditions, including T2DM and obesity. In humans and rodents, glucose tolerance appears to be enhanced by activated thermogenesis in both brown and beige adipocytes (*Czech, 2020; Kaisanlahti e Glumoff, 2019)*. Furthermore, increased amounts of BAT are associated with decreased body fat mass and increased insulin sensitivity and oxidative capacity (*Betz e Enerbäck, 2018*).

In contrast to BAT, the main function of WAT is to store excess energy as triglycerides after feeding and mobilize lipids in the fasting state to meet the energy demands of other tissues *(Yamamoto et al., 2020*). This way, WAT is the most important buffering system for lipid energy balance in the body due to its ability to accumulate and provide energy when needed (*Park, 2014)*.

Morphologically, while brown adipocytes contain many multilocular lipid droplets and a high number of mitochondria, white adipocytes have unilocular lipid droplets and fewer mitochondria *(Shinde, Song e Wang, 2021; Yamamoto et al., 2020*).

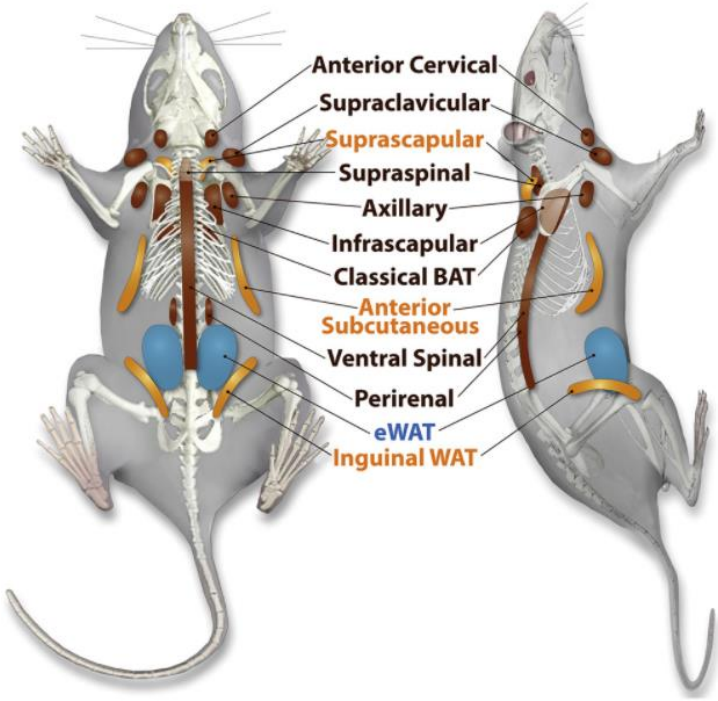

Figure 4 – Rodent fat pads. White adipose tissue depots are indicated in blue, fat pads with the ability to beige are indicated in yellow, classical brown adipose tissue deports are indicated in brown. eWAT - epidydimal white adipose tissue. Image taken from (*Zhang et al., 2018*).

1.1.6. Hepatic steatosis as a major complication of Prediabetes

The liver also plays a prominent role in the pathophysiology of several metabolic disorders such as prediabetes and T2DM, since it is a key organ in the maintenance of lipid and glucose homeostasis. Pathophysiological processes include inflammation, oxidative stress, lipotoxicity, and glucotoxicity that can lead to impaired liver function and consequently liver injury (*Ferrannini, Gastaldelli e Iozzo, 2011; Flier, 2000)*.

Hepatic fat accumulation (steatosis), the hallmark feature of nonalcoholic fatty liver disease (NAFLD), is one of the main pathophysiological complications of prediabetes. NAFLD is the most common cause of liver disease worldwide, representing a major cause of hepatic morbidity and mortality as its global prevalence is estimated to range from 25% to 45% and increasing with the growing prevalence of diabetes and obesity (*Donnelly et al., 2005; Rinella, 2015; Younossi, 2019*).

NAFLD is a disease spectrum characterized by hepatic steatosis in the absence of chronic alcohol consumption and can progress to more severe forms, including nonalcoholic steatohepatitis (NASH), cirrhosis and ultimately hepatocellular carcinoma. This lipid accumulation in hepatocytes results from abnormalities in lipid metabolism, as the rate of the mechanisms that promote fatty acid input in the liver (increased fat and sugar intake from diet, lipolysis and *de novo* lipogenesis) surpass the rate of the mechanisms that promote fatty acid output (fatty acid β-oxidation and very-low-density lipoproteins export) (*Donnelly et al., 2005*).

As the disease progresses, each state presents distinct histological findings. NAFLD includes isolated hepatic steatosis and mild lobular inflammation, while NASH is characterized by the presence of steatosis and features of hepatocellular injury like tissue ballooning, a higher severity of inflammation with or without fibrosis. Cirrhosis is characterized by elevated scar tissue-like states that become more irreversible as the disease progresses and can culminate in hepatocellular carcinoma and death (Figure 5) (*Pagliassotti, 2012; Rinella, 2015*).

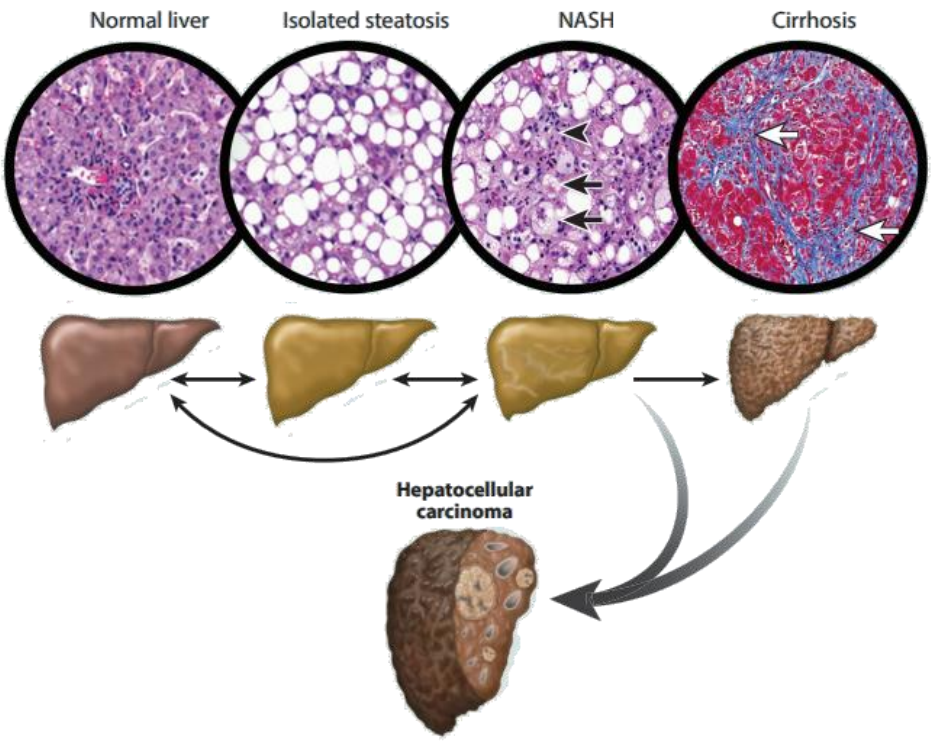

Figure 5 – Spectrum of nonalcoholic fatty liver disease (NAFLD). Hepatocyte cell ballooning (black arrows) and collagen bands surrounding liver nodules (white arrows). NASH - Nonalcoholic steatohepatitis. Image adapted from (*Arab, Arrese e Trauner, 2018*).

Although indispensable, current pharmacological approaches for NAFLD and NASH are poor in efficacy and limited, as they demonstrated good results in inflammation and steatosis, but without reliable effects on fibrosis. Thus, the first approach to the management of this condition is based on the prevention of progression through the correction of the main risk factors (obesity, dyslipidemia, and insulin resistance) through life style modification strategies, such as weight loss and healthy dietary regimens, as these measures can reverse a steatotic liver state into a normal condition *(Diehl e Day, 2017; Oseini e Sanyal, 2017*). Low levels of HDL and high levels of TGs are common findings among NASH patients, as well as elevated liver enzyme levels such as aspartate aminotransferase (AST) and alanine aminotransferase (ALT), which are indicators of liver injury *(Dumitrascu e Neuman, 2018*). The correction of transaminase blood levels is also one of the current strategies for NASH management to avoid its progression (*Oseini e Sanyal, 2017*).

Histologically, hepatic steatosis can be classified in two types: microvesicular steatosis and macrovesicular steatosis. Microvesicular steatosis is characterized by hepatocytes with small lipid vesicles with less than 1 μm in diameter that may or not be

discernible. These hepatocytes are distended with foamy appearing cytoplasm and a typically centrally located nucleus. In macrovesicular steatosis, hepatocytes display large lipid droplets in which there is a single large vacuole of fat that fills up the hepatocyte and displaces the nucleus to the periphery (*Tandra et al., 2011*). While in human settings microvesicular steatosis is considered potentially more malignant than macrovesicular steatosis, which is regarded as benign *(Kristiansen et al., 2019; Tandra et al., 2011*), the opposite occurs in rodent models, as macrovesicular steatosis is associated with worse disease phenotype progression *(Kitamori et al., 2012; Piacentini et al., 2018*).

1.1.6.1. Molecular mechanisms of hepatic steatosis

a) The endoplasmic reticulum (ER) stress and the unfolded protein response (UPR)

NAFLD comprises several metabolic changes that act synergistically in its development and progression, such as insulin resistance, lipotoxicity, and ER stress *(Feng et al., 2014*). Likewise, ER stress is also involved in prediabetes progression to T2DM and development of insulin resistance and is emerging as a key mechanism in metabolic diseases such diabetes and obesity (*Green e Olson, 2011; Lupachyk et al., 2013; Wu et al., 2017*). ER stress is also associated with obesity, the major risk factor for hepatic steatosis and its progression (*Zhang et al., 2014)*. This progression in promoted by a vicious cycle where hepatic lipid accumulation promotes the increase of phosphatidylcholine/phosphatidylethanolamine ratio that leads to the disruption of ER membrane. This promotes ER stress, which in turn leads to increased lipogenesis and VLDL secretion and decreased fatty acid oxidation, promoting steatosis (*Baiceanu et al., 2016; Veen, van der et al., 2017*).

The main functions of the endoplasmic reticulum involve the modification and processing of proteins and synthesis of intracellular proteins. It is also the main site of cholesterol synthesis (*Li e Zhang, 2019; Pagliassotti, 2012*). Most of the lipids synthetized in the ER are transported to other organelles and most of the newly synthesized proteins are inserted into membranes or secreted (*Cooper, 2000*).

ER stress occurs when the protein folding capacity, protein biosynthesis, cell death or secretory pathways are compromised. ER stress occurs due to misfolded protein accumulation in the lumen of the ER that can be induced by overnutrition and metabolic

disorders like diabetes and obesity (*Rocha et al., 2020*). When cell homeostasis is compromised due to multiple stress factors, such as lipotoxicity (as in hepatic steatosis) or oxidative stress, a series of cell self-protection events are initiated in order to maintain cellular homeostasis (*Li e Zhang, 2019*). The cellular response to ER stress is called the unfolded protein response (UPR) which aims to preserve cellular function by three mechanisms: the interruption of protein translation to avoid the generation of more unfolded proteins; the activation of signaling pathways that promote the synthesis of molecular chaperones implicated in protein folding; and the activation of ERAD in order to reduce protein accumulation in ER through the degradation of unfolded/ misfolded proteins. However, if the UPR does not succeed in achieving its primary goal, it will promote apoptosis (*Kawasaki et al., 2012; Rocha et al., 2020*).

The activation of the mammalian UPR encompasses three signaling branches: the double stranded RNA-dependent protein kinase-like ER kinase (PERK), the inositol-requiring enzyme-1 (IRE-1), and the activating transcription factor 6 (ATF6). Under normal conditions, that is, in the absence of ER stress, these proteins are inactivated through association with the ER protein chaperone immunoglobulin heavy chain binding protein (BiP), also referred to as 78-kDa glucose-regulated protein (GRP78). However, under ER stress conditions, these proteins are activated through dissociation from GRP78 that is released and sequestered by unfolded proteins *(Pagliassotti, 2012)*.

Activation of IRE-1 promotes the splicing of X-box-binding protein-1 (XBP1s) mRNA which is then translated into the active XBP1. The active XBP1 promotes the expression of components related to the endoplasmic-reticulum-associated protein degradation (ERAD), to protein folding and quality control. The activation of IRE-1 promotes the degradation of specific mRNAs localized in the ER proximities as an effort to decrease the production of proteins requiring folding in the ER lumen. Additionally, IRE-1 activates the c-Jun N-terminal kinase (JNK) and apoptosis signal-regulating kinase 1 (ASK1) pathway through the binding of TNF receptor-associated factor 2 (TRAF2) *(Baiceanu et al., 2016; Pagliassotti, 2012*).

Activation of ATF6 leads to its release from the ER membrane, then it is transferred to the Golgi apparatus where it is cleaved into an active form by the membrane-bound site-1 (S1P) and site-2 (S2P) proteases. This active form enters the nucleus and induces the expression of UPR components and chaperones *(Baiceanu et al., 2016; Pagliassotti, 2012*).

When activated, PERK phosphorylates and inactivates the α-subunit of the translation initiation factor eIF2 (p-eIF2α) leading to a general decrease in protein translation initiation except for activating transcription factor 4 (ATF4), which induces the expression of factors involved in autophagy, apoptosis and antioxidant defense, such as DNA damage-inducible transcript 3 protein (C/EBP homologous protein; CHOP). ATF4 also increases the expression of GADD34, a member of the growth arrest and DNA damage-inducible family of proteins, which enables the dephosphorylation of eIF2α and therefore reversal of translational attenuation (Figure 6) *(Baiceanu et al., 2016; Pagliassotti, 2012*).

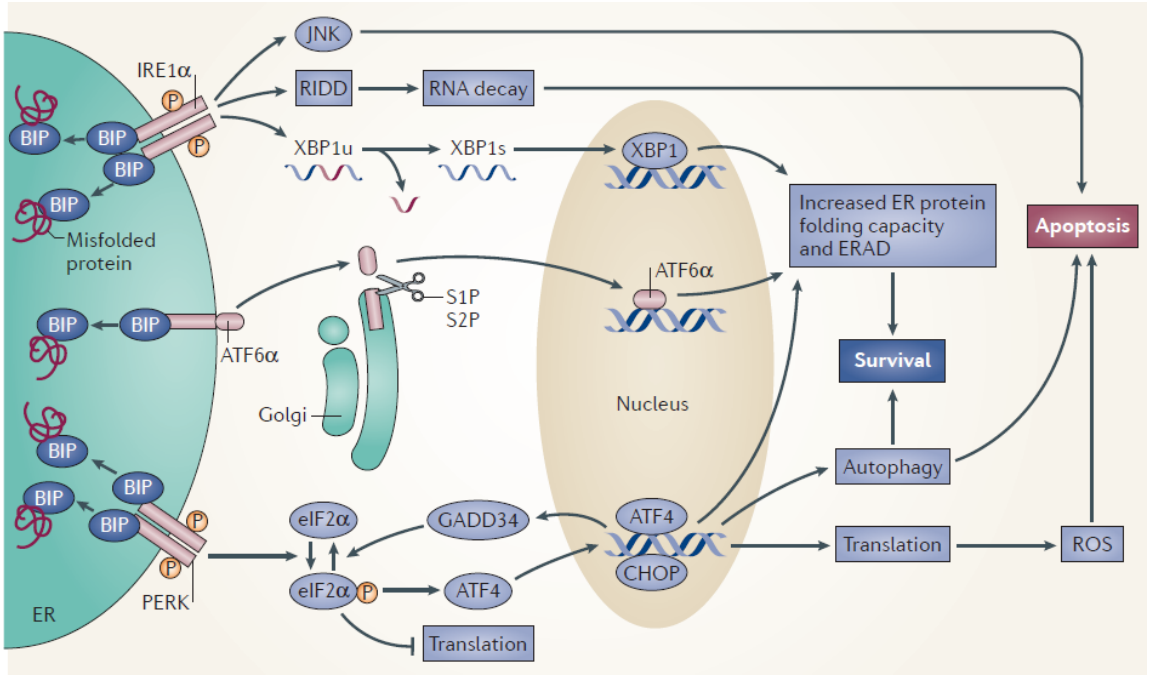

Figure 6 – The unfolded protein response (UPR). ER - Endoplasmic reticulum; BIP - Immunoglobulin heavy-chain binding protein; PERK - PRKR-like ER kinase (PERK); eIF2α - Eukaryotic translation initiation factor 2α; IRE-1 - Inositol-requiring protein 1; XBP1 - X-box binding protein 1; ATF6α - Transcription factor 6α; ERAD - ER-associated protein degradation; CHOP - C/EBP homologous protein; GADD34 - Growth arrest and DNA damage-inducible protein 34; JNK - JUN N-terminal kinase; P - Phosphorylation; RIDD - Regulated IRE-1-dependent decay; ROS - Reactive oxygen species; XBP1s - Transcriptionally active XBP1; XBP1u - Unspliced XBP1. Image taken from *(Wang e Kaufman, 2014)*.

Under physiological conditions, the liver undergoes transient ER stress responses; however, under pathophysiological conditions such as NAFLD, ER stress becomes chronic and so does the UPR. Chronic UPR activation has been demonstrated in livers of obese mice and rats. Although the aim of the UPR is to restore cellular homeostasis, its chronic activation in response to fatty liver may have deleterious consequences, as it promotes hepatic steatosis progression *(Baiceanu et al., 2016)*.

b) Autophagy

Another molecular mechanism associated with hepatic steatosis and dysregulated glucose metabolism is autophagy *(Coccurello et al., 2018)*. Autophagy is a lysosomal catabolic process that ensures cell survival, maintains energy homeostasis during periods of nutrient deprivation and preserves genomic integrity by degrading pathogens or damaged cellular components. This process is activated by many stressors including pathogen infection, hypoxia, oxidative stress, nutrient starvation and can also be induced by the UPR as aggregated or misfolded proteins accumulate *(González-Rodríguez et al., 2014; Park et al., 2013; Rocha et al., 2020; Senft e Ronai, 2015*).

Indeed, there are three distinct types of autophagy, classified by how substrates are trafficked to the lysosomes for degradation: macroautophagy, microautophagy and chaperone-mediated autophagy (*Rocha et al., 2020*). Chaperone-mediated autophagy recognizes only proteins amenable to unfolding and translocate them directly into the lysosome for degradation (*Tekirdag e Cuervo, 2018*). Microautophagy refers to the direct invagination of cytosolic components by lysosomes for degradation. In contrast, macroautophagy, the major type of autophagy, sequesters and transports a heterogeneous set of cargo in vesicles, called autophagosomes, to the lysosome (*Rocha et al., 2020*). Although these pathways are mechanistically distinct, they all carry out degradation via the lysosome (*Park et al., 2013; Rocha et al., 2020*).

In the presence of nutrients and cytokines, autophagy is inhibited by activation of mammalian target of rapamycin (mTOR), which regulates cellular processes, including autophagy, cell growth proliferation and protein synthesis *(Rocha et al., 2020; Witzig et al., 2015*). On the other hand, in the absence of nutrients and increased stress (nutrient starvation conditions, oxidative stress and UPR activation),

mTOR is inhibited and autophagy is initiated (*Khandia et al., 2019*). In addition to the mTOR pathway, autophagy can be induced directly through the stimuli of the phosphoinositide-3-kinase (PI3K) complex which contains Beclin (a mammalian homolog of yeast Atg6), which also plays a major role in macroautophagy nucleation step (*Pauly et al., 2017*). A link between the UPR and autophagy has also been evidenced. PERK-eIF2α pathway is crucial for the induction of autophagy after ER stress, as ATF4 and its target gene CHOP transcriptionally regulate numerous autophagy-related genes (Atgs). Furthermore, IRE-1 is also implicated in autophagy activation as the JUNK and TRAF2-dependent activation of IRE-1 results in the phosphorylation of Bcl-2, enabling Beclin

dissociation and therefore the activation of PI3K complex and autophagy (*Senft e Ronai, 2015*).

This complex process involves several phases: 1) induction and nucleation of phagophore; 2) elongation that leads to the formation of autophagosome; 3) following the maturation, the fusion of the autophagosome with the lysosome occurs to form the autolysosome, in which result in the cargo degradation. The digested components can then be used for energy production or biosynthesis of new products after being transported to the cytosol (*Rocha et al., 2020)*.

The nucleation step begins with phagophore formation, a double-membrane elongation structure that will constitute the autophagosome. This phase of autophagy starts with the interaction between the PI3K-II complex and the unc51 like kinase (ULK). As part of the PI3K complex, Beclin interacts via its BH3 domain with the anti-apoptotic family B-cell lymphoma 2 (Bcl-2), since it recruits autophagic proteins to a primordial autophagosomal structure. This interaction is regulated by numerous proteins capable of promoting and inhibiting the interaction Bcl-2/Beclin with the purpose of repress and activate autophagy. The binging of Bcl-2 to Beclin inhibits autophagy. In order to nucleation step to occur, it is required the dissociation between Bcl-2 and Beclin enabling the activation of PI3K complex and autophagy stimulation (Figure 7) *(Decuypere, Parys e Bultynck, 2012; González-Rodríguez et al., 2014*).

The elongation step is coordinated through two ubiquitin-like conjugation systems: light chain-3 (LC3)-phosphatidylethanolamine (PE) and the ATGs proteins. In order to promote autophagosomal elongation, Atg12-Atg5-Atg16L forms a multicomplex that dissociates once the fully functional autophagosome is formed. This protein complex facilitates the conjugation of PE with LC3 (*Ravikumar et al., 2009)*. Through the action of Atg4 and Atg3, the soluble form of LC3 (LC3-I) is converted in to the autophagic vesicle associated form LC3-II, a molecular marker for autophagosomes. LC3-II is essential for the expansion of the autophagic membrane and is present in both outer and inner surfaces of the autophagosome (*Khandia et al., 2019; Park et al., 2013*). Moreover, the elongation step involves the interaction between cargos that recognize each other through specific receptor proteins. The autophagic adaptor protein p62/Sequestosome-1 (p62/SQSTM1) is crucial for autophagosome formation. The p62/SQSTM1 tag the autophagy substrates with ubiquitin to degradation by interacting with autophagic proteins like LC3-II *(Lamark, Svenning e Johansen, 2017; Park et al., 2013*). The final steps consist in closure and

maturation, in which occurs the enclosure of the membrane resulting in the complete formation of the autophagosome. After this step, the autophagosome is ready to bind with the lysosome for cargo degradation (*Tong, Yan e Yu, 2010*).

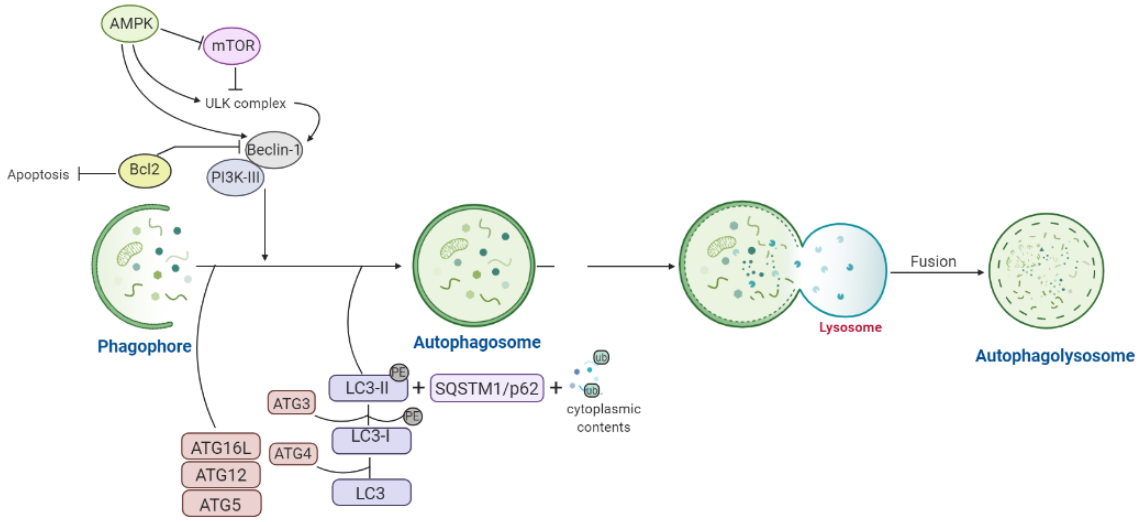

Figure 7 – Autophagolysosome formation. AMPK - AMP - activated protein kinase; mTOR - Mammalian target of rapamycin; ULK - Unc-51-like kinase 1; Bcl-2 - B-cell lymphoma 2; PI3K-III - Phosphoinositide 3-kinase class III; ATG - Autophagy-related proteins; LC - Light chain; SQSTM1/p62 - Sequestosome-1/p62; PE - Phosphatidylethanolamine; Original image adapted from *(Bhattacharya et al., 2018)*

The role of autophagy in the pathophysiology of NAFLD was first suggested by the discovery that this pathway mediates the breakdown of intracellular lipids in hepatocytes and, through this process, it may prevent the progression of hepatic steatosis. Additional studies showed novel critical functions for autophagy, not only in hepatocytes but also in other hepatic cell types, such as stellate cells and macrophages, that regulate insulin sensitivity, hepatocellular injury, and carcinogenesis, arousing great interest in this mechanism due to its extensive implications in the progression of multiple metabolic diseases *(Czaja, 2016)*.

Due to its anti-steatotic properties, autophagy (lipophagy) is a mechanism of great interest as it may play a critical role in the prevention of NAFLD progression to NASH (*Allaire et al., 2019*). This mechanism is deregulated in many liver diseases and its function is decreased under several conditions that predispose to NASH (*González-Rodríguez et al., 2014*). In fact, the autophagic flux, a measure of autophagic degradation activity *(Loos, Toit, du e Hofmeyr, 2014*), is impaired in both humans with NAFLD and in murine models of NAFLD. For instance, the blockade of the autophagic flux was reported in the liver of

mice fed with high fat diets (HFD) compared with mice fed with chow diets (CD), as an increase in LC3-II/LC3-I ratio and p62 was observed *(Allaire et al., 2019; González-Rodríguez et al., 2014*). In a vicious cycle where lipid accumulation promotes insulin resistance, and insulin resistance promotes lipid accumulation, both of these pathophysiological processes impair autophagy. In turn, the impairment of autophagy further worsens both insulin resistance and lipid accumulation (*Allaire et al., 2019; González-Rodríguez et al., 2014*). In this sense, autophagy plays a key role in both steatosis and prediabetes progression, making its modulation a potential therapeutic strategy to prevent disease progression.

Although the relationship between autophagy and T2DM is well established, few studies have focused on the relationship between autophagy and prediabetes *(Fakih et al., 2020; He et al., 2020)*, which highlights the need to investigate further this link. Thus, well-defined and characterized animal models mimicking the development and progression of prediabetes could be important tools to improve our understanding of the pathophysiological mechanisms underlying the evolution of prediabetes to T2DM and associated complications.

1.1.7. Diet-induced animal models of Prediabetes

In line with the global epidemic of T2DM, the increasing prevalence of prediabetes becomes an important concern within the scientific community. This increase in prediabetes prevalence is mainly due to detrimental lifestyle behaviors, including unhealthy eating habits (*Tsalamandris et al., 2019*). As mentioned above, interventions based on the management of risk factors through lifestyle modifications may prevent the progression of prediabetes (*Tsalamandris et al., 2019; Wu et al., 2020*). However, the majority of the population fails to adhere to these lifestyle modifications (*Kim et al., 2014*). Considering the difficulties in controlling this disease, as the epidemiological numbers continue to grow, it becomes imperative to increase our knowledge on the molecular mechanisms and therapeutic targets that will allow more effective strategies for prediabetes.

Over the years, pre-clinical models of disease have been indispensable tools in this quest as a means to evaluate the effect of the various behavioral, environmental and genetic factors that lead to metabolic alterations. The most frequently used animal models of prediabetes are rodents (rats or mice) due to their small size, their short reproduction cycle, and their low cost (*Cefalu, 2006*). While there is a wide diversity of animal models

of both T2DM and obesity, animal models of prediabetes are scarce (*Islam e Venkatesan, 2016; Islam e Shannon, 2012*).

While some models show a genetic predisposition to the disease, others may develop the disease spontaneously or in a diet-induced manner (*Brown e Setchell, 2001; Dawson, Ko e Dawson, 2010; Dourmashkin et al., 2005; Islam e Venkatesan, 2016*). The most commonly used non-genetic rodent models of diabetes are those induced by partial pancreatectomy, or induced by alloxan or streptozotocin simultaneously with dietary modifications *(Islam e Loots, 2009; Lenzen, 2008*). Some spontaneously or genetically induced models of diabetes are used as models for insulin resistance and prediabetes in the early stage of their lifespan (e.g., Goto Kakizaki rats, prediabetic BB-DP rats Zucker Diabetic Fatty (ZDF) rats, prediabetic Chinese hamster, prediabetic SHROB rats, and Otsuka Long Evan Tokushima Fatty Rats (OLETF). However, spontaneously or genetically induced models of diabetes are expensive compared with experimentally-induced non-genetic models such as diet-induced models. Therefore, spontaneously or genetically-induced models of diabetes are not widely available and are not so suitable for routine pharmacological or nutraceutical screening of compounds that prevent prediabetes progression (*Islam e Venkatesan, 2016)*.

The prediabetic phenotype can be induced in rodents by a variety of dietary regimens. The most frequently used are high-fat diets (HFD), high-sugar diets (HSD), and a combination of both, for example the high-fat high-sucrose diets (HFHS). These diets vary greatly in their composition. The fat content in HFD ranges from 45 and 60% calories. HSD are the most diverse and can be administered alone or supplemented to an HFD, being fructose, sucrose and glucose, the most used sources of sugar. In HFHS diets, while fat content ranges from 20-60%, the carbohydrate content ranges from 10-60% in drinking water, diet or both (*Preguiça et al., 2020*). Changes in macronutrient composition of diets, such as the content of protein, fat, carbohydrate as well as water and fiber, considerably affect the induction and progression of disease phenotypes and their associated complications *(Bray et al., 2002; Stanhope et al., 2018*). Despite several studies in animal models have shown that the use of HSD (high-fructose and high-sucrose) promotes the development of glucose intolerance and insulin resistance (*Chen et al., 2011; Oliveira et al., 2014*), fructose, sucrose and glucose display differences in terms of metabolic disruption. For instance, *ad libitum* access to fructose beverages increases adiposity and hepatic lipid accumulation in mice when compared to sucrose. Furthermore, several experimental

studies showed that dietary macronutrient composition is an important environmental factor for prediabetes development (*Hafizur et al., 2015; Lozano et al., 2016; Saravanan et al., 2017*). Therefore, hypercaloric diets should be carefully selected to achieve the most desired outcome as subtle changes in diet formulation, such as the physical state and nutrient source, may affect the extent of the metabolic impairments (*Preguiça et al., 2020*). Although epidemiological studies on the prevalence of diabetes and sugar consumption suggest that HFHS diets are a greater risk factor for these metabolic disorders than HFD or HFS alone (*Basu et al., 2013)*, the most appropriate model will depend on the scientific question to be addressed (*King e Bowe, 2016*).

The phenotype of an animal model of prediabetes has been defined as increased 2h blood glucose values, hyperinsulinaemia, glucose intolerance, moderate/mild hyperglycaemia and hyperlipidaemia (*Hafizur et al., 2015*). In our previous studies, a prediabetic phenotype was successfully induced in Wistar rats by oral consumption of 35% sucrose solution *ad libitum* for 9 weeks. This model displayed glucose intolerance, insulin resistance, hyperinsulinaemia and hypertriglyceridemia; however, obesity or fasting hyperglycaemia, two central features of the disease, were not observed (*Nunes et al., 2013*). To overcome this limitation, in the present study, we fed Wistar rats with a solid high-fat high-sucrose (HFHS) diet for 24 weeks with the purpose of inducing a more aggravated prediabetic phenotype. Preliminary data from our group demonstrated that from week 12 onward the HFHS-induced animal model of prediabetes displayed increased body weight, and from week 16 onward displayed glucose intolerance along with normal levels of fasting glycaemia and insulinemia. However, at week 24, the HFHS-fed animals model displayed elevated postprandial insulin (unpublished data), which represents a compensatory feature of the prediabetic state *(Elks et al., 2015; Marques et al., 2016*) (Figure 8).

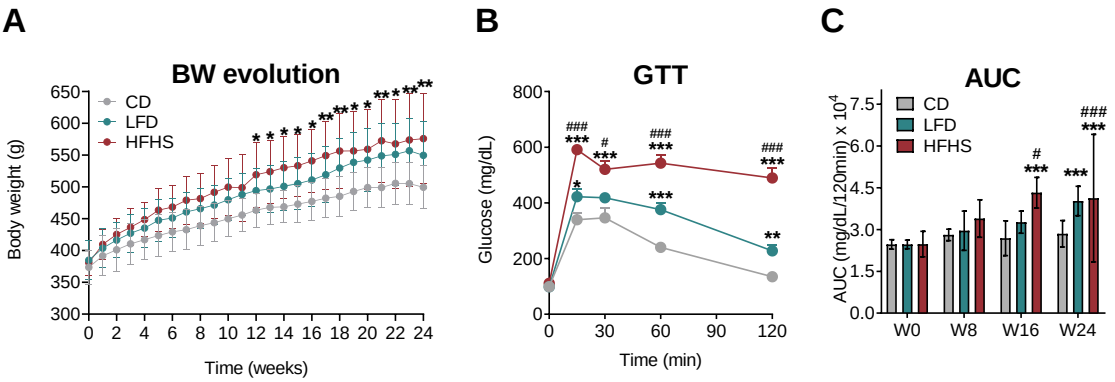

Figure 8 – Body weight evolution and glucose tolerance in response to 24 weeks of CD, LFD and HFHS diets in male Wistar rats. (**A**) Body weight (BW) evolution (grams). (**B**) Changes in blood glucose levels (mg/dl) at different time points after an intraperitoneal injection of a glucose solution (2 g/kg body weight, glucose tolerance test (GTT) assay) at week 24. (**C**) Area under the curve (AUC) of GTT assay, expressed as milligrams per deciliter per 120 minutes. CD - Chow diet; LFD - Low-fat diet; HFHS - High-fat high-sucrose. Data are presented as mean ± SEM (n = 4-8 per group); *p<0.05; **p<0.01 and ***p<0.001 vs CD; # p<0.05 and ### p<0.001 vs LFD.

1.2. Refined vs Unrefined control diets

Most animal models of prediabetes are induced by refined diets with high fat and high sucrose content (HFHS) (*Preguiça et al., 2020*), which are usually compared with unrefined control diets (chow, CD). However, these diets differ markedly, not only in their refinement degrees, but also in their nutrient content (*Lai, Chandrasekera e Barnard, 2014; Pellizzon e Ricci, 2018*).

While unrefined control diets are mainly produced with a combination of ingredients based on cereal grains (e.g., soybean meal, corn, alfalfa, wheat, oats), purified diets are made of a combination of refined ingredients isolated from the whole food source, each ingredient supplying a main nutrient (e.g., fat from soybean oil) along with insoluble fiber (e.g., cellulose) (*Almeida-Suhett et al., 2019*). Another major difference between refined and unrefined diets is their content in phytoestrogen and sucrose. While chow diets (CD) have a high content in phytoestrogen and no sucrose, the opposite occurs in refined diets, in which the phytoestrogen is absent and sucrose is used as a carbohydrate source (*Preguiça et al., 2020*). Due to nutritional variations in cereal grains, batch consistency in unrefined diets is difficult to ensure, and because diet compositions are not fully disclosed by the manufacturers, data reproducibility is often questioned. In contrast, refined diets overcome this limitation by allowing the manipulation of individual

nutrients and enabling the assessment of the effects of a single nutrient on a given phenotype (*Pellizzon e Ricci, 2020*).

Taking this into account, a refined low-fat diet (LFD) produced with the same ingredients as the refined high-fat high-sucrose (HFHS) diet may be a more appropriate control diet than the standard unrefined chow diet (CD). Nonetheless, despite several studies advising on the use of nutrient-matched refined control diets *(Pellizzon e Ricci, 2018, 2018*), there are also reports on the harmful metabolic effects of refined control diets *(Blaisdell et al., 2014, 2017; González-Blázquez et al., 2020*). For example, it is recognized that the healthy potential of cereal-based food can be deteriorated by processing strategies (*Fardet, 2018*). Therefore, it is also important to consider the potential unhealthy impact of refined ingredients on diets (*Blaisdell et al., 2017*) and to further investigate whether the most appropriate control diet for a refined HFHS diet is a standard unrefined chow diet (CD) or a nutrient-matched refined diet (LFD).

1.3. Putative beneficial effects of blueberries on Prediabetes

1.3.1. Health-promoting properties of blueberries

Epidemiological evidence supports the notion that a balanced diet, rich in fruits and vegetables, has a positive impact on human well-being and health, playing an important role in the prevention of several pathologies (e.g., reduction of the risk of cardiovascular and metabolic disease and some forms of cancer). As phenolic compounds and other antioxidants are abundantly present in fruits and vegetables, their consumption may provide some potential health benefits (*Neto, 2007; Rossi et al., 2009; Szajdek e Borowska, 2008*).

Blueberries are among the most popular berries and are found in numerous forms in retail markets (fresh, frozen and processed). Blueberries belong to the genus Vaccinium of Ericaceae family, and *Vaccinium corymbosum* (*V. corymbosum,* highbush blueberries), *Vaccinium ashei* (*V. ashei*; rabbiteye blueberries) and *Vaccinium angustifolium* (*V. angustifolium*, lowbush blueberries) are the most predominant species when considering commercial production (*Riihinen et al., 2008; Zhao, 2007*). Given their polyphenolic content, blueberry incorporation into food products may confer them beneficial properties. Furthermore,

because consumers consider blueberries as healthy foods, their incorporation (either directly or through an extract) in diet may increase the commercial value of a food product while also possibly aiding in the improvement of its flavor, color or even shelf-life (e.g., through their antioxidant activity) (*Lee, Durst e Wrolstad, 2002; Szajdek e Borowska, 2008*).

1.3.2. Antidiabetic effects of blueberries

Blueberries have been the focus of several studies that aim to characterize their health-promoting properties. Many of the beneficial properties of blueberries can be related to the presence of anthocyanins, flavonoids and other phenolic compounds. These beneficial effects may result from the action of isolated compounds, or from multiple compounds acting synergistically. The various anthocyanins, phenolic acids and other bioactive compounds present in blueberries have been recognized for their ability to provide and activate cellular antioxidant defenses, scavenge free radicals, inhibit the expression of genes that induce inflammation, and thus protect against injury and cytotoxicity induced by oxidant and inflammatory agents (*Johnson e Arjmandi, 2013; Kang et al., 2015; Silva et al., 2020)*. Blueberries may have antioxidant and anti-inflammatory effects through different pathways, including inhibition of ROS production, such as hydroxyl radicals and superoxide, and the reduction of inflammatory cytokine levels, including TNF-α and IL-6, in addition to influencing other factors, such as the chemotactic protein of monocytes-1 (MCP-1). NF-kB appears to be a major pathway for the anti-inflammatory effects of blueberries (*Shi et al., 2017*). Furthermore, blueberries may possess other health benefits associated with the presence of bioactive compounds (*Nunes et al., 2021; Silva et al., 2020*), including prebiotic, antibacterial, anticancer and insulin sensitizers. *In vitro* (*Martineau et al., 2006*), *in vivo (DeFuria et al., 2009; Grace et al., 2009; Martineau et al., 2006*) and clinical (*Stull et al., 2010*) studies show that blueberry consumption exerts antidiabetic effects. (*Martineau et al., 2006*) evaluated the ability of a blueberry extract to increase the proliferation of pancreatic β cells in cell culture, suggesting a potential protection against β-cell injury, thus improving insulin sensitivity. Blueberries can protect against the development of glucose intolerance and increased glucose levels in circulation *(Roopchand et al., 2013; Vuong et al., 2007*), suppress appetite (*Molan, Lila e Mawson, 2008*), and normalize lipid markers (*Prior et al., 2010*). Blueberry

reduced the concentration of glucose, TGs and cholesterol in the blood, increased glucose uptake, glucose tolerance and fatty acid oxidation (*Shi et al., 2017*). However, the cellular mechanisms that contribute to the antidiabetic effect of blueberries are not fully elucidated. Some studies in cell culture and in animals suggest that blueberry extracts enhanced glucose uptake *(Martineau et al., 2006; Seymour et al., 2011*), while others observed that blueberry anthocyanins did not increase the uptake of glucose in the L6 myotube cell line (e.g., skeletal muscle cells) (*Roopchand et al., 2013*). However, these studies reported a reduction in glucose production in rat hepatocytes after the addition of blueberry anthocyanins. Anthocyanin rich extracts have been demonstrated to attenuate insulin sensitivity and hyperglycaemia, while a diet supplemented with blueberry powder has been shown to enhance glucose tolerance in post-menopausal mice and insulin sensitivity in humans (*Elks et al., 2015; Stull et al., 2010; Takikawa et al., 2010*). Moreover, blueberry juice and probiotics attenuated mitochondrial oxidative stress through elevation of reduced glutathione and superoxide dismutase levels while reducing ROS production in an animal model of NAFLD. The authors demonstrated that the modulation of SIRT1/PGC-1α pathway is a potential target of blueberry juice and probiotics against hepatic damage induced by NAFLD (*Ren et al., 2019*). Further animal research also showed that the attenuation of hepatic steatosis and enhancement of lipolysis following exposure of hepatic cells to blueberry polyphenols can be promoted by modulation of autophagy (*Zhuge et al., 2020*). Despite many studies pointing to the potential health benefits of blueberry-derived phytochemicals, the effectiveness of blueberry intake in prediabetes has not been established so far (*Nunes et al., 2021*).

As an attempt to fill this knowledge gap, preliminary findings from our group demonstrated that blueberry juice (BJ) supplementation in an animal model of prediabetes induced by an HFHS diet was able to attenuate glucose intolerance without preventing body weight gain (unpublished data) (Figure 9).

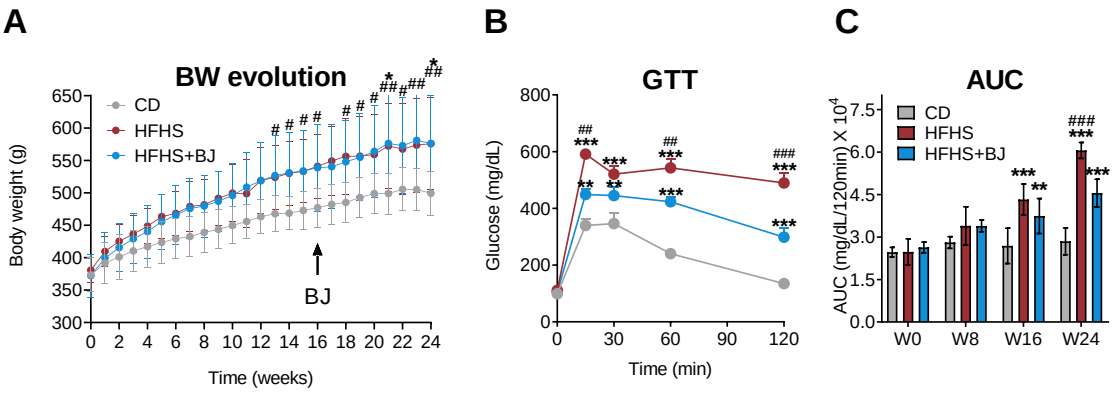

Figure 9 – Effects of blueberry juice (BJ) supplementation on the body weight evolution and glucose tolerance of rats fed a high fat-high sucrose (HFHS) diet. (**A**) Body weight (BW) evolution (grams). (**B**) Changes in blood glucose levels (mg/dl) at different time points after an intraperitoneal injection of a glucose solution (2 g/kg body weight, glucose tolerance test (GTT) assay) at week 23. (**C**) Area under the curve (AUC) of GTT assay, expressed as milligrams per deciliter per 120 minutes. CD - Chow diet; HFHS - High-fat high-sucrose; HFHS+BJ - High-fat high-sucrose plus blueberry juice; Data are presented as mean ± SEM (n = 6-8 per group); (**A**) * p<0.05 HFHS vs CD; # p<0.05 and ## p<0.01 HFHS+BJ vs CD; (**B**)(**C**) * p<0.05; ** p<0.01 and *** p<0.001 vs CD; ## p<0.01 and ### p<0.001vs HFHS+BJ

Chapter II

Aims

Aims

Although pharmacological interventions are indispensable for the management of type 2 diabetes (T2DM), lifestyle modifications are instead recommended as first-line interventions in stages where the disease is not yet fully established, such as in prediabetes, where subtle pathophysiological changes start to evolve in vital organs, including in the liver.

As highlighted above, due to its anti-inflammatory, antioxidant, hypoglycemic and hypolipidemic properties, blueberry may be a valuable nutraceutical intervention with potential to prevent the progression of prediabetes to diabetes, as inflammation, oxidative stress, insulin resistance and dyslipidemia are the main drivers of prediabetes progression and the development of its complications, namely NASH. However, the potential of blueberry to protect against prediabetes under conditions relevant for human pathogenesis and the molecular mechanisms involved remain largely unexplored. It can thus be hypothesized that a nutraceutical approach based on blueberry supplementation may exhibit hepatoprotective effects in prediabetes progression and associated complications.

Animal models of prediabetes are scarce and most are induced by diets rich in fat and/or sugar (HFHS). In most metabolic studies in animals, refined diets are compared with standard control unrefined diets (CD). However, differences in the nutritional composition (particularly phytoestrogen and fiber content) of these diets may lead to unanticipated phenotypic differences and an erroneous interpretation of results.

Accordingly, the central aims of this thesis are:

#1. To evaluate metabolic, histological and molecular alterations in an animal model of prediabetes induced by a high-fat high-sucrose diet in comparison with refined and unrefined control diets.

#2. To identify molecular mechanisms responsible for the putative protective effects of blueberry juice supplementation in Prediabetes-associated metabolic dysfunction.

Chapter III

Materials and Methods

3.1 Experimental design

3.1.1. Experimental setting I – Establishment and characterization of a diet-induced rodent model of prediabetes

Given that unhealthy diets are a key risk factor for prediabetes progression, we decided to establish a prediabetic rat model induced by diet. Considering a wide range of commercially custom diets with distinct nutritional compositions available to induce disease phenotype, in Experimental Setting I, we aimed to establish and characterize the metabolic phenotypes induced by 24 weeks (chronic) intake of an unrefined control diet (CD), a refined low-fat diet (LFD) and a refined high-fat high-sucrose diet (HFHS).

Although CD and LFD may be considered isocaloric, (3-4 kcal/g), they differ in terms of refinement process of ingredients. The nutritional composition of commercially available diets used in this study are presented in Table 2.

Table 2 – Nutritional composition of CD, LFD and HFHS diets.

Diet Composition	Chow Diet (Mucedola 4RF21)	Low Fat Diet (TD.08485)	High Fat High Sucrose Diet (TD.08811)
Energy sources (% by weight)	18.5% Protein 53.5% Carbohydrate 3.0% Fat	17.3% Protein 61.3% Carbohydrate 5.2% Fat	17.3% Protein 47.6% Carbohydrate 23.2% Fat
Energy (Kcal/g)	Protein: 0.74 Carbohydrate: 2.14 Fat: 0.27 Total: 3.15	Protein: 0.69 Carbohydrate: 2.45 Fat: 0.47 Total: 3.6	Protein: 0.69 Carbohydrate: 2.09 Fat: 1.90 Total: 4.7
Proteins (% by weight)			
Casein	---	19.5	19.5
L-Cysteine	---	---	0.3
DL-Methionine	---	0.3	---
Carbohydrates (% by weight)			
Starch	53.5	---	---
Corn Starch	---	43.3	5.7
Maltodextrin	---	10.0	6.0
Cellulose	---	5.0	5.0
Sucrose	---	12.0	34.0
Lipids (% by weight)			
Soybean oil	3.0	1.3	2.0
Anhydrous Milkfat	---	3.7	21.0
Vitamin/Mineral Mixes (% by weight)			
Mineral Mix, AIN-93G-MX (94046)	---	---	4.3
Mineral Mix, AIN-76 (170915)	---	3.5	---
Vitamin Mix, AIN-93-VX (94047)	---	---	1.9

Vitamin Mix, Teklad (40060)	---	1.0	---
Fatty acids (% by weight)			
Saturated fatty acids	22	---	61
Mono-unsaturated fatty acids	22	---	30
Poly-unsaturated fatty acids	56	---	9

In this experimental setting, twenty-two male Wistar rats (13-week-old) were used. Rats were housed two *per* cage in the vivarium of the Coimbra Institute for Clinical and Biomedical Research (iCBR), Faculty of Medicine, University of Coimbra, under controlled environmental conditions with temperature 22 ±1°C, 50-60% relative humidity, a 12h-light 12-h dark cycle, with tap water and food supplied *ad libitum*. Animal experiments were conducted according to the National and European Communities Council Directives of Animal Care and received approval (#9/2018) by the local (iCBR) Animal Welfare Body (ORBEA).

After 2 weeks of acclimation period, rats were randomly divided into three groups and assigned to the following dietary regimens: CD (n=6); LFD (n=8) and HFHS (n=8). Body weight (BW) was monitored weekly and food and fluid intake twice per week.

The design of Experimental Setting I is shown in Figure 10.

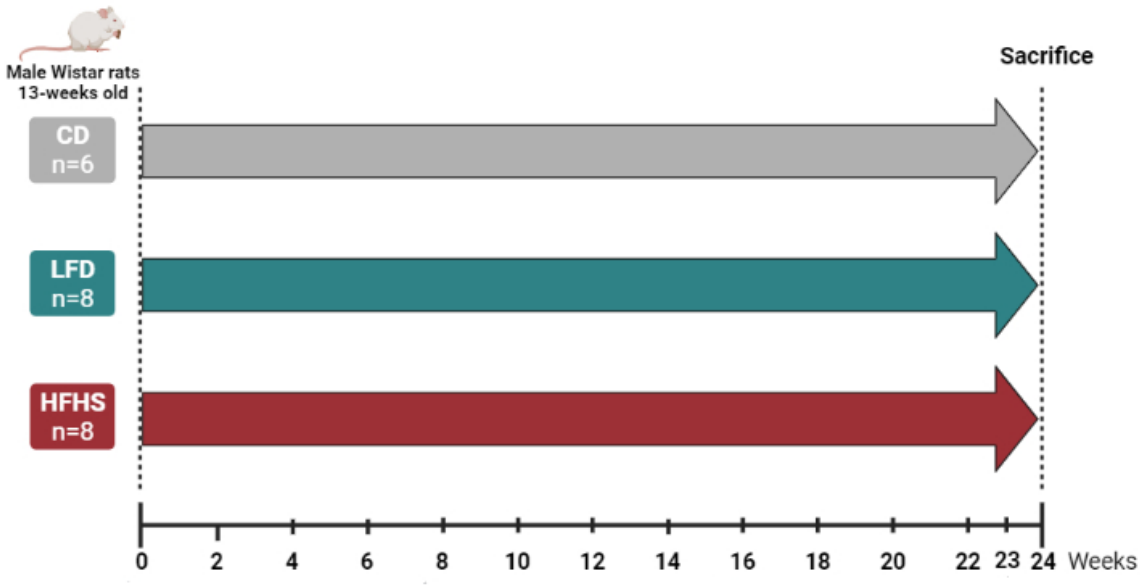

Figure 10 – Experimental Setting I. CD - Chow diet; LFD - Low-fat diet; HFHS - High-fat high-sucrose.

3.1.2. Experimental setting II - Putative protective effects of blueberry juice in HFHS-induced metabolic dysfunction

To assess the putative protective effects of blueberry juice (BJ), a fourth experimental group composed of eight male Wistar rats (13-week-old), were fed the HFHS diet and supplemented with BJ from week 16 until the end of the protocol (24 weeks). At this time point (week 16), the early metabolic impairments were found in rats fed HFHS diet. In order to comply with the 3Rs Reduction Principle, the multiple evaluations carried out in the fourth experimental group (HFHS+BJ) were compared with the CD and HFHS experimental groups from the Experimental setting I.

Blueberries (*Vaccinium corymbosum* L. from Cultivar: Liberty) were supplied by the Cooperativa Agropecuária dos Agricultores de Mangualde (COAPE) and stored at -80°C until processing. In order to obtain a juice and to ensure that blueberry pulp, seeds and peel were all consumed, blueberries were weighed and blended with drinking water. To ensure that 25g of blueberry *per* kg of rat's BW were daily consumed, the volume of drinking water was adjusted.

Animals were monitored weekly for BW and food consumption as in Experimental Setting I. Until week 16, fluid (water) intake was measured twice a week and after that point onward, fluid (BJ) intake was measured daily (Figure 11).

Animal experiments were conducted according to the National and European Communities Council Directives of Animal Care and received approval (9/2018) by the local (iCBR) Animal Welfare Body (ORBEA).

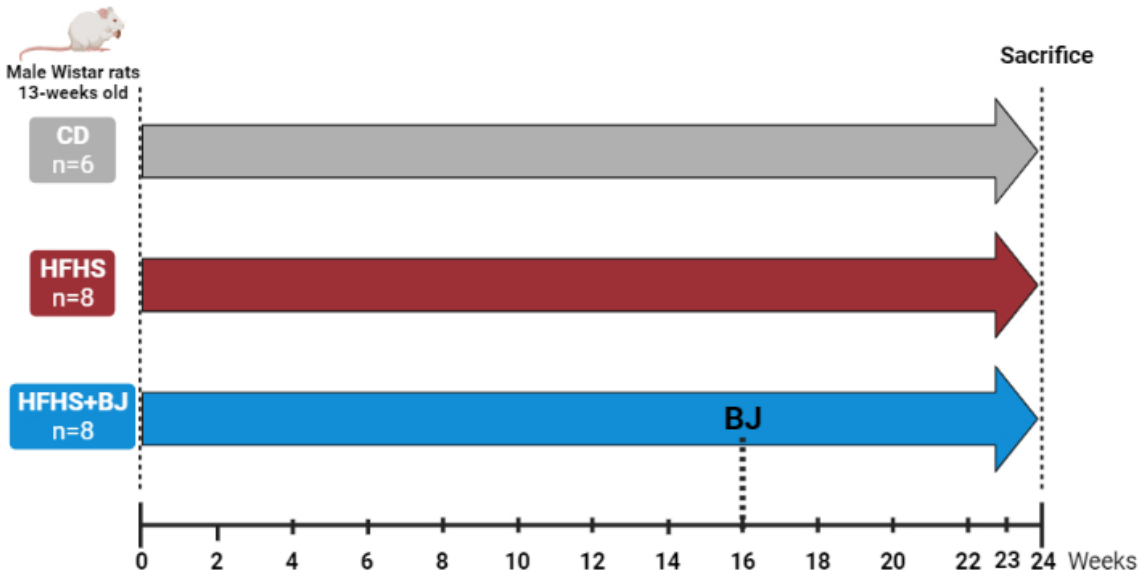

Figure 11 – Experimental Setting II. CD - Chow diet; HFHS - High fat high sucrose; HFHS+BJ - High-fat high-sucrose plus blueberry juice.

3.2 Tissue collection

At week 24, animals were anaesthetized in a chamber saturated with isoflurane (IsoFlo®, Abbott) followed by intraperitoneal injection of 150 mg/kg of ketamine chloride (1 g/mL; Imalgene®) in chlorpromazine 2.5% (Largactil®). Blood was immediately collected through heart puncture to serum tubes (BD Vacutainer SST II 47 Advance) and then centrifuged at 3500 rpm for 15 minutes (4 °C) and stored at -20 °C. Upon sacrifice, rats were transcardially perfused with ice-cold PBS (1x) and epididymal white adipose tissue (eWAT), interscapular brown adipose tissue (iBAT) and liver were isolated, washed and weighed. Samples were divided into 3 sections for distinct purposes: a first section was kept in a neutral buffered formalin solution to be used for histological analysis; for fluorescence microscopy, samples were placed in OCT CryoMatrix (6769006, ThermoScientific); for protein analysis, samples were snap frozen in liquid nitrogen. Samples were stored at -80 °C for later analysis.

3.3 Liver, eWAT and iBAT histomorphology

3.3.1. Hematoxylin and Eosin (H&E) staining

Liver, eWAT and iBAT samples were formalin-fixed and embedded in paraffin wax. Cryosections (5 µm) from each block were deparaffinized in xylene and hydrated to a decrescent series of ethanol until distilled water. Afterwards, tissue sections were immersed in hematoxylin stain Solution, Gill 1 (Sigma Aldrich, Saint Louis, MO, USA) for 2 minutes and washed in tap water. Then, they were counterstained with 0.5% aqueous eosin (Sigma Aldrich; MO, USA) for 30 seconds and then dehydrated, cleared, and mounted.

3.3.2. Image analysis and data quantification

3.3.2.1. Liver

Two high-resolution images per animal, 5 to 7 animals per group, imaged at 40x magnification were captured under the same parameter settings for hepatocyte morphometry analysis using a Zeiss microscope Mod. Axioplan 332 2 (Zeiss, Jena, Germany). To evaluate the liver morphology and the degree of steatosis, approximately 200 hepatocytes *per* animal were analyzed using the FIJI (ImageJ v2) plugin Cell Counter.

Each acquired image was imported to ImageJ and analyzed individually. The number of total hepatocytes in each image was calculated by manually counting all the visible hepatocyte nuclei. The total number of hepatocytes with microvesicular steatosis morphology (microsteatotic hepatocytes - distended hepatocytes with foamy appearing cytoplasm; small lipid vesicles less than 1 µm in diameter that may or may not be discernible, with typically centrally located nucleus *(Kristiansen et al., 2019; Sethunath et al., 2018*) and the total number of hepatocytes with macrovesicular steatosis morphology (macrosteatotic hepatocytes - cells with large fat vacuoles and peripherally displaced nucleus (*Kristiansen et al., 2019; Sethunath et al., 2018*) were also manually counted separately as showed in **Annex 1**.

To assess the total steatosis score (%), the ratio between the total number of steatotic hepatocytes (number of hepatocytes with microvesicular steatosis plus the

number of hepatocytes with macrovesicular steatosis) and the total number of hepatocytes times 100 were calculated.

$$Total\ Steatosis\ Score\ (\%) = \frac{(Microsteatotic + Macrosteatotic\ hepatocytes)}{total\ number\ of\ hepatocytes} \times 100$$

To assess the microvesicular steatosis score (%), the ratio between the number of hepatocytes with microvesicular steatosis and the total number of hepatocytes times 100 were calculated.

$$Microsteatosis\ Score\ (\%) = \frac{Microsteatotic\ hepatocytes}{Total\ number\ of\ hepatocytes} \times 100$$

To assess the macrovesicular steatosis score (%), the ratio between the number of hepatocytes with macrovesicular steatosis and the total number of hepatocytes times 100 were calculated.

$$Macrosteatosis\ Score\ (\%) = \frac{Macrosteatotic\ hepatocytes}{Total\ number\ of\ hepatocytes} \times 100$$

3.3.2.2. Epididymal white adipose tissue

Five to ten high-resolution images *per* animal, 5 to 8 animals *per* group, were captured by a Axiocam 105 color (Zeiss, Jenna, Germany) camera under the same parameter settings for adipocyte morphometry analysis, using a Zeiss microscope Mod. Axioplan 332 2 (Zeiss, Jenna, Germany). Slides were imaged at 10x magnification. To quantify the mean adipocyte area, mean adipocyte diameter, adipocyte area distribution and adipocyte diameter distribution, an average of 512 adipocytes *per* animal were analyzed using the FIJI (ImageJ v2) plugin Adiposoft.

Images were captured and imported into ImageJ software. To obtain a more precise quantification of adipocyte dimensions (area and diameter), the contrast between the adipocyte outlines (cytoplasmatic membrane) and the inner side of the adipocytes (lipid droplet) should be maximized to facilitate the recognition of the adipocyte outlines by the ImageJ plugin Adiposoft. To achieve this, each image acquired was splitted in three channels (red, green, blue). Of the three channels, the green-channel enabled a higher

contrast. As a consequence, only the green-channel image of each image acquired was saved through a screenshot for further analysis. All the green-channel images saved were imported again, one by one, into ImageJ software and analyzed by the ImageJ plugin Adiposoft as showed in **Annex 2**.

To ensure that only adipocytes were counted, each image was manually inspected. The artifacts and broken adipocytes unduly analyzed and accounted by the software were recorded and eliminated manually from the output-excel sheet that contained the diameter and area data of all the adipocytes in each image.

Mean adipocyte area and mean adipocyte diameter were calculated for each animal and for each group. In order to calculate the adipocyte area and diameter distribution, classes were defined for each parameter and all the data acquired by the software were assigned into the defined classes.

3.3.2.3. Interscapular brown adipose tissue

Five high-resolution images *per* animal (5 to 8 animals *per* group) were captured by Axiocam 105 Color (Zeiss, Jenna, Germany) camera under the same parameter settings for adipocyte morphometry analysis, using a Zeiss microscope Mod. Axioplan 332 2 (Zeiss, Jenna, Germany). Slides were imaged at 20x magnification. FIJI (ImageJ v2) plugin Adiposoft was used to quantify the mean lipid droplet area and distribution.

iBAT images were captured and imported into ImageJ software as described in the eWAT section. Similarly, iBAT images were analyzed by the ImageJ plugin Adiposoft and showed in **Annex 2**.

Mean lipid droplet area was calculated for each animal and for each group. In order to calculate the lipid droplet area distribution, classes were defined for each parameter and all the data acquired by the software analysis were assigned into the defined classes.

3.4 Quantification of hepatic triglyceride levels

Triglyceride (TG) content of liver samples was measured by an enzymatic colorimetric assay using a commercial kit (Ref.1155010, Triglycerides MR, Cromatest ®, Linear Chemicals, Barcelona, Spain). Briefly, 50 mg of frozen tissue was homogenized in 1 mL of isopropanol. The homogenate was sonicated and then centrifuged at 3000 rpm for

5 minutes at 4°C, and the supernatant was analyzed following the manufacturer's instructions.

3.5 Quantification of hepatic ALT and AST levels

Serum aspartate aminotransferase (AST) and alanine aminotransferase (ALT) concentrations were determined through automatic validated methods and equipment (Hitachi 717 analyzer, Roche Diagnostics GMBH, Mannheim, Germany), as previously described in (Madureira *et al.*, 2016).

3.6 Protein expression by western blotting

3.6.1. Protein extraction and quantification

Approximately 100 mg of frozen iBAT and 50 mg of liver were homogenized by mechanical dissociation using a handheld tissue homogenizer in cold (4°C) radioimmunoprecipitation assay (RIPA) lysis buffer containing 50 mM Tris-HCl (pH 8.0), 150 mM NaCl, 0.1% (v/v) sodium dodecyl sulphate (SDS), 1% (v/v) Triton X-100, 5 mM ethylenediaminetetraacetic acid (EDTA), supplemented with 1 pill of protease inhibitor cocktail (11836170001, Roche Diagnostics GmbH, Germany), 1 mM of phenylmethylsulfonyl fluoride (PMSF) and 1 mM of sodium orthovanadate (Na_3VO_4). iBAT and liver homogenates were left on ice for 1 hour, and vortexed every 15 min. iBAT sample lysates were centrifuged for 15 min at 15,000 rpm at 4°C and liver sample lysates were centrifuged for 20 min at 13,000 rpm at 4°C. After centrifugation, the supernatant fractions (corresponding to total extracts) were collected and centrifuged again. This process was repeated three times in iBAT samples and twice in liver samples. After the last centrifugation, the supernatant fractions were collected and one aliquot (20 µL) of protein lysate of each sample was used to determine protein concentration. The remaining samples were stored at -80°C.

The protein concentration was determined using the bicinchoninic acid (BCA) assay (Pierce™ BCA Protein Assay Kit, Pierce Biotechnology, Rockfor, IL, USA) using bovine albumin serum (BSA) standard solutions. Absorbance reading was performed at 570 nm using BioTek Synergy™ HT and Gen5 Data Analysis Software after the plate was

incubated for 30 min at 37°C. Total protein concentration in each sample was calculated considering the calibration curve obtained through the BCA assay.

3.6.2. Polyacrylamide gel electrophoresis and immunodetection

iBAT and liver protein samples were denatured with sample buffer (6x) (0.35 M Tris-HCl (pH 6.8), 30% (v/v) glycerol, 0.65 M dithiothreitol (DTT), 10% (w/v) SDS, 0.03% (w/v) bromophenol blue) for 5 minutes at 95°C.

For the western blot analysis, 10 μg of iBAT protein and 30 μg of liver protein were loaded *per* lane and separated by electrophoresis on a 10-15% SDS-polyacrylamide gel electrophoresis (SDS-PAGE) in running buffer (125 mM Tris-base, 950 mM glycine and 0.5% (w/v) SDS, pH 8.3) at 70 volts for 20 minutes and then at 100 volts for 150-210 minutes until the prestained marker (A8889.0500 Protein Marker VI (10-245), AppliChem GMbH, Germany) reached the desired level depending on the molecular weight of the target protein, at 4°C. After electrophoresis and activation of 0.45 μm polyvinylidene difluoride (PVDF) membranes (Amersham™ Hybond™, GE Healthcare, USA), proteins were electro-transferred in transfer buffer (100 mM N-cyclohexyl-3-aminopropanesulfonic acid (CAPS), pH 11) at 100 volts, for 90 minutes at 4°C. Following protein transfer, Ponceau S staining (GB21.0500, GRiSP) was performed to assess the transfer quality and efficiency and to confirm equal amount of protein in each well. Distaining was performed with 0.1M NaOH and Tris-buffered saline (150 mM NaCl, 20 mM Tris-HCl, pH 7,6) containing 0.1 % (v/v) Tween-20 (TBS-T) wash. Thereafter, in order to prevent non-specific binding, membranes were blocked in 5 % (w/v) non-fat dry milk in TBS-T or 5 % (w/v) bovine serum albumin (BSA) in TBS-T (Table 3), for 1 hour with agitation, at room temperature.

Membranes were then incubated with primary antibodies (Table 3), overnight at 4°C with agitation. All the primary antibodies used in this thesis were subjected to validation as shown in **Annex 3**.

After incubation, membranes were washed 3 times with TBS-T, for 10 minutes and incubated with adequate secondary antibodies (Table 3), for 1 hour at room temperature with agitation. After secondary antibody incubation, membranes were washed again 3 times with TBS-T for 10 minutes. At the end of this procedure, the intensity of the bands

was detected by enhanced chemiluminescence substrate (ECL) (R-03031-D25, R-03025-D25 WesternBright™ ECL and Peroxide, advansta, USA) and (R-03027-C50, R-03025-C50, WesternBright™ Sirius and Peroxide, advansta, USA) in the ImageQuant™ LAS500 (GE Healthcare Life Sciences).

To ensure equal protein loading, membranes were reincubated with antibodies against housekeeping proteins, including β-tubulin, β-actin, glyceraldehyde 3-phosphate dehydrogenase (GAPDH), and calnexin (Table 3). Results were normalized against these loading proteins and expressed as percent of control. Optical density of the bands was quantified by densitometry, using Image J Software.

Table 3 – Primary and secondary antibodies used in Western blot analysis and experimental conditions.

Antibody	Reference	Source	Animal Origin	Blocking Solution	Solution	Dilution	Incubation Time
Primary Antibodies							
Anti-PGC1α	Ab191838	Abcam	Rabbit	5% Milk in TBS-T	1% Milk in TBS-T	1:1500	48h
Anti-UCP1	Ab23841	Abcam	Rabbit	5% Milk in TBS-T	1% Milk in TBS-T	1:1500	24h
Anti-eIF2α	5324	Cell Signaling Technology	Rabbit	5% BSA in TBS-T	1% BSA in TBS-T	1:2000	24 h
Anti-Phospho-eIF2α	3398	Cell Signaling Technology	Rabbit	5% BSA in TBS-T	1% BSA in TBS-T	1:2000	24 h
Anti-IRE1α	3294	Cell Signaling Technology	Rabbit	5% BSA in TBS-T	1% BSA in TBS-T	1:1000	24 h
Anti-CHOP	2895	Cell Signaling Technology	Mouse	5% BSA in TBS-T	1% BSA in TBS-T	1:1000	24 h
Anti-SQSTM1 /p62	5114S	Cell Signaling Technology	Rabbit	5% BSA in TBS-T	1% BSA in TBS-T	1:1000	24 h
Anti-LC3	PA1-16931	Thermo Fisher Scientific	Rabbit	5% BSA in TBS-T	1% BSA in TBS-T	1:1000	24 h
Loading Controls							
Anti-β-tubulin	T7816	Sigma-Aldrich	Mouse	5% BSA in TBS-T	1% BSA in TBS-T	1:1000	24 h
Anti-β-actin	AB0145-200	Sicgen	Goat	5% BSA in TBS-T	1% BSA in TBS-T	1:1000	24 h
Anti-Calnexin	AB0041-200	Sicgen	Goat	5% BSA in TBS-T	1% BSA in TBS-T	1:1000	24 h
Anti-GAPDH	AB0049-200	Sicgen	Goat	5% BSA in TBS-T	1% BSA in TBS-T	1:5000	24 h
Secondary Antibodies							
Anti-Rabbit	R-0572-050	Advansta	Goat		Same as respective antibody	1:10000	1 h
Anti-Mouse	R-05071-500	Advansta	Goat		Same as respective antibody	1:10000	1 h
Anti-Goat	AB1011-1000	Sicgen	Goat		Same as respective antibody	1:10000	1 h

3.7 Data processing and statistical analysis

Results were expressed as mean ± standard error of the mean (SEM) using GraphPad Prism software, version 6.01 (GraphPad Software, Inc., La Jolla, CA, USA).

The normality of the distributions was determined through the Kolmogorov-Smirnov test. To analyze the differences between groups, when a normal distribution was observed, the parametric one-way ANOVA followed by Tukey Post´hoc test for multiple comparisons was used. Differences between two groups were analyzed using Unpaired t-test with Welch´s correction. Differences were considered statistically significant at p values < 0.05.

Chapter IV

Results

4.1. Establishment of a Diet-induced Rodent Model of Prediabetes: Impact of Control Diet composition

4.1.1. Changes in body weight and fat mass

The study of prediabetes has been hampered by the scarcity of animal models, most of which are induced by refined diets with high content of fat and/or sugar (*Preguiça et al., 2020*). To characterize the metabolic phenotype of a diet-induced animal model of prediabetes and the role of the nutritional composition of control diets, 13-week-old male Wistar rats were fed for 24 weeks with a prediabetes-inducing refined high-fat high-sucrose (HFHS) diet, in comparison with a nutrient-matched refined low-fat diet (LFD) and a standard unrefined control diet (CD) (Figure 12A). The detailed composition of the diets is presented in Table 2. The HFHS diet-fed group showed a significant increase in total body weight (BW) gain over the 24-week study period in comparison with the CD-fed group (~55% increase, $p<0.05$), while no significant differences were found between the LFD-fed group and the other two groups (Figure 12B). In line with an increase in BW gain, rats fed a HFHS diet also showed increased visceral epididymal white adipose tissue (eWAT) mass when compared with rats fed a CD (~150% increase, $p<0.001$) (Figure 12C). Interestingly, the LFD group displayed a significantly higher eWAT mass in comparison to CD-fed animals (~90% increase, $p<0.05$) (Figure 12C). Similar results were found when the eWAT mass was normalized to the BW (Figure 12D).

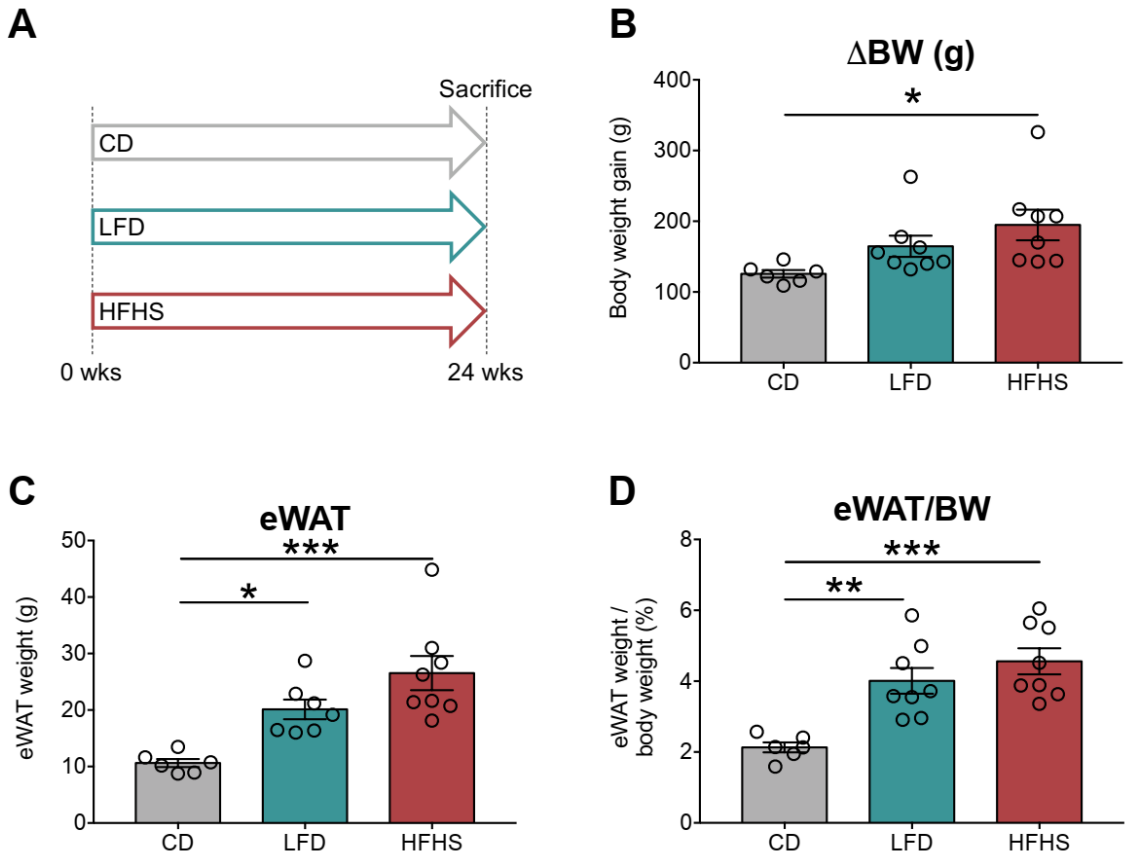

Figure 12 – Body weight gain and epididymal white adipose tissue (eWAT) mass in response to 24 weeks of CD, LFD and HFHS diets in male Wistar rats. (**A**) Schematic diagram of the experimental design of the study. (**B**) Total body weight (BW) gain (g) at the end of the experiment. (**C**) eWAT weight (g). (**D**) eWAT weight expressed as a percentage of BW. Data are presented as mean ± SEM (n = 6-8 per group); *p<0.05; **p<0.01 and ***p<0.001, using a one-way ANOVA followed by a Tukey multiple comparison test.

4.1.2. Histological analysis of eWAT

Given our observations that HFHS feeding induced BW gain and adiposity, and that adipose tissue expansion may result from increased adipocyte size (hypertrophy) and/or adipocyte number (hyperplasia), we next used hematoxylin and eosin (H&E) staining of eWAT sections to evaluate changes in adipocyte size, diameter, and number in rats fed a CD, a LFD or a HFHS diet.

Histological analysis revealed an increase in adipocyte size in HFHS and LFD groups in comparison with the CD group (Figure 13A). To further explore these changes, we performed a more refined quantitative histological analysis to determine cell size (area and diameter) (Figure 13B and C). Both HFHS and LFD groups presented a significant increase in the mean adipocyte area and diameter when compared to the CD group. Analysis of the frequency distribution of adipocyte area and diameter across the tissue

depot showed that both LFD- and HFHS-fed rats presented higher proportions of large adipocytes in combination with lower proportions of small adipocytes, when compared to CD-fed rats (Figure 13D and E). To further characterize the morphological changes of epididymal white adipocytes, we quantified the number of adipocytes per section for each animal and found a negative correlation between adipocyte number per section and eWAT mass ($r=0.593$; $p=0.0074$) (Figure 13F).

In combination, these findings indicate that the expansion of visceral adipose tissue observed in a HFHS diet-induced model of prediabetes and also in rats fed a control LFD results mainly from adipocyte hypertrophy rather than adipocyte hyperplasia.

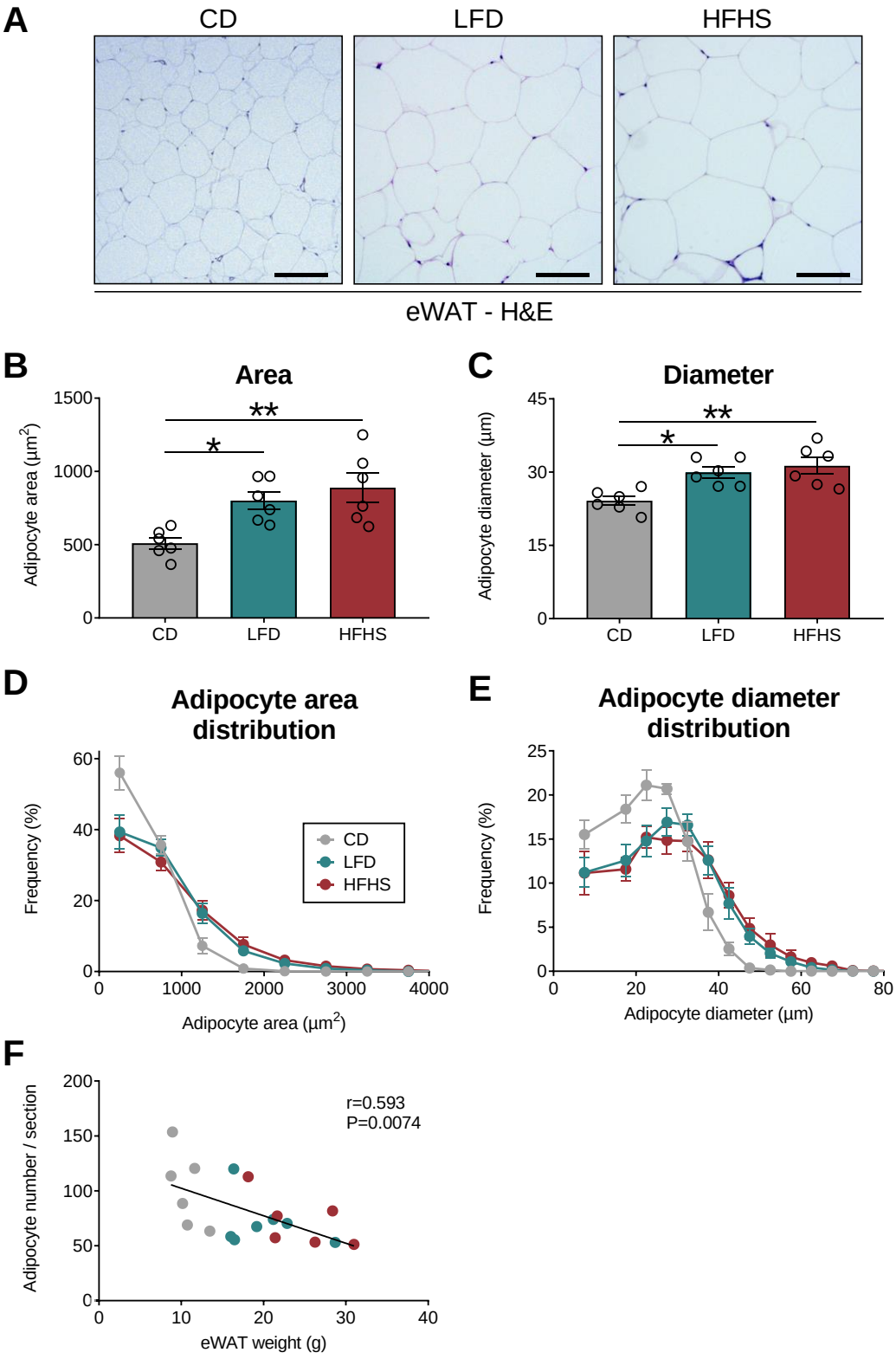

Figure 13 – Analysis of the morphology and dimensions of adipocytes in eWAT. (**A**) Representative images of hematoxylin and eosin (H&E) staining of epididymal white adipose tissue (eWAT) sections showing adipocytes at 10× magnification (scale bar = 100 µm). (**B**) Mean adipocyte area (µm²) and (**C**) mean adipocyte diameter (µm) in eWAT sections. **(D, E)** Frequency distribution (%) of adipocyte area (**D**) and diameter (**E**). (**F**) Negative linear correlation between the number of adipocytes per section and eWAT weight. Data are presented as mean ± SEM (n = 6-7 per group); *p<0.05 and **p<0.01, using a one-way ANOVA followed by a Tukey multiple comparison test.

4.1.3. Histological analysis and thermogenic markers in iBAT

4.1.3.1. Histological analysis of iBAT

Like WAT, BAT is also a highly active metabolic tissue playing a key role in energy homeostasis. However, while the major function of WAT is energy storage, BAT is primarily involved in energy expenditure. When BAT is activated, for example in response to an HFD, the rate of fatty acid oxidation increases, leading to heat production *(Cernea e Dobreanu, 2013; Czaja, 2016; Mousovich-Neto et al., 2019*). Considering that our findings indicate a positive energy balance manifested through increased BW gain and adiposity, and previous results indicate that the HFHS group had higher caloric intake (~492 kcal/week) when compared to the LFD and CD groups (~420 and ~460 kcal/week, respectively), to investigate whether the weight gain observed in the HFHS diet-induced prediabetes model is due to increased caloric intake, decreased energy expenditure or both, we examined changes in lipid droplet size and number and the expression of key thermogenic markers in iBAT of rats fed with CD, LFD and HFHS diets.

Although no significant differences were found between groups with respect to iBAT weight (Figure 14A), the visual inspection of the H&E-stained iBAT sections suggested a decrease in lipid droplet size of brown adipocytes in the LFD and HFHS groups compared to the CD group (Figure 14B). To quantify these differences, the number of lipid droplets per section and the mean lipid droplet area for each animal were determined (Figure 3C and D). The number of lipid droplets increased significantly in the HFHS group in comparison with LFD (~51% increase, $p<0.05$) and CD groups (~74% increase, $p<0.01$) (Figure 14C). Consistent with that, we also found a decrease in the lipid droplet areas of HFHS-fed rats in comparison with CD-fed rats (~57% decrease, $p<0.001$) and a trend towards a decrease when compared to the LFD-fed rats ($p=0.057$) (Figure 3D), suggesting an inverse relationship between lipid droplet number and lipid droplet area and supporting the previous qualitative results (Figure 14B).

We next explored the frequency distribution of adipocyte lipid droplet areas among the three groups (Figure 14E). The frequency distribution of lipid droplet areas of iBAT adipocytes showed that HFHS increases the generation of smaller lipid droplets (<10 μm^2) while reducing the number of larger lipid droplets (>20 μm^2). The opposite pattern was seen in the CD group, whereas an intermediate pattern was seen in the LFD group.

When lipid droplet area was plotted as a function of iBAT weight, we found three distinct populations corresponding to each dietary group (Figure 14F). While CD-fed animals displayed a slight variation in iBAT weight along with high dispersion of adipocyte lipid droplet areas, HFHS-fed animals displayed a substantial variation in iBAT weight along with a slight variation in adipocyte lipid droplet areas. Consistently, LFD-fed animals displayed an intermediate populational distribution between the HFHS and the CD-fed animals.

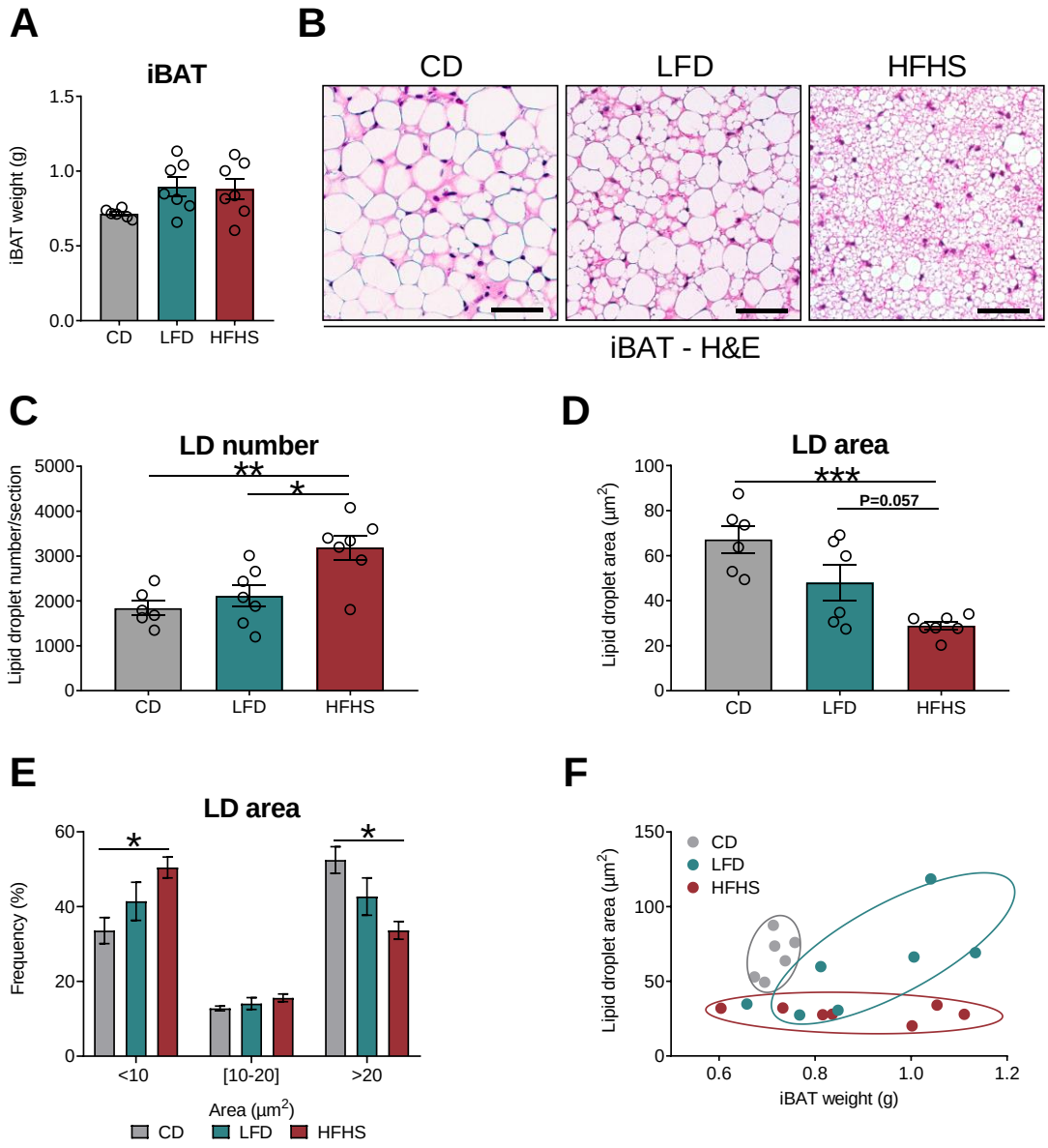

Figure 14 – Interscapular brown adipose tissue (iBAT) mass and adipocyte dimensions. (**A**) iBAT weight (g). (**B**) Representative images of hematoxylin and eosin (H&E) staining of iBAT sections showing adipocyte lipid droplets (LD) at 20× magnification (scale bar = 50 µm). (**C**) Mean LD number per section. (**D**) Mean LD area (µm²). (**E**) Frequency distribution (%) of LD areas. (**F**) Scatter plot of the mean LD area in function of iBAT weight. Data are presented as mean ± SEM (n = 6-8 per group); *p<0.05; **p<0.01 and ***p<0.001, using a one-way ANOVA followed by a Tukey multiple comparison test.

4.1.3.2. Expression of thermogenesis markers in iBAT

To further investigate if the positive energy balance in HFHS-fed rats was also caused by a decrease in energy expenditure, we evaluated thermogenesis activation through the measurement of protein expression levels of uncoupling protein-1 (UCP-1) and peroxisome proliferator-activated receptor-gamma coactivator-1alpha (PGC-1α) by Western blotting (Figure 15A and B). We found an increase in UCP-1 expression in HFHS diet-fed rats in comparison with both the LFD- (~123% increase, $p<0.01$) and CD-fed group (~163% increase, $p<0.0001$) (Figure 15A). Similarly, protein expression of PGC-1α was also significantly increased in the HFHS group in comparison with the LFD group (~191% increase, $p<0.05$) and the CD group (~188% increase, $p<0.05$) (Figure 15B), suggesting an increase in energy expenditure through thermogenesis activation in the HFHS-fed rats.

Together, these results suggest that the increase in BW and adiposity observed in the HFHS diet-induced model of prediabetes was probably due to increased caloric intake.

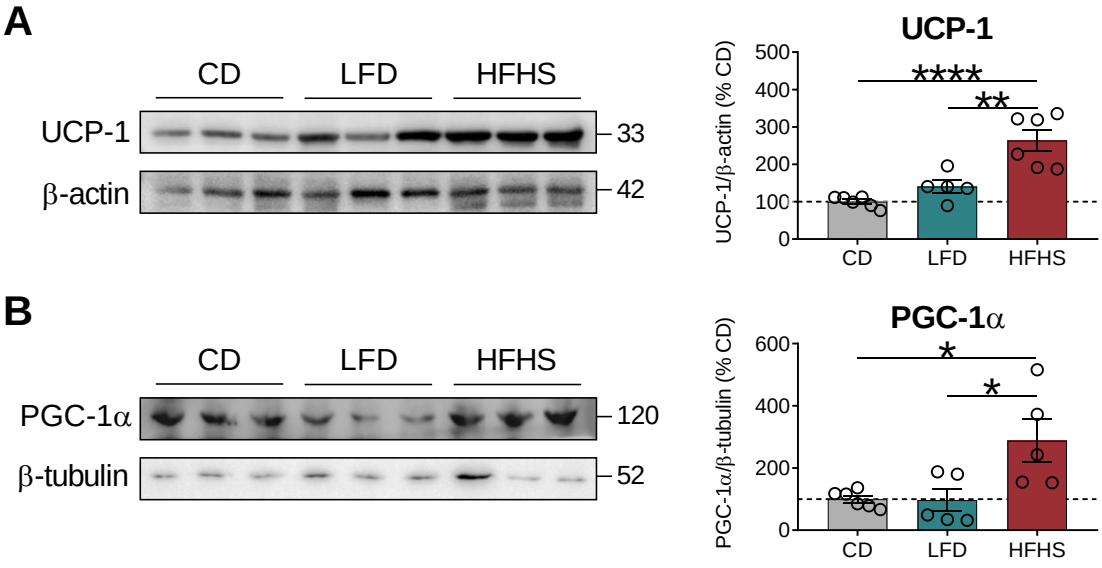

Figure 15 – Thermogenesis markers in interscapular brown adipose tissue (iBAT). (**A**) Immunoblotting of thermogenesis markers UCP-1 and (**B**) PGC-1α and their protein levels in iBAT protein extracts from rats fed with CD, LFD and HFHS diets for 24 weeks. Data are presented as mean ± SEM (n = 5-6 rats per group); *p<0.05; **p<0.01 and ****p<0.0001, using a one-way ANOVA followed by a Tukey multiple comparison test.

4.1.4. Analysis of hepatic phenotype

We next focused our analysis on the liver, another metabolic organ that plays a key role in the regulation of glucose and lipid metabolism *(Cotrozzi et al., 1997; Nguyen et al., 2008*) and is known to accumulate lipids derived from adipose tissue lipolysis and diet *(Malone e Hansen, 2019; Smith e Adams, 2011*).

No significant differences in the absolute liver weights were found between groups (Figure 16A), despite a significant decrease in the relative liver weight was noted in the HFHS group (~21% decrease, $p<0.01$) (Figure 16B). There was also no difference between groups in the plasma levels of alanine transaminase (ALT) and aspartate aminotransferase (AST), two commonly used markers of liver injury (Figure 16C and D). However, we found a reduction in serum triglyceride levels of HFHS-fed rats when compared to LFD-fed rats (~38% decrease, $p<0.05$) (Figure 16E), in parallel with an increase in hepatic triglyceride content when compared to both CD- (409% increase, $p<0.001$) and LFD-fed rats (~74% increase, $p<0.05$) (Figure 16F). LFD-fed animals also displayed an increase in the hepatic triglyceride content in comparison to CD-fed animals (~86% increase, $p<0.05$ using student´s t-test) (Figure 16F), compatible with a fatty liver phenotype.

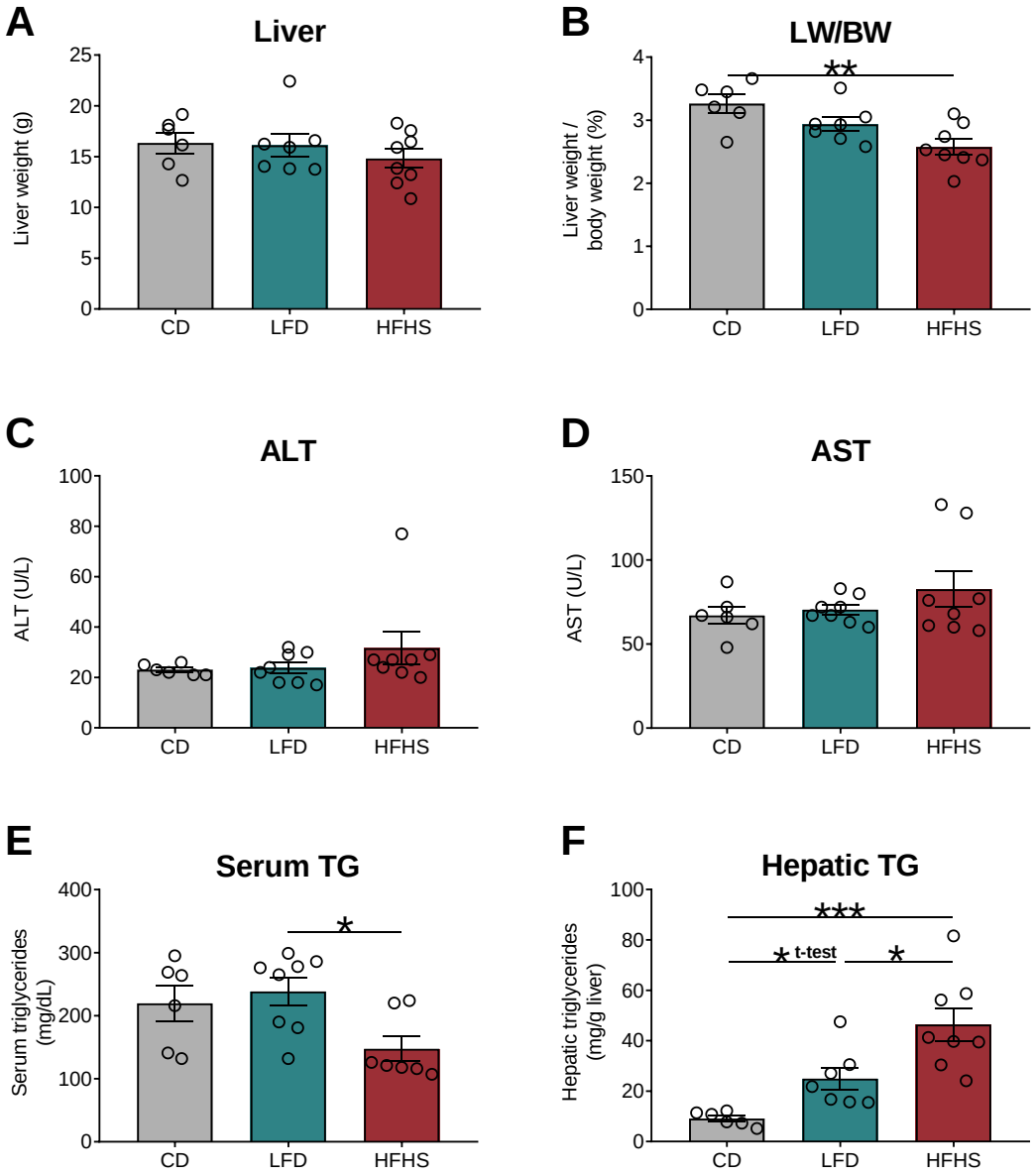

Figure 16 – Liver weight, hepatic enzymes and triglyceride content. (**A**) Absolute liver weight (LW, g). (**B**) LW expressed as a percentage of body weight (LW/BW). (**C**) Plasma levels (U/L) of alanine transaminase (ALT) (**D**) and aspartate transaminase (AST). (**E**) Serum and (**F**) hepatic triglyceride (TG) content. Data are presented as mean ± SEM (n = 6-8 per group); *p<0.05; **p<0.01 and ***p<0.001, using a one-way ANOVA followed by a Tukey multiple comparison test; unpaired t-test using Welch´s correction was used to compare differences between CD- and LFD-fed group.

4.1.5. Histological assessment and quantification of hepatic steatosis

To evaluate the presence of hepatic steatosis, we performed hematoxylin and eosin (H&E) staining, which detects steatosis by the presence of vacuoles. While CD-fed rats exhibit normal liver morphology, both LFD- and HFHS-fed rats exhibit vacuoles in the H&E-stained liver sections.

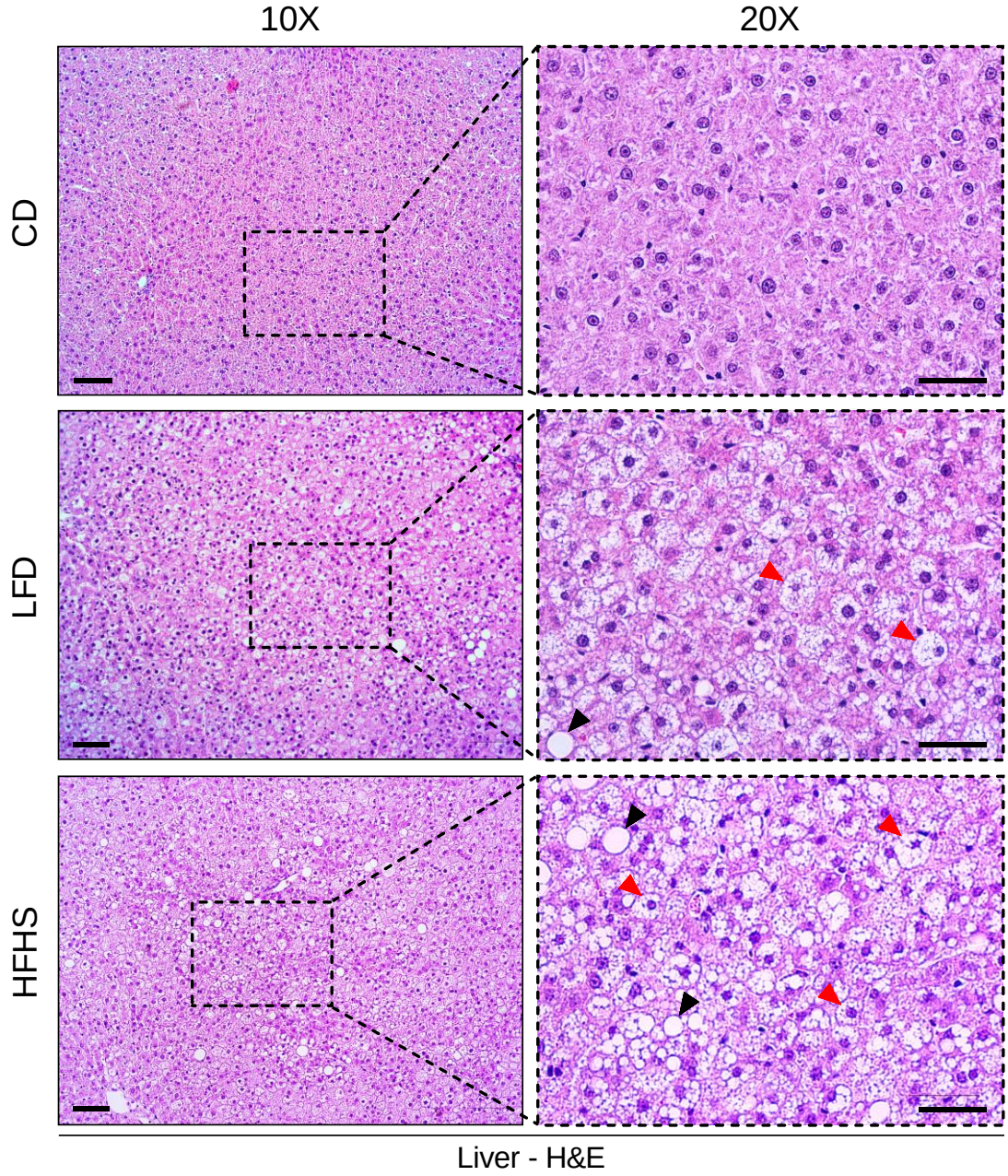

Figure 17 – Histological evaluation of hepatic steatosis. Representative images of hematoxylin and eosin (H&E) staining of liver sections from male Wistar rats after 24 weeks of different dietary regimens showing normal (nonsteatotic), microsteatotic (red arrows) and macrosteatotic (black arrows) hepatocytes at 10× and 20× magnification (scale bar = 100 μm).

We then quantified the total hepatic steatosis score by calculating the percentage of steatotic hepatocytes using H&E-stained liver sections. We found an increase in total steatosis score in the HFHS group when compared to the LFD (~53% increase, $p<0.05$) and CD-fed groups (~495% increase, $p<0.0001$). Surprisingly, LFD-fed animals also presented an increase in the percentage of steatotic hepatocytes when compared to CD-fed animals (~289% increase, $p<0.01$) (Figure 18A).

To further quantify the distinct steatotic phenotypes present in each group, we assessed the macrosteatosis and microsteatosis scores by calculating the percentage of macrosteatotic and microsteatotic hepatocytes, respectively. No differences in the macrosteatosis score were found between groups; however, marked differences were observed in the microsteatosis score, similarly to the total steatosis score (Figure 18B).

Therefore, our findings showed that microsteatosis is the main contributor to overall steatosis, the predominant phenotype developed in the prediabetic animal model.

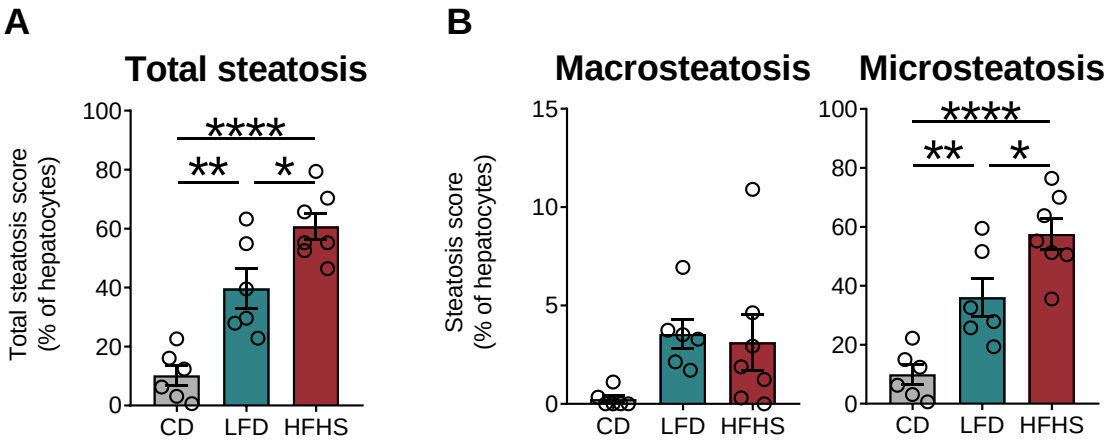

Figure 18 – Quantitative assessment of hepatic steatosis. (**A**) Total steatosis score expressed as a percentage of hepatocytes. (**B**) Macrosteatosis and microsteatosis scores are expressed as a percentage of hepatocytes. Data are presented as mean ± SEM (n = 6-7 per group); *p<0.05; **p<0.01 and ****p<0.0001, using a one-way ANOVA followed by a Tukey multiple comparison test.

4.1.6. Molecular mechanisms associated with hepatic steatosis

4.1.6.1. Endoplasmic reticulum stress response

The endoplasmic reticulum (ER) stress is upregulated in hepatic steatosis (*Zhang et al., 2014)* and is now widely accepted as both a cause and a consequence of this pathology *(Henkel, 2018*). Furthermore, HFD-fed Wistar rats showed increased ER stress markers *(Kandeil et al., 2019*). Thus, ER stress may be an underlying mechanism of hepatic lipid overload. Therefore, we analyzed protein expression of ER stress markers by Western blotting in livers from all groups (Figure 19).

Inositol-requiring enzyme 1 (IRE-1) expression was increased in both the HFHS and LFD groups when compared to the CD-fed group (~236% increase, $p<0.01$; ~178% increase, $p<0.05$) (Figure 19A). The expression of the total and phosphorylated forms of eukaryotic initiation factor 2-α (eIF2α and P-eIF2α) was increased in the HFHS group when compared to the CD group (~40% increase, $p<0.05$; ~120% increase, $p<0.01$). Moreover, P-eIF2α expression was also increased in the LFD group in comparison to the CD group (~91% increase, $p<0.05$) (Figure 19B and C). Finally, C/EBP homologous protein (CHOP) expression was increased in HFHS-fed rats in comparison with LFD (~64% increase, $p<0.001$) and CD groups (~95% increase, $p<0.0001$) (Figure 19D).

These results indicate that the ER stress response is upregulated in the prediabetic animal model, suggesting an adaptive response to hepatic lipid accumulation.

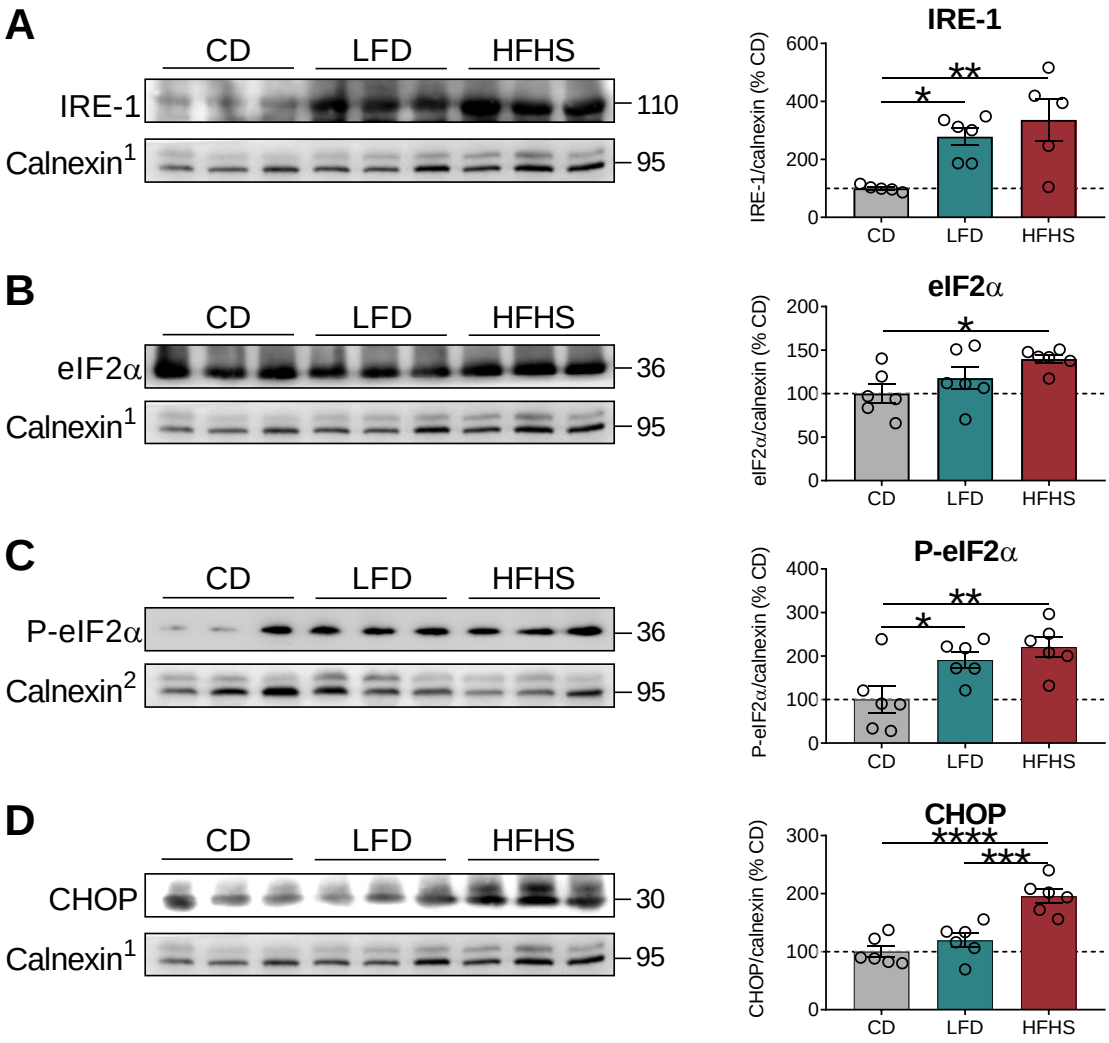

Figure 19 – Endoplasmic reticulum (ER) stress markers in the liver. (**A**) Representative Western blot images of ER stress markers IRE-1, (**B**) eIF2α, (**C**) P-eIF2α and (**D**) CHOP, and their protein levels in liver protein extracts from rats fed with CD, LFD and HFHS diets for 24 weeks. Data are presented as mean ± SEM (n = 6 rats per group); *p<0.05; **p<0.01; ***p<0.001 and ****p<0.0001, using a one-way ANOVA followed by a Tukey multiple comparison test.

4.1.6.2. Autophagy

Impaired autophagy has been implicated in the pathogenesis of hepatic steatosis. For example, the autophagic function is decreased in the liver under conditions that predispose to the development of NASH (*Czaja, 2016*) and in insulin resistance states *(Álvarez-Mercado et al., 2021*). Furthermore, studies in hepatic tissue and murine hepatocytes demonstrated that autophagy inhibition promoted increased triglyceride storage (*Ezquerro et al., 2016*).

To investigate the possibility that impaired autophagy may underlie hepatic lipid accumulation, we analyzed the expression of three classical autophagic markers, namely microtubule-associated protein 1 light chain 3-II (LC3-II), Beclin and protein p62/sequestosome-1 (p62/SQSTM1), by Western blotting (Figure 20). Although no statistically significant difference in LC3-II expression was found between groups, there was a trend towards an increase in the HFHS-fed group when compared to the CD group (~196% increase, p=0.063) (Figure 20B). We observed a significant increase in Beclin expression in HFHS-fed rats when compared with the LFD (~128% increase, p<0.01) and CD group (~181% increase, p<0.01) (Figure 20C). No statistical significance was found in the expression levels of p62, however, a clear trend towards increase was observed in the HFHS and LFD groups in comparison with the CD-fed group (~116% increase, p=0.067; ~119% increase, p=0.060) (Figure 20D).

Our findings suggest that autophagy is upregulated in both prediabetic animal model and LFD-fed rats.

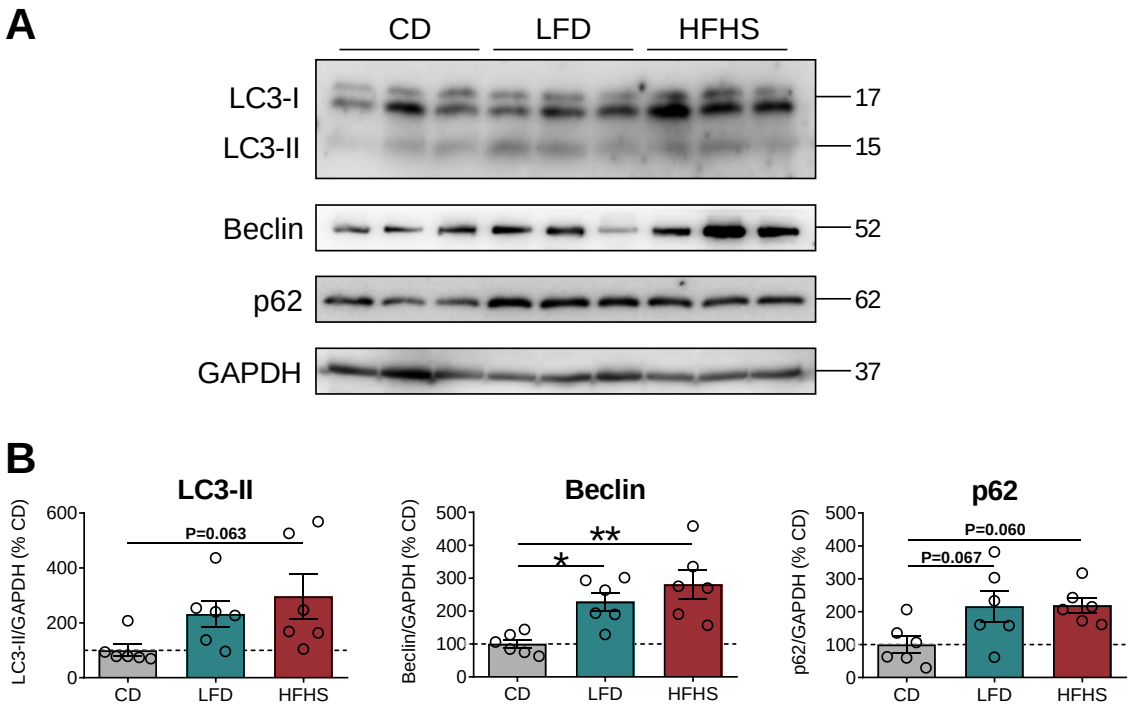

Figure 20 – Autophagy markers in the liver. (**A**) Representative Western blot images of autophagy markers LC3-II, Beclin and p62, and, (**B**) corresponding protein levels in liver protein extracts from male Wistar rats fed with CD, LFD and HFHS diets for 24 weeks. Data are presented as mean ± SEM (n = 6 rats per group); *p<0.05 and **p<0.01, using a one-way ANOVA followed by a Tukey multiple comparison test.

Overall, the metabolic, histological, and molecular alterations induced by the refined HFHS diet are compatible with a prediabetic phenotype. Unexpectedly, when compared to the most commonly used standard unrefined CD, the nutrient-matched refined LFD also induced several metabolic and molecular abnormalities (Table 4).

Table 4 – Summary of results of experimental setting I.

	CD	LFD	HFHS
Body Weight Gain	=	=	↑
Adiposity	=	↑	↑
Glucose Intolerance	=	↑	↑↑
BAT activation	=	=	↑
Hepatic Steatosis	=	↑	↑↑
ER stress	=	↑	↑↑
Autophagy	=	↑	↑↑

= – Unaltered; ↑ – Mild; ↑↑ – Exacerbated.

4.2. Effects of Blueberry Juice Supplementation on HFHS Diet-induced Prediabetes

4.2.1. Effects of BJ on body and eWAT weight

The importance of a healthy diet to prevent prediabetes progression is now well established, being nutraceutical approaches preferable to pharmacological interventions in a prediabetic state. Given that blueberries have antioxidant, anti-inflammatory and hypoglycemic properties, it might be an important nutraceutical tool in the prevention of prediabetes development to overt T2DM (*Nunes et al., 2021*). However, despite the beneficial effects of blueberries, the molecular mechanisms underlying their beneficial effects remain largely unknown.

After investigating histological and molecular alterations in a diet-induced animal model of prediabetes, we next evaluated the ability of BJ supplementation (25g/Kg/day) to attenuate HFHS-induced alterations, and its effects on molecular mechanisms associated with hepatic steatosis. Considering the metabolic and molecular abnormalities induced by the LFD, we selected the CD as a control group for the subsequent analysis.

Male Wistar rats (8-weeks-old) were provided three dietary regimens for 24 weeks: the standard control diet (CD), the prediabetes-inducing diet (HFHS), and the HFHS diet supplemented with BJ from week 16 to 24 (HFHS+BJ) (Figure 21A). Total body weight gain over the 24-week study period was significantly increased in both HFHS diet-fed group and in the group supplemented with BJ when compared with the CD-fed group (~62% increase, $p<0.05$; ~55% increase, $p<0.05$, respectively) (Figure 21B). In line with an increase in body weight gain, rats fed with HFHS diet and rats supplemented with BJ also showed an increase in the visceral eWAT mass when compared with CD-fed rats (~151% increase, $p<0.001$; ~129% increase, $p<0.01$) (Figure 21C). Similar results were found when the eWAT weight was normalized to the body weight (Figure 21D).

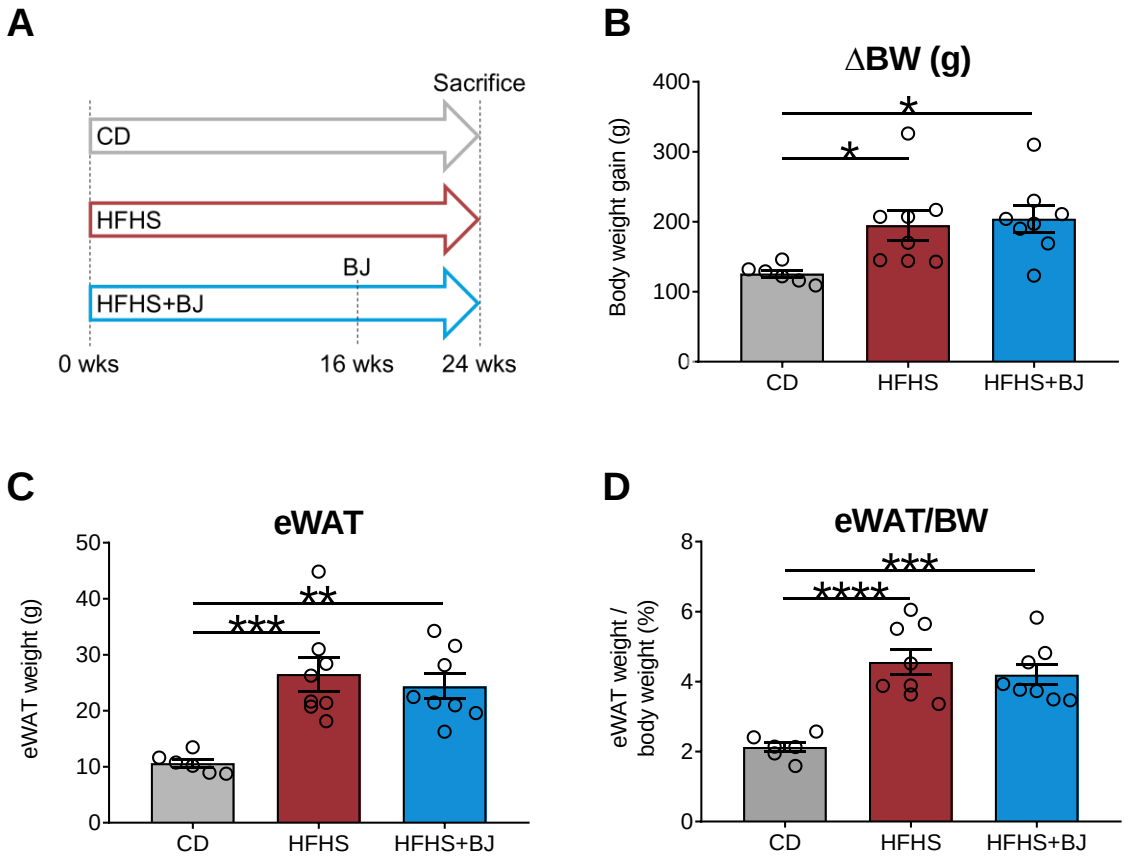

Figure 21 – Body weight gain and epididymal white adipose tissue (eWAT) mass in response to 24 weeks of CD, HFHS and HFHS diet supplemented with blueberry juice (BJ) for 8 weeks. (**A**) Schematic diagram of the experimental design of the study. (**B**) Total body weight gain (g) at the end of the experiment. (**C**) eWAT weight (g). (**D**) eWAT weight is expressed as a percentage of body weight (BW). Data are presented as mean ± SEM (n = 6-8 per group); *p<0.05; **p<0.01; ***p<0.001 and ****p<0.0001, using a one-way ANOVA followed by a Tukey multiple comparison test.

4.2.2. Histological effects of BJ on eWAT

Although our findings suggest that BJ supplementation was unable to attenuate body weight gain and adiposity induced by the HFHS diet, we next used H&E staining of eWAT sections to evaluate changes in adipocyte size, diameter and number per section of rats fed with CD, HFHS and HFHS+BJ. Histological analysis revealed no differences in adipocyte size between the HFHS and the HFHS+BJ groups, although both groups displayed increased adipocyte dimensions in comparison to the CD-fed group (Figure 22A).

To further explore these differences, we performed a more refined quantitative histological analysis by assessing cell size parameters (area and diameter). Corroborating the qualitative analysis of H&E histology, both HFHS and HFHS+BJ groups presented a significant increase in the mean adipocyte area and diameter when compared to the CD group (Figure 22B and C).

We then explored the frequency distribution of adipocyte area and diameter across the tissue depot. This analysis showed that both HFHS and HFHS+BJ-fed rats presented higher proportions of large adipocytes together with lower proportions of small adipocytes when compared to CD-fed rats (Figure 22D and E).

To further characterize the effects of BJ supplementation on the morphological changes of epididymal white adipocytes induced by the HFHS diet, we quantified the number of adipocytes per section for each animal and found a negative correlation between adipocyte number per section and eWAT mass ($r=0.661$; $p=0.0015$) (Figure 11F). The overlapping pattern between the HFHS and HFHS+BJ groups in comparison with the CD group suggests that the increase in eWAT weight in both groups was mainly due to adipocyte hypertrophy rather than adipocyte hyperplasia, and that 8 weeks of BJ supplementation was unable to attenuate changes in adipose tissue morphology induced by HFHS diet.

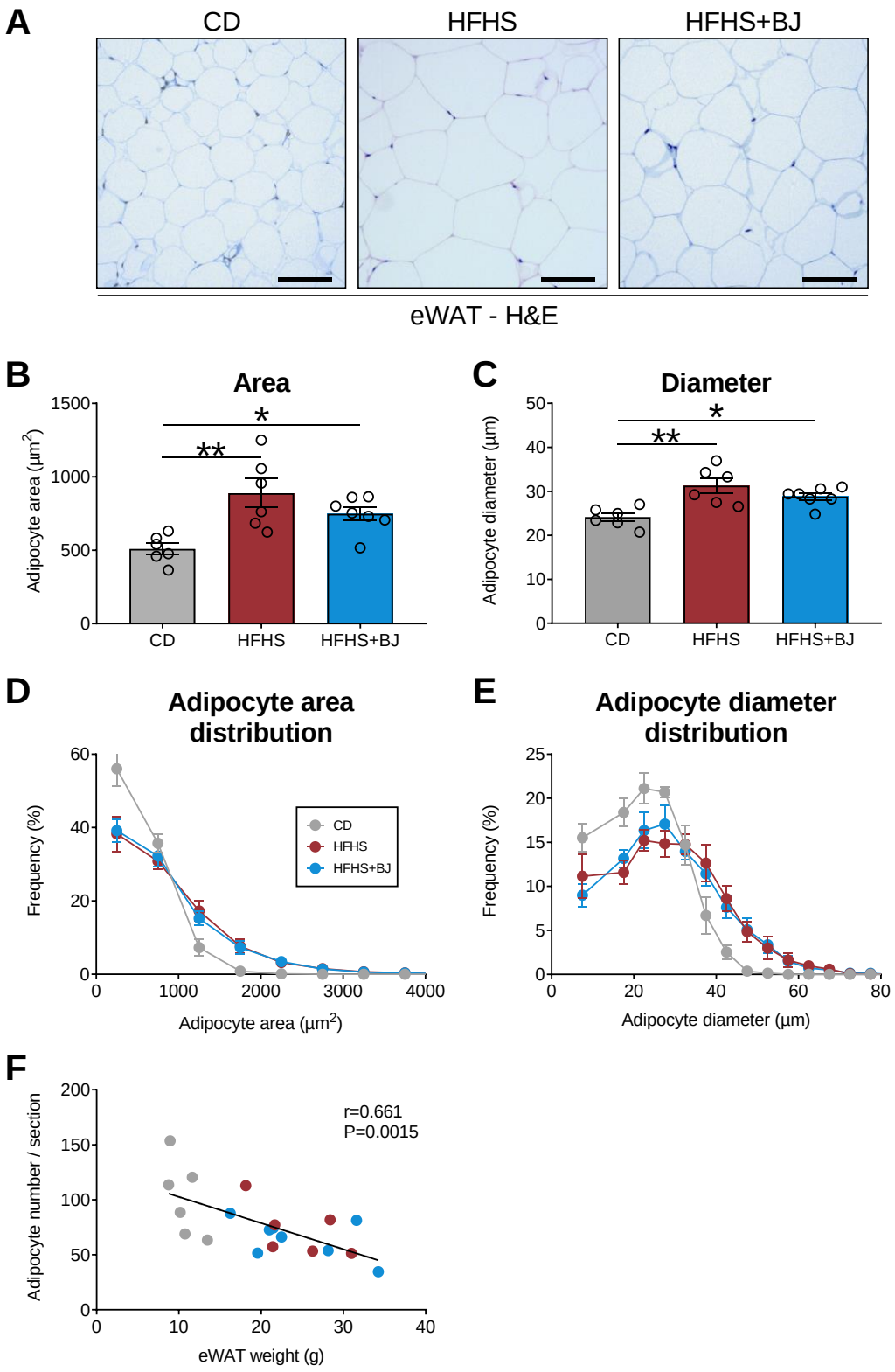

Figure 22 – Analysis of the morphology and dimensions of adipocytes in eWAT. (**A**) Representative images of hematoxylin and eosin (H&E) staining of epididymal white adipose tissue (eWAT) sections showing adipocytes at 10× magnification (scale bar = 100 µm). (**B**) Mean adipocyte area (µm2) and (**C**) mean adipocyte diameter (µm) in eWAT sections. (**D**, **E**) Frequency distribution (%) of adipocyte area (**D**) and diameter (**E**). (**F**) Negative linear correlation between the number of adipocytes per section and eWAT weight. Data are presented as mean ± SEM (n = 6-7 per group); *p<0.05 and **p<0.01, using a one-way ANOVA followed by a Tukey multiple comparison test.

4.2.3. Effects of BJ on iBAT morphology and thermogenic markers

4.2.3.1. BJ attenuates HFHS-associated histological alterations in iBAT

To understand the cause of the higher body weight and body fat in HFHS and HFHS+BJ rats, we examined changes in lipid droplet size and number, and also studied the expression of key thermogenic markers, in iBAT of rats fed with CD, HFHS and HFHS+BJ.

iBAT weight was increased in the HFHS+BJ group when compared to the CD-fed group (~32% increase, $p<0.05$) (Figure 23A). We then examined H&E-stained iBAT sections. As described above (Figure 14B), the lipid droplet area of the HFHS group is smaller than that of the CD group. Surprisingly, we observed that the group supplemented with BJ displayed an increase in lipid droplet size when compared to the HFHS group (Figure 23B).

To further evaluate the effects of BJ consumption on iBAT morphology and quantify these differences, the number of lipid droplets per section and the mean lipid droplet area for each animal were determined. The HFHS-fed group presented an increase in the number of lipid droplets per section in comparison to both the CD- and HFHS+BJ-fed groups (~82% increase, $p<0.0001$; ~60% increase, $p<0.01$) (Figure 23C), in parallel with a decrease in the mean area of the lipid droplets (~58% decrease, $p<0.0001$; ~53% decrease, $p<0,001$) (Figure 23D).

We explored the frequency distribution of iBAT adipocyte lipid droplet areas among the three groups (Figure 23E) and observed that the HFHS+BJ group displayed fewer small lipid droplets (<10 μm^2) and more large lipid droplets (>20 μm^2) than the HFHS group. In contrast, when compared to the CD group, the HFHS+BJ group displayed more small lipid droplets (<10 μm^2) and fewer large lipid droplets (>20 μm^2).

We then plot the lipid droplet area as a function of iBAT weight and found three distinct populational distributions corresponding to each distinct dietary regimen (Figure 23F). HFHS+BJ-fed animals displayed greater dispersion in both lipid droplet area and iBAT weight than the HFHS- and CD-fed rats, presenting an intermediate distribution between the two groups.

Taken together, these results demonstrate that BJ supplementation may have attenuated morphological alterations in iBAT induced by HFHS diet.

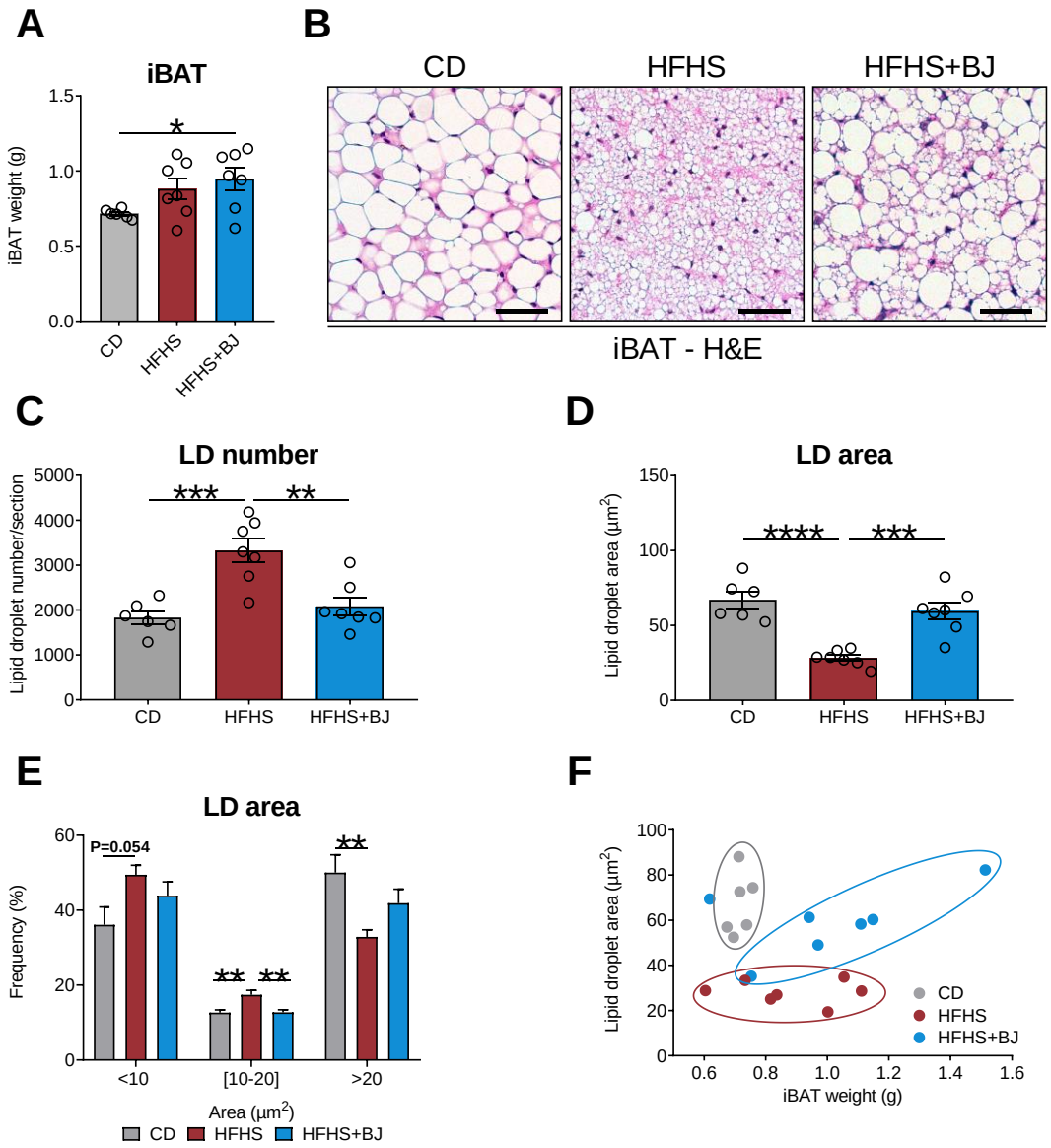

Figure 23 – Interscapular brown adipose tissue (iBAT) mass and adipocyte dimensions. (**A**) iBAT weight (g). (**B**) Representative images of hematoxylin and eosin (H&E) staining of iBAT sections showing adipocyte lipid droplets (LD) at 20× magnification (scale bar = 50 µm). (**C**) Mean LD number per section. (**D**) Mean LD area (µm²). (**E**) Frequency distribution (%) of LD areas. (**F**) Scatter plot of the mean LD Area in function of iBAT weight. Data are presented as mean ± SEM (n = 6-8 per group); *p<0.05; **p<0.01; ***p<0.001 and ****p<0.0001, using a one-way ANOVA followed by a Tukey multiple comparison test.

4.2.3.2. BJ decreases HFHS-induced expression of thermogenic markers in iBAT

To investigate if BJ supplementation affected thermogenesis activation in the prediabetic model, we measured the protein expression levels of the thermogenic markers UCP-1 and PGC-1α in iBAT by Western blotting (Figure 24A and B).

When compared to CD, the HFHS-fed group displayed an increase in the expression of both UCP-1 and PGC-1α (~94% increase, $p<0.001$; ~80% increase, $p<0.01$). Surprisingly, BJ supplementation led to a decrease in UCP-1 expression, when compared to the HFHS group (~28% decrease, $p<0.05$), suggesting that BJ may have suppressed iBAT thermogenesis, thus, contributing to the positive energy balance reflected as an increase in body weight gain and adiposity.

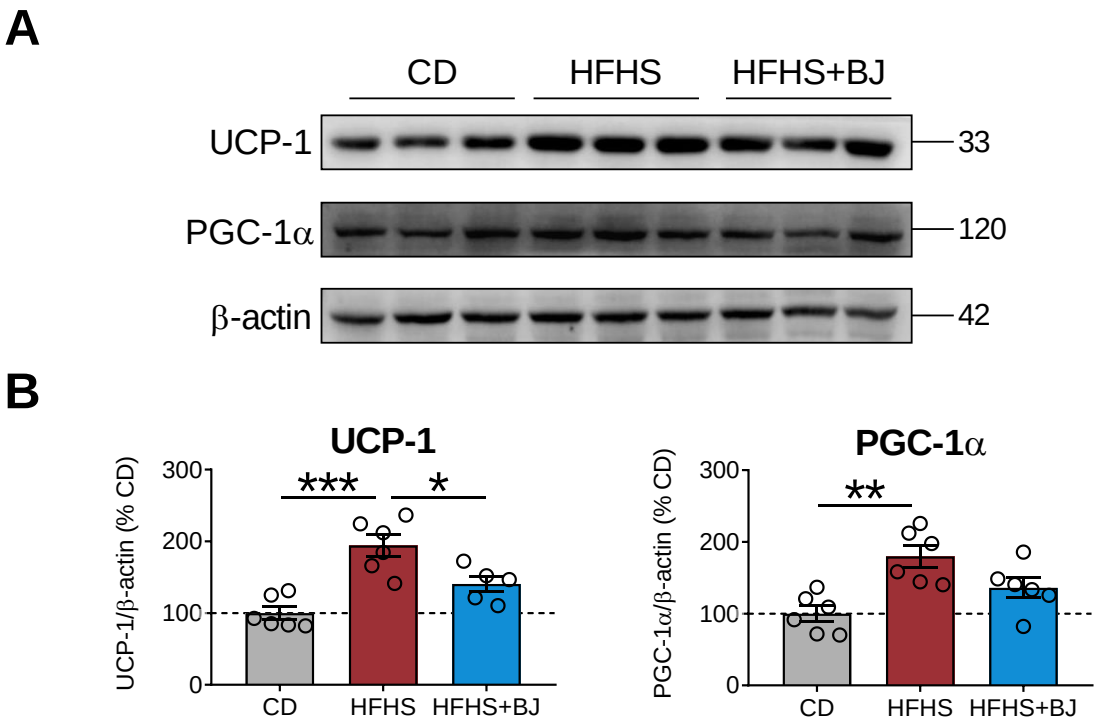

Figure 24 – Thermogenic markers in interscapular brown adipose tissue (iBAT). (**A**) Immunoblotting of thermogenic markers UCP-1 and (**B**) PGC-1α, and their corresponding protein levels in iBAT protein extracts from male Wistar rats fed with CD and HFHS diet for 24 weeks and HFHS diet supplemented with BJ for 8 weeks. Data are presented as mean ± SEM (n = 5-6 rats per group); *p<0.05; **p<0.01 and ***p<0.001, using a one-way ANOVA followed by a Tukey multiple comparison test.

4.2.4. Effects of BJ on HFHS-induced hepatic steatosis

Because HFHS diet induced hepatic steatosis and BJ has been shown to play a crucial role in liver protection in rats (*Wang et al., 2010, 2013*), we next investigated the putative hepatoprotective effects of 8-week BJ supplementation in a rat model of prediabetes.

No significant differences were observed in liver weight among groups (Figure 25A). However, the relative liver weight was decreased in both the HFHS and HFHS+BJ groups in comparison with the CD group (~21% decrease, $p<0.01$; ~13% decrease, $p<0.05$, respectively) (Figure 25B). The plasma levels of liver injury markers ALT and AST were not different between groups (Figure 25C and D). However, we found an increase in serum triglyceride levels in the group supplemented with BJ when compared to HFHS-fed rats (~654% increase, $p<0.05$) (Figure 25E), in parallel with an increase in hepatic triglyceride content when compared to both CD- (~822% increase, $p<0.0001$) and HFHS-fed rats (~409% increase, $p<0.05$) (Figure 25F).

Thus, 8 weeks of BJ supplementation aggravated the fatty liver phenotype induced by the HFHS diet.

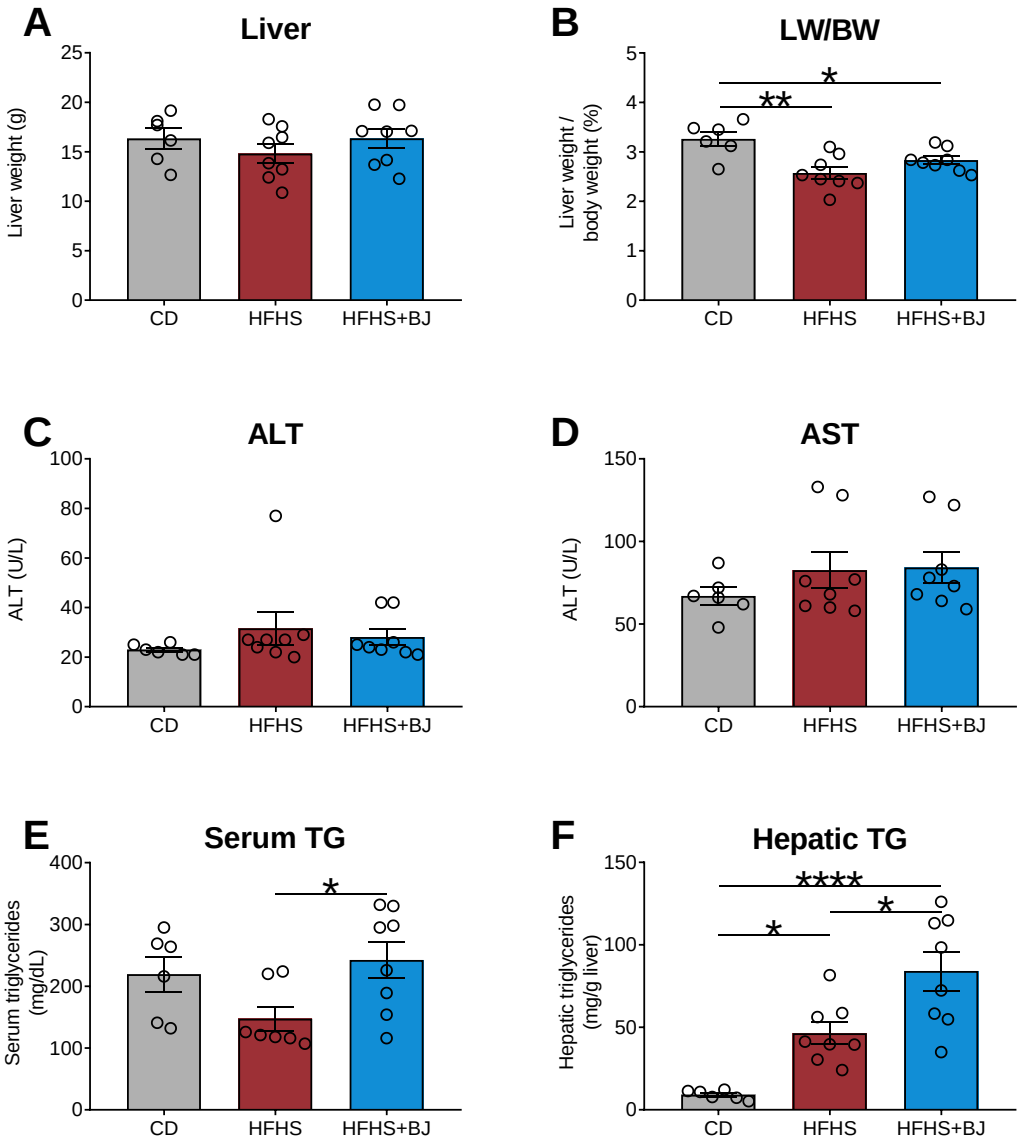

Figure 25 – Liver weight, hepatic enzymes and triglyceride content. (**A**) Absolute liver weight (LW, g). (**B**) LW is expressed as a percentage of body weight (LW/BW). (**C**) Plasma levels (U/L) of alanine transaminase (ALT) (**D**) and aspartate transaminase (AST). (**E**) Serum and (**F**) hepatic triglyceride (TG) content. Data are presented as mean ± SEM (n = 6-8 per group); *p<0.05; **p<0.01 and ****p<0.0001, using a one-way ANOVA followed by a Tukey multiple comparison test.

4.2.5. BJ aggravates the microsteatotic phenotype

To further characterize the effects of BJ supplementation on the hepatic phenotype induced by the HFHS diet, we performed a qualitative assessment of hepatic steatosis in H&E-stained liver sections, which revealed the presence of vacuoles in both HFHS- and HFHS+BJ-fed rats.

These qualitative results suggest the presence of fatty liver phenotype in both groups and that hepatic steatosis was not attenuated by BJ supplementation.

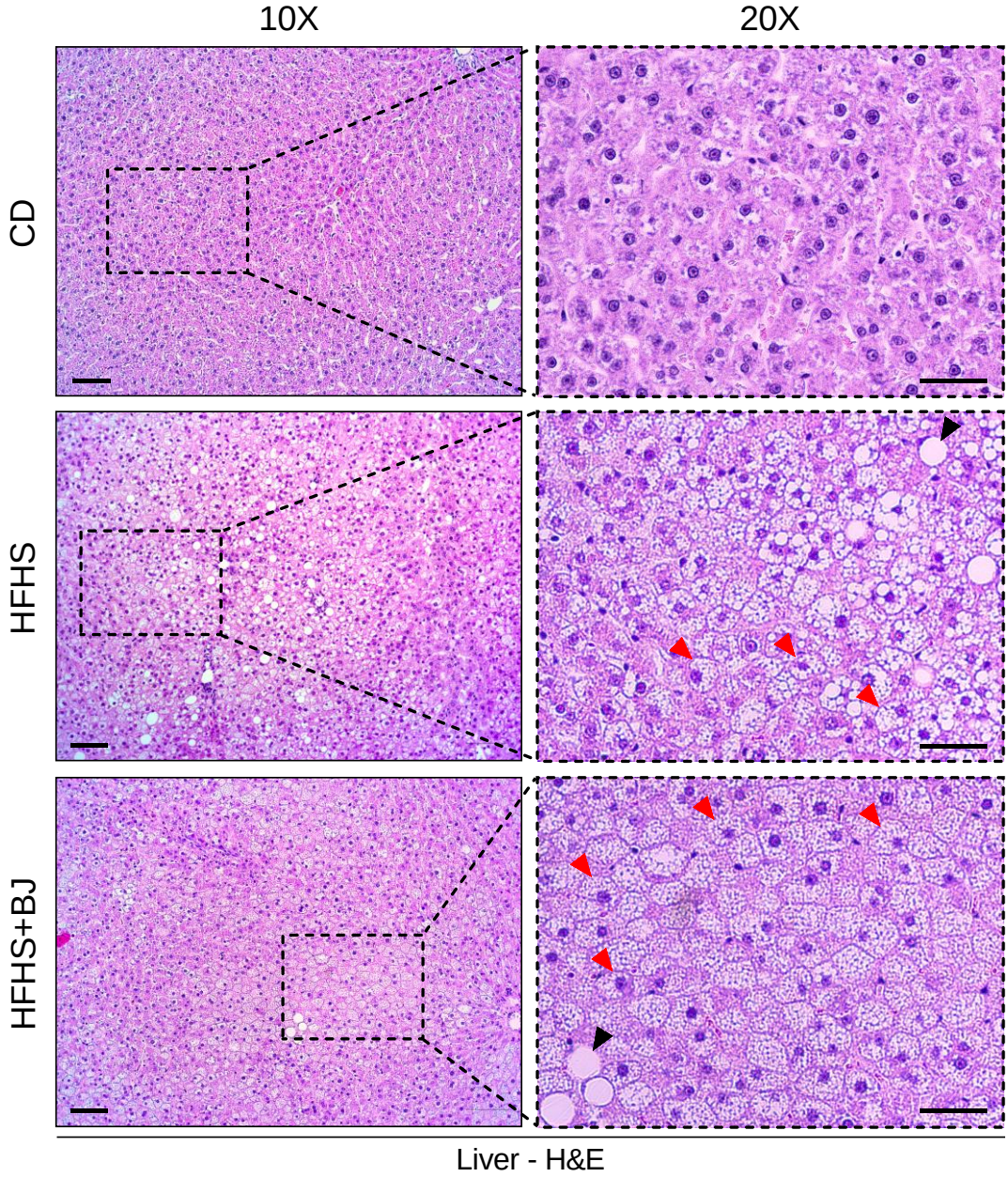

Figure 26 – Histological evaluation of hepatic steatosis. Representative images of hematoxylin and eosin (H&E) staining of liver sections from rats after 24 weeks of different dietary regimens and 8-week BJ ingestion showing normal (nonsteatotic), microsteatotic (red arrows) and macrosteatotic (black arrows) hepatocytes at 10× and 20× magnification (scale bar = 100 μm).

We quantified the total hepatic steatosis score by calculating the percentage of steatotic hepatocytes using H&E-stained liver sections. We found an increase in the percentage of steatotic hepatocytes in HFHS-fed rats relative to the CD-fed group (~497% increase, p<0.0001) (Figure 27A). A further increase was found in the group supplemented with BJ when compared to CD- (~658% increase, p<0.0001) and HFHS-fed rats (~27% increase, p<0.05).

To further quantify the distinct steatotic phenotypes present in each group, we evaluated the percentage of macrosteatotic and microsteatotic hepatocytes. No differences in the macrosteatosis score were found between groups, despite significant differences in microsteatosis score were noted, similar to the total steatosis score (Figure 27B).

These results indicate that 8 weeks of BJ supplementation may have aggravated hepatic lipid deposition which was manifested as an increase in microsteatotic phenotype.

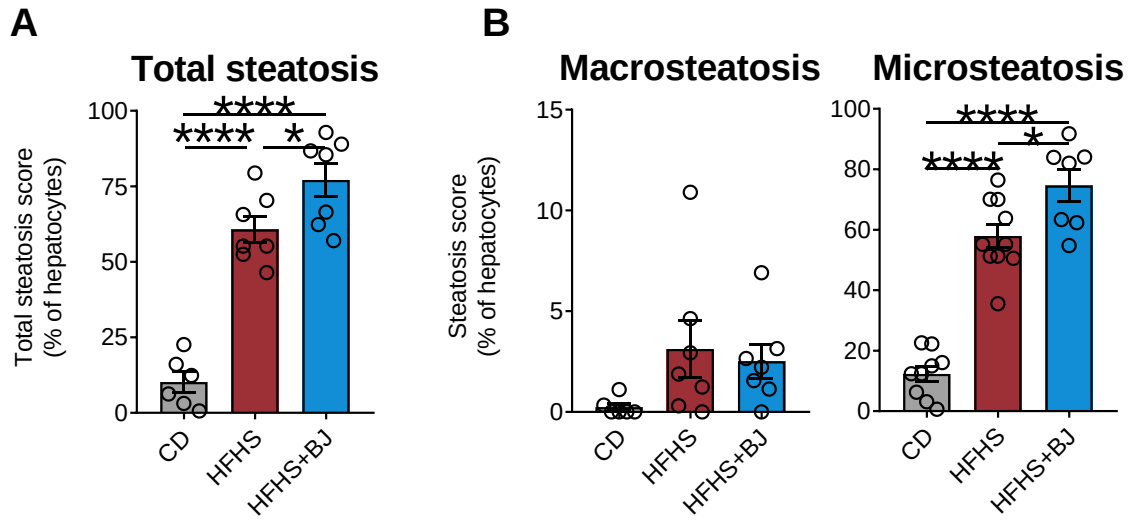

Figure 27 – Quantitative assessment of hepatic steatosis. (**A**) Total steatosis score expressed as a percentage of hepatocytes. (**B**) Macro and microsteatosis scores are expressed as a percentage of hepatocytes. Data are presented as mean ± SEM (n = 6-7 per group); *p<0.05 and ****p<0.0001, using a one-way ANOVA followed by a Tukey multiple comparison test.

4.2.6. Influence of BJ supplementation on molecular mechanisms associated with hepatic steatosis

4.2.6.1. BJ attenuates HFHS-induced impaired endoplasmic reticulum stress response

The association between ER stress and hepatic steatosis is widely accepted. However, no previous studies have addressed the effects of BJ supplementations on ER stress in the liver of prediabetic rats.

Thus, to investigate the hepatic effects of BJ supplementation on ER stress in a HFHS diet-induced animal model of prediabetes, we analyzed protein expression of several well-known ER stress markers, namely IRE-1, eIF2α, P-eIF2α and CHOP (Figure 28). The expression of all ER stress markers increased significantly in the HFHS group when compared to the CD-fed group (IRE-1: ~120% increase, $p<0.01$; eIF2α: ~80% increase, $p<0.05$; P-eIF2α: ~45% increase, $p<0.05$; CHOP: ~77% increase, $p<0.01$). Surprisingly, BJ supplementation significantly decreased the expression of IRE-1, P-eIF2α and CHOP when compared to the HFHS-fed group (IRE-1: ~49% decrease, $p<0,01$; P-eIF2α: ~28% decrease, $p<0,05$; CHOP: ~54% decrease, $p<0,01$), suggesting that BJ supplementation decreased the activation of the ER stress response in diet-induced prediabetic rats.

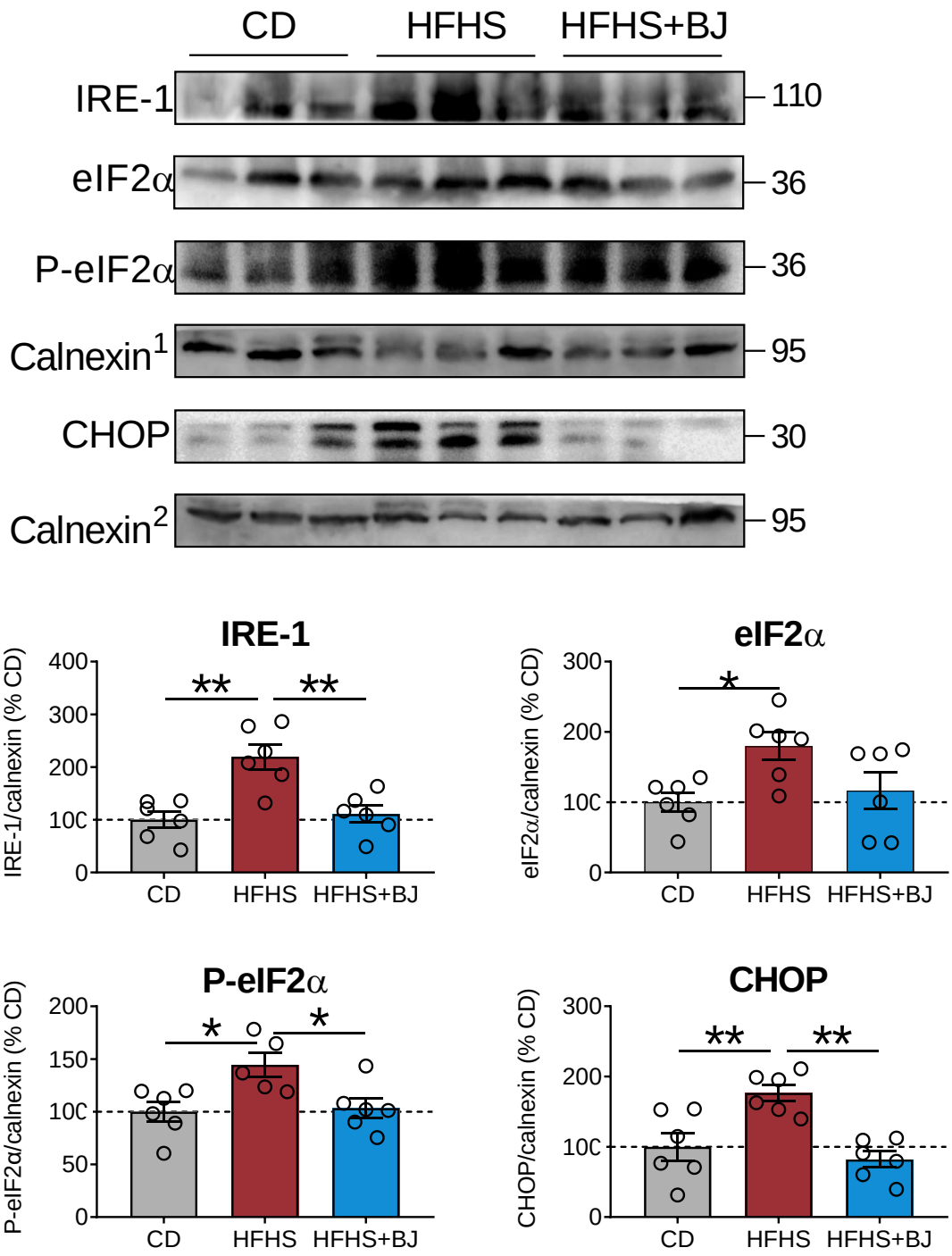

Figure 28 – Endoplasmic reticulum (ER) stress markers in the liver. Representative Western blot images of ER stress markers IRE-1, eIF2α, p-eIF2α and CHOP, and their corresponding protein levels in liver protein extracts from rats fed with CD, HFHS diet and HFHS diet supplemented with BJ for 8 weeks. Data are presented as mean ± SEM (n = 6 rats per group); *p<0.05 and **p<0.01, using a one-way ANOVA followed by a Tukey multiple comparison test.

4.2.6.2. BJ arrested HFHS-induced autophagy

Although autophagy has been implicated in the pathogenesis of hepatic steatosis, no previous studies have addressed the effects of BJ supplementation on hepatic autophagy in rat models of prediabetes.

Thus, to investigate the hepatic effects of BJ supplementation on autophagy activation induced by HFHS diet we analyzed the expression of several autophagy markers by Western blotting (Figure 29). Our results demonstrated a significant increase in LC3-II and p62 and a trend towards an increase in Beclin expression in the HFHS group when compared to the CD-fed group (LC3-II: ~110% increase, $p<0.05$; p62: ~120% increase, $p<0.05$; Beclin: ~53% increase, $p=0.097$). The group supplemented with BJ displayed a decrease in Beclin (~47% decrease, $p<0.05$) and p62 expression (~57% decrease, $p<0.01$) in comparison with the HFHS group, suggesting that BJ supplementation may have arrested autophagy activation induced by the HFHS diet in the model of prediabetes.

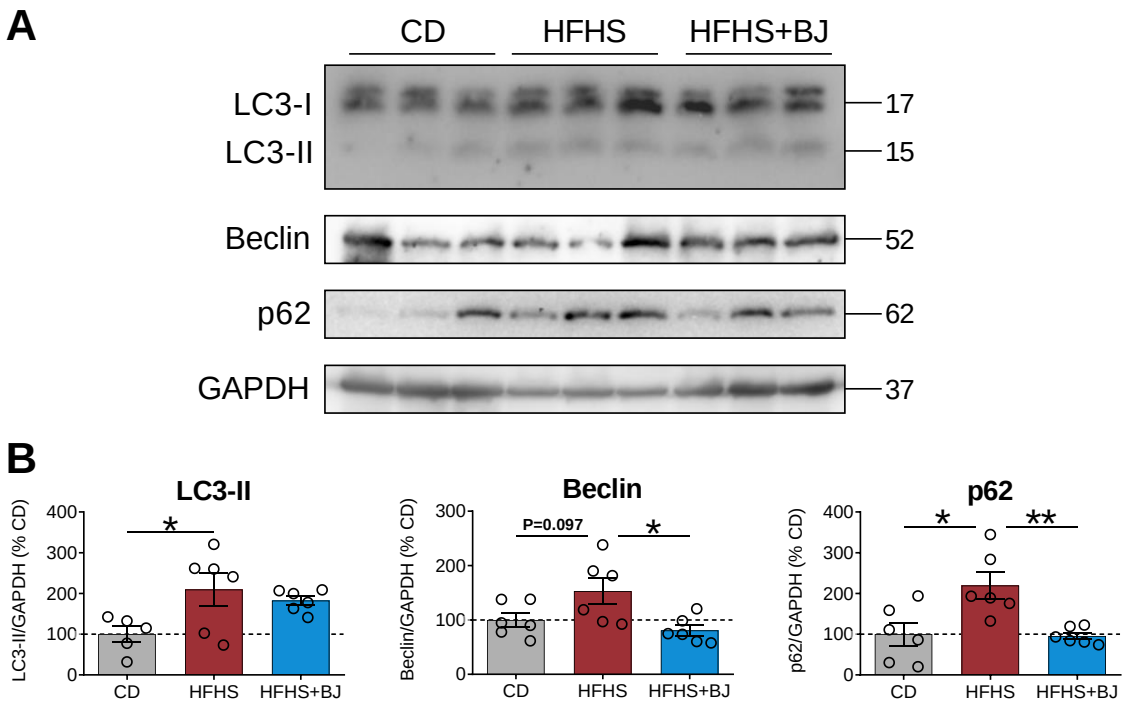

Figure 29 – Autophagy markers in the liver. (**A**) Representative Western blot images of autophagy markers LC3-II, Beclin and p62, and (**B**) corresponding protein levels in liver protein extracts from rats fed with CD, HFHS diet and HFHS diet supplemented with BJ for 8 weeks. Data are presented as mean ± SEM (n = 6 rats per group); *p<0.05 and **p<0.01, using a one-way ANOVA followed by a Tukey multiple comparison test.

Despite preliminary results demonstrated that BJ supplementation attenuated glucose intolerance, this set of results indicate that BJ impaired lipid metabolism given the deleterious metabolic, histological and molecular alterations observed in the liver and adipose tissue of a rat model of prediabetes induced by an HFHS diet (Table 5).

Table 5 – Summary of results of experimental setting II.

	CD	HFHS	HFHS + BJ
Body Weight Gain	=	↑	↑
Adiposity	=	↑	↑
Glucose Intolerance	=	↑↑	↑
BAT activation	=	↑	=
Hepatic Steatosis	=	↑	↑↑
ER stress	=	↑	=
Autophagy	=	↑	=

= – Unaltered; ↑ – Mild; ↑↑ – Exacerbated.

Chapter V

Discussion

Discussion

Along with the increasing prevalence of prediabetes, there is a growing necessity to explore more about this condition and to develop effective therapeutic strategies to prevent its establishment and progression. This concern is accompanied by the need for new and improved animal models of prediabetes that adequately mimic the disease phenotype in humans. Additionally, taking into account the processing degree of control diets ingredients, there is a lack of consensus on the choice of the most appropriate control diet to compare with refined diets that induce the disease phenotype. Therefore, a major goal of this study was to investigate metabolic, histological and molecular alterations in a HFHS diet-induced prediabetic rat model in comparison with two control diets, a standard unrefined control diet (CD) and a nutrient-matched refined low-fat diet (LFD).

In the present study, we used a solid HFHS diet, which displays several advantages when compared to HSD-induced prediabetes models previously used by our group, in which sucrose was supplemented in the beverage (*Nunes et al., 2013*). One of the major differences between the prediabetes model characterized in the present study and the previously mentioned is the introduction of high-fat content in the dietary regimen. Considering that the goal of an animal model is to mimic the human pathophysiology, it might be preferable that the way the disease phenotype is induced also mimics human settings. Thus, considering that Western diets have a high content in both carbohydrates and fat, and that epidemiological studies indicate that HFHS diets are a greater risk factor for metabolic diseases than HSD or HFD alone (*Basu et al., 2013*), we used a HFHS diet to induce the prediabetic phenotype. Furthermore, a solid HFHS diet presents advantages when compared to a HFD supplemented with sucrose in the beverage. For instance, while in HFD the fat content ranges from 55-60% kcal derived from fat, solid HFHS diets have 40-45% kcal derived from fat, thus being more representative of the fat content in human Western diets (~30% calories from fat) (*Kleinert et al., 2018*). Moreover, HFHS diets may have up to three times the amount of sucrose than HFD and therefore, may be more appropriate to study sugar-related pathologies such as prediabetes. Additionally, although more expensive than the supplementation with sucrose in the beverage, the HFHS diet allows to ensure that the animals consume the same ratio of fat to sucrose throughout the study.

Considering that the features of prediabetes in rodent models are the presence of mild hyperglycaemia, glucose intolerance, insulin resistance, hyperinsulinaemia and hyperlipidemia (*Hafizur et al., 2015*), the HFHS-induced animal model successfully achieved a prediabetic phenotype because it displayed glucose intolerance and increased insulin levels from week 16 onwards, representing compensatory hyperinsulinemia, which indicates that the animals reached the stage that precedes β-cell exhaustion (a T2DM hallmark). Furthermore, the fasting normoglycaemia observed reinforces the early stage of the disease which is a feature of prediabetes

Contrarily to the previously used HSD model (*Nunes et al., 2013*), the HFHS model used in this study led to increased body weight gain (~55%) and adiposity (~155% increase eWAT mass), which is in line with a prediabetic phenotype, since obesity is a major risk factor of this disease. However, while HSD-induced model displayed hypertriglyceridemia (*Nunes et al., 2013*), HFHS-fed rats were normoglycemic. Interestingly, *(Brom, van den et al., 2016)* also reported an increase in body weight gain (26%) and a twofold increase in eWAT mass in a HFHS diet-induced Wistar model of prediabetes, along with hypertriglyceridemia. The discrepancies between our results and those reported by (*Brom, van den et al., 2016*) could be due to differences in the experimental design settings such as the duration of HFHS-feeding (24 weeks vs 8 weeks), and the age of the animals at the beginning of the study (13 weeks vs 4 weeks).

Several studies have reported increased body weight gain and adiposity in Wistar rats fed HFD and HFHS diets (*Fourny et al., 2021; Malafaia et al., 2013; Matias et al., 2018)*, and that the expansion of visceral fat depots (e.g., eWAT) in HFD-fed Wistar rats occurs mostly as a result of adipocyte hypertrophy (*Moura e Dias, de et al., 2021*), being the increased body weight and adiposity observed in the HFHS-fed rats in accordance with the literature.

Surprisingly, we also found an increase in insulin levels in the LFD-fed group at week 24 along with increased adiposity, without changes in body weight, suggesting the presence of metabolic abnormalities induced by the refined control diet. Although we observed no changes in body weight gain in the LFD-fed rats, there are reports that a refined diet may increase body weight in rats (*Blaisdell et al., 2014*) and adiposity in mice, probably due to the lack of fermentable fiber in the refined LFD, which is a major substrate that shapes microbiota composition (*Chassaing et al., 2015; Dalby et al., 2017*).

BAT is recognized as the major site for non-shivering thermogenesis, controlling whole-body energy expenditure and body fat due to the abundance of mitochondria with high expression of UCP-1 *(Romestaing et al., 2007; Saito, 2013*). It was hypothesized that Wistar rats first increase lipid storage in peripheral WAT and then overexpress UCP-1-related thermogenesis markers in BAT as an adaptive process in response to excess lipid consumption (*Romestaing et al., 2007*). Considering that thermogenesis contributes roughly to 15-20% of total energy expenditure in rodents, the impact of this mechanism on energy balance and regulation of body weight is significant *(Wood Dos Santos et al., 2018*). Previous reports showed an increase in thermogenesis and UCP-1 expression in rats during HFD feeding (*Romestaing et al., 2007*). This was further confirmed in our study, as the HFHS promoted a significant increase in thermogenic markers UCP-1 and PGC-1α. Although many studies have reported an increase in brown adipocyte lipid droplet size due to HFD feeding (*Wu et al., 2018*), we observed a decrease in lipid droplet size in the HFHS-induced animal model of prediabetes. Interestingly, in a study using Wistar rats, the consumption of 10% sucrose solution for 21 days also resulted in a reduction in brown adipocyte lipid droplet size accompanied by an increase in UCP-1 and PGC-1α immunoexpression, without changes in BAT mass (V*elickovic et al., 2018*). The increase in thermogenesis markers in parallel with the decrease in lipid droplet size suggests that the lipid content present in BAT served as the main substrate for mitochondrial oxidation and provide the signal to uncouple mitochondria in BAT *(Fedorenko, Lishko e Kirichok, 2012*). Despite several studies reported larger iBAT depots along with increase in UCP-1 content in HFD-fed rats (*Romestaing et al., 2007*), likewise (V*elickovic et al., 2018*), we observed no differences in iBAT mass in the HFHS-fed group.

The prediabetes model displayed significantly higher energy intake (~492 kcal/week) in comparison with both control groups (CD: ~460 kcal/week; LFD: ~420 kcal/week) (unpublished data), along with increased thermogenesis markers. Nonetheless, it displayed a positive energy balance reflected by increased body weight and adiposity. Thus, although BAT possesses the ability to increase thermogenic activity in response to high energy intake to prevent body weight gain (*Hatting et al., 2017*), in the present study, increased BAT activity was not sufficient to prevent diet-induced body weight gain.

When compared to the CD group, the LFD group displayed an increase in adiposity without differences in total body weight gain, thermogenesis markers and brown

adipocytes lipid droplets size, suggesting that the increase in adiposity in the LFD group was not enough to induce alterations in BAT activity.

The expansion of the adipose tissue is also associated with lipid mobilization (*Shulman, 2014)*. Ectopic fat accumulation in the liver (hepatic steatosis) causes insulin resistance, playing a key role in prediabetes progression to T2DM *(Byrne, 2013*). In the present study, we observed that the HFHS diet-induced animal model of prediabetes exhibit increased levels of hepatic triglycerides and developed hepatic steatosis with the predominance of a microvesicular steatotic phenotype. Unexpectedly, control LFD-fed rats presented similar changes. In both groups, these alterations occurred without alterations in serum enzyme markers of hepatic injury, ALT and AST.

(*Kandeil et al., 2019*) reported that Wistar rats fed a HFD for 12 weeks displayed microvesicular steatosis in parallel with increase in AST and ALT enzymes. However, hepatic steatosis may be present in Wistar rats without alteration in the levels of ALT and AST *(Kučera et al., 2011; Zarghani et al., 2016; Zhang et al., 2014*). While some studies in Wistar rats fed HFD report a macrovesicular steatotic phenotype (*Zhang et al., 2014*), others report a microvesicular steatotic phenotype (*Kandeil et al., 2019; Kučera et al., 2011*). Nonetheless, a study evaluating steatosis phenotypes in HFD-fed Lewis, Wistar, and Sprague Dawley rats, concluded that, the hepatic steatosis morphologic features were strain-specific. While Lewis show solely microvesicular steatosis and Sprague Dawley show solely macrovesicular steatosis, Wistar rats developed both macro and microvesicular steatosis (*Rosenstengel et al., 2011*).

Hepatic lipid overload due to enhanced *de novo* lipogenesis or increased free fat acids flux from diet or peripheral tissues has been associated with ER stress and impaired autophagy (*Carreres et al., 2021; Ezquerro et al., 2016; Rada et al., 2020*). Moreover, hepatic steatosis is a well-known trigger of ER stress in the liver (*Wang, Wei e Pagliassotti, 2006*). We found an increase in ER stress markers IRE-1, eIF2α, P-eIF2α and CHOP in the animal model of prediabetes in comparison to the control CD group, which might indicate an upregulation of the IRE-1 and PERK pathways of the unfolded protein response (UPR). Because a major function of the UPR is to maintain hepatic lipid homeostasis, the activation of this stress response plays a key role in the prevention of hepatic steatosis development and progression (*Henkel e Green, 2013*). Given that mice with genetic ablations of IRE-1 and eIF2α displayed dysregulated response to ER stress and exacerbated hepatic steatosis with the development of microvesicular steatosis phenotype *(Rutkowski*

et al., 2008; Wang et al., 2012), the increase in the ER stress markers observed in the present study might indicate that UPR upregulation is responding to ER stress, triggered by hepatic steatosis, in order to resolve it. Our results are consistent with previous studies showing impaired IRE-1/Xbp1 pathway of the UPR associated with hepatic steatosis, considering that Wistar rats fed a HFD displayed an increased expression of the ER stress genes CHOP, XBP1, and GRP78 in the liver, accompanied by intrahepatic fat accumulation (*Kandeil et al., 2019*).

Wang *et all* reported an increase in CHOP expression in livers from rats fed a diet rich in saturated fat when compared with rats fed a diet enriched in polyunsaturated fat, which is also in agreement with our results, considering the composition of the diets used in this study (HFHS diet – saturated fat (61%), polyunsaturated (9%); and CD – saturated (22%), polyunsaturated (56%)) (*Wang, Wei* e *Pagliassotti, 2006*). We observed no differences in CHOP expression in the LFD-fed group when compared to the CD group, which might be due to the low amounts of both saturated and polyunsaturated fats present in the LFD.

Surprisingly, the ER stress sensor IRE-1 was also increased in the LFD group when compared to the CD group, which might indicate that the refined LFD may also have deleterious effects in the liver by promoting ER stress.

Autophagy impairment may also be an underlying cause of hepatic steatosis (*Rada et al., 2020*). Moreover (*Cahová et al., 2010)* demonstrated that autophagy is stimulated by high-fat or high-sugar diet-induced triglyceride accumulation in the liver from Wistar rats. In situations of nutrient abundance and absence of stress, Bcl-2 binds to Beclin and autophagy is inhibited. In contrast, in a situation of nutrient scarcity or stress, the Bcl-2/Beclin complex dissociates and enables the nucleation phase of autophagy (*Wei et al., 2008*). Thus, the observed increase of Beclin expression might indicate that the nucleation phase of autophagy is enhanced in both the animal model of prediabetes and in the control LFD group. The elongation phase is characterized by the lipid conjugation of LC3-I into LC3-II which results in the recruitment of ubiquitinated p62 bind to the cargo molecules destined for degradation and the enclosure of the autophagosome. The amount of LC3-II is closely correlated with the number of autophagosomes (*Ohsumi, 2001*) and both LC3-II and p62 are degraded in conditions where autophagy is fully functional (*Jeong et al., 2019; Larsen et al., 2010*), being these markers usually used to assess autophagy. Although no significant differences were found between groups, we observed a trend towards the

increase in the expression of both LC3-II in prediabetic rats, and in p62 in prediabetic and LFD-fed rats. Overall, these results suggest that autophagy is being activated in both prediabetic and LFD-fed rats, which might be viewed as an adaptive response to the diet-induced hepatic steatosis to resolve it in this early stage of disease. Whether autophagy activation will be a contributor to disease in advanced stages deserve further elucidation,

Overall, the HFHS-fed rats successfully developed a prediabetic phenotype exhibiting glucose intolerance, hyperinsulinemia, increased body weight and adiposity, and hepatic steatosis. Furthermore, the upregulation of the UPR response and autophagy in the liver suggest an adaptive response to the diet-induced hepatic lipid accumulation to resolve it.

Studies investigating the impact of refined diets on rodent phenotypes are scarce. Furthermore, while there are reports on the harmful effects of refined diets (*Blaisdell et al., 2014, 2017; González-Blázquez et al., 2020*), there are also studies advising the use of nutrient-matched refined control diets (*Pellizzon e Ricci, 2018, 2018*). Nonetheless, in the present study, the nutrient-matched refined control diet (LFD) displayed deleterious significant differences when compared to the unrefined standard control diet (CD) in multiple metabolic histologic and molecular parameters evaluated. Furthermore, our results suggest that the severity of prediabetic features depends on the nutrient composition of the control diet, underlining the importance of its careful selection in interpreting metabolic studies. Considering that the purpose of a control diet is to mimic conditions of a good health status, we consider the unrefined CD more suitable than the refined LFD to use as a control in the experimental setting II.

The second major goal of this study was to identify the molecular mechanisms associated with the putative protective effects of BJ in a diet-induced animal model of prediabetes.

BJ supplementation for 8 weeks did not affect HFHS diet-induced weight gain or adiposity. Similar findings were reported by (*DeFuria et al., 2009*) that showed that whole blueberry powder supplementation in HFD-fed mice did not protect against weight gain, adiposity or eWAT adipocyte hypertrophy.

Despite the absence of effects of BJ in the total weight gain and in the eWAT hypertrophy, BJ supplementation decreased thermogenic markers UCP-1 e PGC-1α along with an increase in brown adipocyte lipid droplet size. These results suggest a decrease

in mitochondrial oxidation of the lipidic content present in brown adipocytes, resulting in a decrease in the signal to uncouple mitochondria *(Fedorenko, Lishko e Kirichok, 2012*).

Although previous research from our group have showed no significant differences in energy intake between the prediabetic animals (~492 kcal/week) and the prediabetic animals supplemented with BJ (~505 kcal/week) (unpublished data), a decrease in the thermogenesis markers UCP-1 and PGC-1α was observed in the group supplemented with BJ. Considering that both groups displayed a positive energy balance manifested through the increase in total weight gain and adiposity, our results suggest that thermogenesis may not have played a significant role in body weight regulation, and that the decrease in BAT activity was not mainly influenced by lower caloric intake but rather by the BJ intake.

Bartelt and colleagues hypothesized that larger BAT mass could be a promoting factor of weight loss and triglyceride clearance (*Bartelt, Merkel e Heeren, 2012)*. Although the iBAT mass was increased, no differences were found in body weight gain in the HFHS+BJ group compared to the control group. Furthermore, (*Almeida, De et al., 2013*) demonstrated that control rats with less BAT mass produced more heat and consequently expended more energy, in comparison with rats with larger BAT mass that where still hyperinsulinemic, hyperglycemic and obese.

Despite no alterations in enzyme markers of hepatic injury (ALT and AST), BJ-supplemented rats displayed an aggravated fatty liver phenotype, characterized by an increase in the total and microsteatosis scores, accompanied by increased serum levels of triglycerides. Considering that thermogenic activation may result in fat oxidation, contributing to liver protection (*Romestaing et al., 2007*), and that multiple studies demonstrated that increased BAT activity promotes the clearance of triglycerides (*Wickramasinghe e Weaver, 2018)*, the apparently decrease in thermogenic activation observed in the prediabetic animals supplemented with BJ, may be one of the underlying causes of the increase in serum and hepatic TGs and hepatic steatosis score. Nonetheless, these results contrast with previous studies showing the efficacy of a wide variety of polyphenols in inducing thermogenesis and fatty acid oxidation (*Wood Dos Santos et al., 2018)*. For instance, a study using a phenolic blueberry extract in mice reported an improvement in genetically- and diet-induced metabolic syndrome, which was linked to improved hepatic lipid metabolism and increased energy expenditure in BAT (*Guo et al., 2019*).

To the best of our knowledge, there is only one study reporting beneficial effects of a blueberry polyphenol (malvidin) on hepatic ER stress (*Ma et al., 2020*). Here, we found that BJ supplementation decreased the expression of the ER stress markers IRE-1, P-eIF2α and CHOP, suggesting the downregulation of the IRE-1 and PERK pathways, which might be one of the underlying causes of hepatic triglyceride accumulation. In contrast to our results, (*Ma et al., 2020*) showed that malvidin upregulated CHOP expression in activated rat hepatic stellate T6 cells (HSC-T6), being beneficial for the liver health.

The supplementation with blueberry polyphenols has been associated with beneficial hepatic effects through autophagy induction. For instance, (*Zhuge et al., 2020*) reported that the supplementation with blueberry polyphenol extract in a mouse model of AFLD improved hepatic steatosis by lowering the hepatic triglyceride content, reporting a decrease in p62 and enhanced LC3-II/LC3-I proportion in the liver. Similarly, the downregulation of p62 and increase in LC3-II and Beclin was also associated with the induction of autophagy in mice supplemented with pterostilbene, an active constituent of blueberries (*Wang et al., 2019*). In contrast to these studies, we observed a decrease in the expression of Beclin and p62 and a trend towards the decrease in the expression of LC3-II in the group supplemented with BJ, suggesting that both nucleation and elongation phases of autophagy are downregulated. Thus, our findings indicate that BJ supplementation promoted the arrest of autophagy. Autophagy inhibition decreases the breakdown of lipid stores, resulting in hepatic triglyceride accumulation in mice. Moreover, it has been reported that diabetic OLETF rats, as well as obese leptin-deficient ob/ob mice, displayed hepatic lipid accumulation associated with decreased autophagy levels (*Ezquerro et al., 2016*). Thus, the arrest in autophagy observed in the prediabetic model supplemented with BJ might be one of the underlying causes of the increase in serum and hepatic TGs content and hepatic steatosis.

Despite our preliminary results demonstrated beneficial effects of BJ on glucose tolerance, in the present study we observed that BJ supplementation decreased thermogenesis markers in iBAT, downregulated ER stress response and arrested autophagy in the liver. Furthermore, BJ also increased serum and hepatic TG content and steatosis scores, without effects on body weight gain and adiposity.

Considering the high fat and sucrose content in the HFHS diet, and the abundance of polyphenols in blueberries, the simultaneous consumption both may had elevated the functional workload in the liver, which may have promoted the exhaustion of the ER stress

response and autophagy. On the other hand, the downregulation of these stress response mechanisms could be due to a "metabolic energy shift" between these, to other mechanisms that might aid in the metabolization of the HFHS diet and the polyphenols present in BJ. There are other studies reporting distinct effects of blueberry derived polyphenols in both ER stress and autophagy (*Ma et al., 2020; Zhuge et al., 2020*). The discrepancies between our results and the previous mentioned reports could be due to multiple factors such as the dose administered, the duration of treatment and most probably due to the complex and highly variable polyphenolic composition of blueberries.

Further studies should contribute to clarify if the blueberry composition, the dose and the duration of treatment are major causes for the worsening of lipid metabolism in the liver and adipose tissue in HFHS diet-induced prediabetic rats despite the improvement of glucose tolerance.

Chapter VI

Concluding Remarks

Concluding remarks

Our study successfully characterized an animal model of prediabetes induced by a high-fat high-sucrose diet, which displayed glucose intolerance, hyperinsulinemia, increased body weight and adiposity, and hepatic steatosis (Table 6). Prediabetic rats exhibited an increase in iBAT thermogenesis markers, accompanied by an upregulation of hepatic autophagy and ER stress response, suggesting an adaptive response to the diet-induced metabolic abnormalities at this early stage of disease.

Rats fed a nutrient-matched refined control diet displayed significant metabolic abnormalities, namely adiposity and hepatic steatosis when compared to rats fed an unrefined standard control diet, suggesting that the severity of prediabetic features depends on the nutrient composition of the control diet, underlining the importance of its careful selection in interpreting metabolic studies.

Despite the improvement of glucose tolerance, blueberry juice supplementation increased serum and hepatic triglyceride content, decreased thermogenesis markers in iBAT, downregulated ER stress response and arrested autophagy in the liver of prediabetic rats (Table 6). Further studies should be performed in order to elucidate whether the worsened lipid metabolism in the liver and adipose tissue induced by blueberry could be explained by its specific composition, by the dose used and/or by the duration of treatment. The results of this thesis recommend that blueberry consumption should be carefully considered at this stage of prediabetes.

Table 6 – Summary of results.

	CD	LFD	HFHS	HFHS + BJ
Body Weight Gain	=	=	↑	↑
Adiposity	=	↑	↑	↑
Glucose Intolerance	=	↑	↑↑	↑
BAT activation	=	=	↑	=
Hepatic Steatosis	=	↑	↑↑	↑↑↑
ER stress	=	↑	↑↑	=
Autophagy	=	↑	↑↑	=

= – Unaltered; ↑ – Mild; ↑↑ – Exacerbated; ↑↑↑ – Severe.

Chapter VII

References

References

AILSHUL, Mark D. - Energy balance and obesity in man. **Nutrition Today**. . ISSN 15389839. 10:5–6 (1975) 29–30. doi: 10.1097/00017285-197509000-00009.

AKASH, Muhammad Sajid Hamid; REHMAN, Kanwal; LIAQAT, Aamira - Tumor Necrosis Factor-Alpha: Role in Development of Insulin Resistance and Pathogenesis of Type 2 Diabetes Mellitus. **Journal of Cellular Biochemistry**. . ISSN 10974644. 119:1 (2018) 105–110. doi: 10.1002/jcb.26174.

ALBRACHT-SCHULTE, Kembra *et al.* - Omega-3 fatty acids in obesity and metabolic syndrome: a mechanistic update. **The Journal of Nutritional Biochemistry**. . ISSN 0955-2863. 58:2018) 1–16. doi: https://doi.org/10.1016/j.jnutbio.2018.02.012.

ALLAIRE, Manon *et al.* - Autophagy in liver diseases: Time for translation? **Journal of Hepatology**. . ISSN 16000641. 70:5 (2019) 985–998. doi: 10.1016/j.jhep.2019.01.026.

ALMEIDA-SUHETT, Camila P. *et al.* - Control diet in a high-fat diet study in mice: Regular chow and purified low-fat diet have similar effects on phenotypic, metabolic, and behavioral outcomes. **Nutritional Neuroscience**. 22:1 (2019) 19–28. doi: 10.1080/1028415X.2017.1349359.

ALMEIDA, Douglas L. DE *et al.* - Early overfeed-induced obesity leads to brown adipose tissue hypoactivity in rats. **Cellular Physiology and Biochemistry**. . ISSN 14219778. 32:6 (2013) 1621–1630. doi: 10.1159/000356598.

ÁLVAREZ-MERCADO, Ana Isabel *et al.* - New Insights Into the Role of Autophagy in Liver Surgery in the Setting of Metabolic Syndrome and Related Diseases. **Frontiers in Cell and Developmental Biology**. . ISSN 2296634X. 9:June (2021) 1–31. doi: 10.3389/fcell.2021.670273.

ARAB, Juan Pablo; ARRESE, Marco; TRAUNER, Michael - Recent Insights into the Pathogenesis of Nonalcoholic Fatty Liver Disease. **Annual Review of Pathology: Mechanisms of Disease**. . ISSN 15534014. 13:2018) 321–350. doi: 10.1146/annurev-pathol-020117-043617.

BAICEANU, Andrei *et al.* - Endoplasmic reticulum proteostasis in hepatic steatosis. **Nature Reviews Endocrinology**. . ISSN 17595037. 12:12 (2016) 710–722. doi: 10.1038/nrendo.2016.124.

BANSAL, Nidhi - Prediabetes diagnosis and treatment: A review. **World journal of diabetes**. . ISSN 1948-9358 (Print). 6:2 (2015) 296–303. doi: 10.4239/wjd.v6.i2.296.

BARTELT, Alexander; MERKEL, Martin; HEEREN, Joerg - A new, powerful player in lipoprotein metabolism: brown adipose tissue. **Journal of molecular medicine (Berlin, Germany)**. Germany. . ISSN 1432-1440 (Electronic). 90:8 (2012) 887–893. doi: 10.1007/s00109-012-0858-3.

BASU, Sanjay *et al.* - The relationship of sugar to population-level diabetes prevalence: an econometric analysis of repeated cross-sectional data. **PloS one**. . ISSN 1932-6203 (Electronic). 8:2 (2013) e57873. doi: 10.1371/journal.pone.0057873.

BETZ, Matthias J.; ENERBÄCK, Sven - Targeting thermogenesis in brown fat and muscle to treat obesity and metabolic disease. **Nature Reviews Endocrinology**. . ISSN 17595037. 14:2 (2018) 77–87. doi: 10.1038/nrendo.2017.132.

BEULENS, Jwj *et al.* - Risk and management of pre-diabetes. **European journal of preventive cardiology**. England. . ISSN 2047-4881 (Electronic). 26:2_suppl (2019) 47–54. doi: 10.1177/2047487319880041.

BHATTACHARYA, Debalina *et al.* - Is autophagy associated with diabetes mellitus and its complications? A review. **EXCLI journal**. . ISSN 1611-2156 (Print). 17:2018) 709–720. doi: 10.17179/excli2018-1353.

BLAISDELL, Aaron P. *et al.* - Food quality and motivation: a refined low-fat diet induces obesity and impairs performance on a progressive ratio schedule of instrumental lever pressing in rats. **Physiology & behavior**. United States. . ISSN 1873-507X (Electronic). 128:2014) 220–225. doi: 10.1016/j.physbeh.2014.02.025.

BLAISDELL, Aaron P. *et al.* - An obesogenic refined low-fat diet disrupts attentional and behavioral control processes in a vigilance task in rats. **Behavioural Processes**. . ISSN 0376-6357. 138:2017) 142–151. doi: https://doi.org/10.1016/j.beproc.2017.03.007.

BODEN, G. - Effects of free fatty acids (FFA) on glucose metabolism: significance for insulin resistance and type 2 diabetes. **Experimental and clinical endocrinology & diabetes : official journal, German Society of Endocrinology [and] German Diabetes Association**. Germany. . ISSN 0947-7349 (Print). 111:3 (2003) 121–124. doi: 10.1055/s-2003-39781.

BRAY, George A. *et al.* - The influence of different fats and fatty acids on obesity, insulin resistance and inflammation. **The Journal of nutrition**. United States. . ISSN 0022-3166 (Print). 132:9 (2002) 2488–2491. doi: 10.1093/jn/132.9.2488.

BROM, Charissa E. VAN DEN *et al.* - Myocardial Perfusion and Function Are Distinctly Altered by Sevoflurane Anesthesia in Diet-Induced Prediabetic Rats. **Journal of Diabetes Research**. . ISSN 2314-6745. 2016:2016) 5205631. doi: 10.1155/2016/5205631.

BROWN, Nadine M.; SETCHELL, Kenneth D. R. - Animal Models Impacted by Phytoestrogens in Commercial Chow: Implications for Pathways Influenced by Hormones. **Laboratory Investigation**. . ISSN 1530-0307. 81:5 (2001) 735–747. doi: 10.1038/labinvest.3780282.

BYRNE, Christopher D. - Ectopic fat, insulin resistance and non-alcoholic fatty liver disease. **The Proceedings of the Nutrition Society**. England. . ISSN 1475-2719 (Electronic). 72:4 (2013) 412–419. doi: 10.1017/S0029665113001249.

CAHOVÁ, M. *et al.* - The autophagy-lysosomal pathway is involved in TAG degradation in the liver: the effect of high-sucrose and high-fat diet. **Folia biologica**. Czech Republic. . ISSN 0015-5500 (Print). 56:4 (2010) 173–182.

CARRERES, Lydie *et al.* - Modeling Diet-Induced NAFLD and NASH in Rats: A Comprehensive Review. **Biomedicines**. . ISSN 2227-9059. 9:4 (2021). doi: 10.3390/biomedicines9040378.

CEFALU, William T. - Animal Models of Type 2 Diabetes: Clinical Presentation and Pathophysiological Relevance to the Human Condition. **ILAR Journal**. . ISSN 1084-2020. 47:3 (2006) 186–198. doi: 10.1093/ilar.47.3.186.

CERNEA, Simona; DOBREANU, Minodora - Diabetes and beta cell function: From mechanisms to evaluation and clinical implications. **Biochemia Medica**. . ISSN 13300962. 23:3 (2013) 266–280. doi: 10.11613/BM.2013.033.

CHASSAING, Benoit *et al.* - Lack of soluble fiber drives diet-induced adiposity in mice. **American Journal of Physiology - Gastrointestinal and Liver Physiology**. . ISSN 15221547. 309:7 (2015) G528–G541. doi: 10.1152/ajpgi.00172.2015.

CHEN, Gou-Chun *et al.* - Two unhealthy dietary habits featuring a high fat content and a sucrose-containing beverage intake, alone or in combination, on inducing metabolic syndrome in Wistar rats and C57BL/6J mice. **Metabolism: clinical and experimental**. United States. . ISSN 1532-8600 (Electronic). 60:2 (2011) 155–164. doi: 10.1016/j.metabol.2009.12.002.

CHEN, Li *et al.* - Mechanisms Linking Inflammation to Insulin Resistance. **International Journal of Endocrinology**. . ISSN 16878345. 2015:2015). doi: 10.1155/2015/508409.

CLEMENTE-POSTIGO, Mercedes *et al.* - The role of Autophagy in white adipose tissue function: Implications for metabolic health. **Metabolites**. . ISSN 22181989. 10:5 (2020) 1–29. doi: 10.3390/metabo10050179.

COCCURELLO, Roberto *et al.* - Effects of caloric restriction on neuropathic pain, peripheral nerve degeneration and inflammation in normometabolic and autophagy defective prediabetic Ambra1 mice. **PLoS ONE**. . ISSN 19326203. 13:12 (2018) 1–26. doi: 10.1371/journal.pone.0208596.

COOPER, Geoffrey M. - **The Cell: A Molecular Approach** [Em linha]. 2nd editio ed. [S.l.] : Sunderland (MA): Sinauer Associates, 2000 Disponível em WWW:<URL:https://www.ncbi.nlm.nih.gov/books/NBK9839/>.

COTROZZI, G. *et al.* - [Role of the liver in the regulation of glucose metabolism in diabetes and chronic liver disease]. **Annali italiani di medicina interna : organo ufficiale della Societa italiana di medicina interna**. Italy. . ISSN 0393-9340 (Print). 12:2 (1997) 84–91.

CZAJA, Mark J. - Function of Autophagy in Nonalcoholic Fatty Liver Disease. **Digestive Diseases and Sciences**. . ISSN 15732568. 61:5 (2016) 1304–1313. doi: 10.1007/s10620-015-4025-x.

CZECH, Michael P. - Mechanisms of insulin resistance related to white, beige, and brown adipocytes. **Molecular Metabolism**. . ISSN 22128778. 34:January (2020) 27–42. doi: 10.1016/j.molmet.2019.12.014.

DALBY, Matthew J. *et al.* - Dietary Uncoupling of Gut Microbiota and Energy Harvesting from Obesity and Glucose Tolerance in Mice. **Cell Reports**. . ISSN 2211-1247. 21:6 (2017) 1521–1533. doi: https://doi.org/10.1016/j.celrep.2017.10.056.

DAWSON, Ted M.; KO, Han Seok; DAWSON, Valina L. - Genetic animal models of Parkinson's disease. **Neuron**. . ISSN 1097-4199 (Electronic). 66:5 (2010) 646–661. doi: 10.1016/j.neuron.2010.04.034.

DECUYPERE, Jean-Paul; PARYS, Jan B.; BULTYNCK, Geert - Regulation of the Autophagic Bcl-2/Beclin 1 Interaction. **Cells**. . ISSN 2073-4409. 1:3 (2012) 284–312. doi: 10.3390/cells1030284.

DEFRONZO, Ralph A. - Pathogenesis of type 2 diabetes mellitus. **Medical Clinics of North America**. . ISSN 00257125. 88:4 (2004) 787–835. doi: 10.1016/j.mcna.2004.04.013.

DEFRONZO, Ralph A.; ABDUL-GHANI, Muhammad A. - Preservation of β-cell function: The key to diabetes prevention. **Journal of Clinical Endocrinology and Metabolism**.

. ISSN 0021972X. 96:8 (2011) 2354–2366. doi: 10.1210/jc.2011-0246.

DEFURIA, Jason *et al.* - Dietary blueberry attenuates whole-body insulin resistance in high fat-fed mice by reducing adipocyte death and its inflammatory sequelae. **The Journal of nutrition**. . ISSN 1541-6100 (Electronic). 139:8 (2009) 1510–1516. doi: 10.3945/jn.109.105155.

Diagnosis and classification of diabetes mellitus. - **Diabetes care**. . ISSN 1935-5548 (Electronic). 34 Suppl 1:Suppl 1 (2011) S62-9. doi: 10.2337/dc11-S062.

DIEHL, Anna M.; DAY, Christopher - Cause, Pathogenesis, and Treatment of Nonalcoholic Steatohepatitis. **New England Journal of Medicine**. . ISSN 0028-4793. 377:21 (2017) 2063–2072. doi: 10.1056/nejmra1503519.

DIREÇÃO-GERAL DA SAÚDE - Diagnóstico e Classificação da Diabetes Mellitus. **Norma da Direção Geral da Saúde (002/2011)**. Diagnóstico e Classificação da Diabetes Mellitus (2011) 1–13.

DONATH, Marc Y. *et al.* - Islet inflammation in type 2 diabetes: from metabolic stress to therapy. **Diabetes care**. . ISSN 19355548. 31 Suppl 2:2008). doi: 10.2337/dc08-s243.

DONNELLY, Kerry L. *et al.* - Sources of fatty acids stored in liver and secreted via lipoproteins in patients with nonalcoholic fatty liver disease. **Journal of Clinical Investigation**. . ISSN 00219738. 115:5 (2005) 1343–1351. doi: 10.1172/JCI23621.

DOURMASHKIN, J. T. *et al.* - Different forms of obesity as a function of diet composition. **International Journal of Obesity**. . ISSN 1476-5497. 29:11 (2005) 1368–1378. doi: 10.1038/sj.ijo.0803017.

DUMITRASCU, Dan L.; NEUMAN, Manuela G. - Non-alcoholic fatty liver disease: An update on diagnosis. **Clujul Medical**. . ISSN 20668872. 91:2 (2018) 147–150. doi: 10.15386/cjmed-993.

EDWARDS, Catherine M.; CUSI, Kenneth - Prediabetes: A Worldwide Epidemic. **Endocrinology and metabolism clinics of North America**. United States. . ISSN 1558-4410 (Electronic). 45:4 (2016) 751–764. doi: 10.1016/j.ecl.2016.06.007.

ELKS, Carrie M. *et al.* - Blueberries improve glucose tolerance without altering body composition in obese postmenopausal mice. **Obesity (Silver Spring, Md.)**. . ISSN 1930-739X (Electronic). 23:3 (2015) 573–580. doi: 10.1002/oby.20926.

EZQUERRO, Silvia *et al.* - Acylated and desacyl ghrelin are associated with hepatic lipogenesis, β-oxidation and autophagy: Role in NAFLD amelioration after sleeve gastrectomy in obese rats. **Scientific Reports**. . ISSN 20452322. 6:December (2016) 1–12. doi: 10.1038/srep39942.

FAKIH, Walaa *et al.* - Dysfunctional cerebrovascular tone contributes to cognitive impairment in a non-obese rat model of prediabetic challenge: Role of suppression of autophagy and modulation by anti-diabetic drugs. **Biochemical pharmacology**. England. . ISSN 1873-2968 (Electronic). 178:2020) 114041. doi: 10.1016/j.bcp.2020.114041.

FARDET, Anthony - Characterization of the Degree of Food Processing in Relation With Its Health Potential and Effects. **Advances in food and nutrition research**. United States. . ISSN 1043-4526 (Print). 85:2018) 79–129. doi: 10.1016/bs.afnr.2018.02.002.

FEDORENKO, Andriy; LISHKO, Polina V; KIRICHOK, Yuriy - Mechanism of fatty-acid-dependent UCP1 uncoupling in brown fat mitochondria. **Cell**. . ISSN 1097-4172 (Electronic). 151:2 (2012) 400–413. doi: 10.1016/j.cell.2012.09.010.

FENG, Nan *et al.* - Common variants in PERK, JNK, BIP and XBP1 genes are associated with the risk of prediabetes or diabetes-related phenotypes in a Chinese population. **Chinese medical journal**. China. . ISSN 2542-5641 (Electronic). 127:13 (2014) 2438–2444.

FERRANNINI, Ele; GASTALDELLI, Amalia; IOZZO, Patricia - Pathophysiology of Prediabetes. **Medical Clinics of North America**. . ISSN 00257125. 95:2 (2011) 327–339. doi: 10.1016/j.mcna.2010.11.005.

FLIER, Barbara B. Kahn And Jeffrey S. - Obesity and insulin resistance. **The Journal of Clinical Investigation**. . ISSN 00970549. 18:4 (2000) 301–306. doi: 10.1007/BF01185522.

FOURNY, Natacha *et al.* - Male and Female Rats Have Different Physiological Response to High-Fat High-Sucrose Diet but Similar Myocardial Sensitivity to Ischemia-Reperfusion Injury. **Nutrients**. . ISSN 2072-6643. 13:9 (2021). doi: 10.3390/nu13092914.

GLOYN, Anna L. *et al.* - Glucokinase (GCK) and other susceptibility genes for β-cell dysfunction: The candidate approach. **Biochemical Society Transactions**. . ISSN 03005127. 36:3 (2008) 306–311. doi: 10.1042/BST0360306.

GONZÁLEZ-BLÁZQUEZ, Raquel *et al.* - Relevance of control diet choice in metabolic studies: impact in glucose homeostasis and vascular function. **Scientific Reports**. . ISSN 2045-2322. 10:1 (2020) 2902. doi: 10.1038/s41598-020-59674-0.

GONZÁLEZ-RODRÍGUEZ, A. *et al.* - Impaired autophagic flux is associated with increased endoplasmic reticulum stress during the development of NAFLD. **Cell Death and Disease**. . ISSN 20414889. 5:4 (2014). doi: 10.1038/cddis.2014.162.

GRACE, Mary H. *et al.* - Hypoglycemic activity of a novel anthocyanin-rich formulation from lowbush blueberry, Vaccinium angustifolium Aiton. **Phytomedicine : international journal of phytotherapy and phytopharmacology**. . ISSN 1618-095X (Electronic). 16:5 (2009) 406–415. doi: 10.1016/j.phymed.2009.02.018.

GREEN, Christopher D.; OLSON, L. Karl - Modulation of palmitate-induced endoplasmic reticulum stress and apoptosis in pancreatic β-cells by stearoyl-CoA desaturase and Elovl6. **American Journal of Physiology - Endocrinology and Metabolism**. . ISSN 01931849. 300:4 (2011) 640–649. doi: 10.1152/ajpendo.00544.2010.

GUILHERME, Adilson *et al.* - Adipocyte dysfunctions linking obesity to insulin resistance and type 2 diabetes. **Nature Reviews Molecular Cell Biology**. . ISSN 14710072. 9:5 (2008) 367–377. doi: 10.1038/nrm2391.

GUO, Jielong *et al.* - Blueberry Extract Improves Obesity through Regulation of the Gut Microbiota and Bile Acids via Pathways Involving FXR and TGR5. **iScience**. . ISSN 2589-0042. 19:2019) 676–690. doi: https://doi.org/10.1016/j.isci.2019.08.020.

GUSTAFSON, Birgit *et al.* - Inflammation and impaired adipogenesis in hypertrophic obesity in man. **American Journal of Physiology - Endocrinology and Metabolism**. . ISSN 01931849. 297:5 (2009). doi: 10.1152/ajpendo.00377.2009.

HAFIZUR, Rahman M. *et al.* - A 'Humanized' rat model of pre-diabetes by high fat diet-feeding to weaning wistar rats. **Integrative Obesity and Diabetes**. 1:2 (2015) 44–48. doi: 10.15761/iod.1000111.

HAGMAN, Derek K. *et al.* - Palmitate inhibits insulin gene expression by altering PDX-1 nuclear localization and reducing MafA expression in isolated rat islets of Langerhans.

Journal of Biological Chemistry. . ISSN 00219258. 280:37 (2005) 32413–32418. doi: 10.1074/jbc.M506000200.

HATTING, Maximilian *et al.* - Adipose Tissue CLK2 Promotes Energy Expenditure during High-Fat Diet Intermittent Fasting. **Cell Metabolism**. . ISSN 19327420. 25:2 (2017) 428–437. doi: 10.1016/j.cmet.2016.12.007.

HE, Qin *et al.* - Mesenchymal stem cell-derived exosomes exert ameliorative effects in type 2 diabetes by improving hepatic glucose and lipid metabolism via enhancing autophagy. **Stem cell research & therapy**. . ISSN 1757-6512 (Electronic). 11:1 (2020) 223. doi: 10.1186/s13287-020-01731-6.

HENKEL, Anne; GREEN, Richard M. - The unfolded protein response in fatty liver disease. **Seminars in liver disease**. . ISSN 1098-8971 (Electronic). 33:4 (2013) 321–329. doi: 10.1055/s-0033-1358522.

HENKEL, Anne S. - Unfolded Protein Response Sensors in Hepatic Lipid Metabolism and Nonalcoholic Fatty Liver Disease. **Seminars in Liver Disease**. . ISSN 10988971. 38:4 (2018) 320–332. doi: 10.1055/s-0038-1670677.

HOSTALEK, Ulrike - Global epidemiology of prediabetes - present and future perspectives. **Clinical Diabetes and Endocrinology**. . ISSN 2055-8260. 5:1 (2019) 5. doi: 10.1186/s40842-019-0080-0.

IKEDA, Kenji; YAMADA, Tetsuya - UCP1 Dependent and Independent Thermogenesis in Brown and Beige Adipocytes. **Frontiers in endocrinology**. . ISSN 1664-2392 (Print). 11:2020) 498. doi: 10.3389/fendo.2020.00498.

INTERNATIONAL DIABETES FEDERATION - **IDF Diabetes Atlas Seventh**. 9th. ed. ISBN 9782930229874.

ISLAM, Md Shahidul; LOOTS, Du Toit - Experimental rodent models of type 2 diabetes: a review. **Methods and findings in experimental and clinical pharmacology**. Spain. . ISSN 0379-0355 (Print). 31:4 (2009) 249–261. doi: 10.1358/mf.2009.31.4.1362513.

ISLAM, Md Shahidul; VENKATESAN, Vijayalakshmi - Experimentally-induced animal models of prediabetes and insulin resistance: A review. **Acta Poloniae Pharmaceutica - Drug Research**. . ISSN 00016837. 73:4 (2016) 827–834.

ISLAM, Md; SHANNON, Rachel - Experimentally Induced Rodent Models of Type 2 Diabetes. **Methods in molecular biology (Clifton, N.J.)**. 933:2012) 161–174. doi: 10.1007/978-1-62703-068-7_10.

JEONG, Se-Jin *et al.* - p62/SQSTM1 and Selective Autophagy in Cardiometabolic Diseases. **Antioxidants & redox signaling**. . ISSN 1557-7716 (Electronic). 31:6 (2019) 458–471. doi: 10.1089/ars.2018.7649.

JOHNSON, Sarah A.; ARJMANDI, Bahram H. - Evidence for anti-cancer properties of blueberries: a mini-review. **Anti-cancer agents in medicinal chemistry**. Netherlands. . ISSN 1875-5992 (Electronic). 13:8 (2013) 1142–1148. doi: 10.2174/18715206113139990137.

KAISANLAHTI, A.; GLUMOFF, T. - Browning of white fat: agents and implications for beige adipose tissue to type 2 diabetes. **Journal of Physiology and Biochemistry**. . ISSN 18778755. 75:1 (2019). doi: 10.1007/s13105-018-0658-5.

KANDEIL, Mohamed A. *et al.* - Zingiber officinale extract and omega-3 fatty acids ameliorate endoplasmic reticulum stress in a nonalcoholic fatty liver rat model. **Journal**

of Food Biochemistry. . ISSN 17454514. 43:12 (2019) 1–9. doi: 10.1111/jfbc.13076.

KANETO, Hideaki *et al.* - Oxidative stress, ER stress, and the JNK pathway in type 2 diabetes. **Journal of molecular medicine (Berlin, Germany)**. Germany. . ISSN 0946-2716 (Print). 83:6 (2005) 429–439. doi: 10.1007/s00109-005-0640-x.

KANG, Jie *et al.* - Phenolic acids of the two major blueberry species in the US Market and their antioxidant and anti-inflammatory activities. **Plant foods for human nutrition (Dordrecht, Netherlands)**. Netherlands. . ISSN 1573-9104 (Electronic). 70:1 (2015) 56–62. doi: 10.1007/s11130-014-0461-6.

KAWASAKI, Noritaka *et al.* - Obesity-induced endoplasmic reticulum stress causes chronic inflammation in adipose tissue. **Scientific Reports**. . ISSN 20452322. 2:2012) 1–7. doi: 10.1038/srep00799.

KHANDIA, Rekha *et al.* - A Comprehensive Review of Autophagy and Its Various Roles in Infectious, Non-Infectious, and Lifestyle Diseases: Current Knowledge and Prospects for Disease Prevention, Novel Drug Design, and Therapy. **Cells**. . ISSN 2073-4409. 8:7 (2019) 674. doi: 10.3390/cells8070674.

KIM, G. W. *et al.* - Antiobesity pharmacotherapy: New drugs and emerging targets. **Clinical Pharmacology and Therapeutics**. . ISSN 00099236. 95:1 (2014) 53–66. doi: 10.1038/clpt.2013.204.

KIM, Hyunsook *et al.* - Hepatic gene expression related to lower plasma cholesterol in hamsters fed high-fat diets supplemented with blueberry peels and peel extract. **Journal of Agricultural and Food Chemistry**. . ISSN 00218561. 58:7 (2010) 3984–3991. doi: 10.1021/jf903230s.

KING, Aileen; BOWE, James - Animal models for diabetes: Understanding the pathogenesis and finding new treatments. **Biochemical pharmacology**. England. . ISSN 1873-2968 (Electronic). 99:2016) 1–10. doi: 10.1016/j.bcp.2015.08.108.

KITAMORI, Kazuya *et al.* - Development of novel rat model for high-fat and high-cholesterol diet-induced steatohepatitis and severe fibrosis progression in SHRSP5/Dmcr. **Environmental Health and Preventive Medicine**. . ISSN 1347-4715. 17:3 (2012) 173–182. doi: 10.1007/s12199-011-0235-9.

KLAUS, Susanne - Adipose Tissue as a Regulator of Energy Balance. **Current Drug Targets**. . ISSN 13894501. 5:3 (2005) 241–250. doi: 10.2174/1389450043490523.

KLEINERT, Maximilian *et al.* - Animal models of obesity and diabetes mellitus. **Nature reviews. Endocrinology**. England. . ISSN 1759-5037 (Electronic). 14:3 (2018) 140–162. doi: 10.1038/nrendo.2017.161.

KRISTIANSEN, Maria N. B. *et al.* - Molecular Characterization of Microvesicular and Macrovesicular Steatosis Shows Widespread Differences in Metabolic Pathways. **Lipids**. . ISSN 15589307. 54:1 (2019) 109–115. doi: 10.1002/lipd.12121.

KUČERA, O. *et al.* - The effect of rat strain, diet composition and feeding period on the development of a nutritional model of non-alcoholic fatty liver disease in rats. **Physiological research**. Czech Republic. . ISSN 1802-9973 (Electronic). 60:2 (2011) 317–328. doi: 10.33549/physiolres.932022.

KUMAR, Mukesh *et al.* - Insulin activates intracellular transport of lipid droplets to release triglycerides from the liver. **Journal of Cell Biology**. . ISSN 15408140. 218:11 (2019) 3697–3713. doi: 10.1083/JCB.201903102.

LAI, M.; CHANDRASEKERA, P. C.; BARNARD, N. D. - You are what you eat, or are you? The challenges of translating high-fat-fed rodents to human obesity and diabetes. **Nutrition & diabetes**. . ISSN 2044-4052 (Print). 4:9 (2014) e135. doi: 10.1038/nutd.2014.30.

LAMARK, Trond; SVENNING, Steingrim; JOHANSEN, Terje - Regulation of selective autophagy: The p62/SQSTM1 paradigm. **Essays in Biochemistry**. . ISSN 00711365. 61:6 (2017) 609–624. doi: 10.1042/EBC20170035.

LAMBADIARI, Vaia; TRIANTAFYLLOU, Konstantinos; DIMITRIADIS, George D. - Insulin action in muscle and adipose tissue in type 2 diabetes: The significance of blood flow. **World journal of diabetes**. . ISSN 1948-9358 (Print). 6:4 (2015) 626–633. doi: 10.4239/wjd.v6.i4.626.

LARSEN, Kenneth Bowitz *et al.* - A reporter cell system to monitor autophagy based on p62/SQSTM1. **Autophagy**. United States. . ISSN 1554-8635 (Electronic). 6:6 (2010) 784–793. doi: 10.4161/auto.6.6.12510.

LEE, J.; DURST, R. W.; WROLSTAD, R. E. - Impact of Juice Processing on Blueberry Anthocyanins and Polyphenolics: Comparison of Two Pretreatments. **Journal of Food Science**. . ISSN 0022-1147. 67:5 (2002) 1660–1667. doi: https://doi.org/10.1111/j.1365-2621.2002.tb08701.x.

LENZEN, S. - The mechanisms of alloxan- and streptozotocin-induced diabetes. **Diabetologia**. Germany. . ISSN 0012-186X (Print). 51:2 (2008) 216–226. doi: 10.1007/s00125-007-0886-7.

LENZEN, Sigurd - Oxidative stress: The vulnerable β-cell. **Biochemical Society Transactions**. . ISSN 03005127. 36:3 (2008) 343–347. doi: 10.1042/BST0360343.

LEÓN-PEDROZA, José Israel *et al.* - Low-grade systemic inflammation and the development of metabolic diseases: From the molecular evidence to the clinical practice. **Cirugía y Cirujanos (English Edition)**. . ISSN 24440507. 83:6 (2015) 543–551. doi: 10.1016/j.circen.2015.11.008.

LI, Wen; ZHANG, Lining - **Regulation of ATG and Autophagy Initiation**. ISBN 9789811506017.

LOOS, Ben; TOIT, André DU; HOFMEYR, Jan-Hendrik S. - Defining and measuring autophagosome flux—concept and reality. **Autophagy**. . ISSN 1554-8635 (Electronic). 10:11 (2014) 2087–2096. doi: 10.4161/15548627.2014.973338.

LOZANO, Iona *et al.* - High-fructose and high-fat diet-induced disorders in rats: impact on diabetes risk, hepatic and vascular complications. **Nutrition & metabolism**. . ISSN 1743-7075 (Print). 13:2016) 15. doi: 10.1186/s12986-016-0074-1.

LUC, K. *et al.* - Oxidative stress and inflammatory markers in prediabetes and diabetes. **Journal of Physiology and Pharmacology**. . ISSN 18991505. 70:6 (2019) 809–824. doi: 10.26402/jpp.2019.6.01.

LUPACHYK, Sergey *et al.* - Endoplasmic reticulum stress contributes to prediabetic peripheral neuropathy. **Experimental Neurology**. . ISSN 00144886. 247:2013) 342–348. doi: 10.1016/j.expneurol.2012.11.001.

MA, Yanhong *et al.* - Malvidin induces hepatic stellate cell apoptosis via the endoplasmic reticulum stress pathway and mitochondrial pathway. **Food science & nutrition**. . ISSN 2048-7177 (Print). 8:9 (2020) 5095–5106. doi: 10.1002/fsn3.1810.

MADUREIRA, Ana Raquel *et al.* - Safety profile of solid lipid nanoparticles loaded with rosmarinic acid for oral use: In vitro and animal approaches. **International Journal of Nanomedicine**. . ISSN 11782013. 11:2016) 3621–3640. doi: 10.2147/IJN.S104623.

MALAFAIA, Andressa Bressan *et al.* - Obesity induction with high fat sucrose in rats. **Arquivos brasileiros de cirurgia digestiva : ABCD = Brazilian archives of digestive surgery**. . ISSN 23176326. 26 Suppl 1:Suplemento 1 (2013) 17–21.

MALONE, John I.; HANSEN, Barbara C. - Does obesity cause type 2 diabetes mellitus (T2DM)? Or is it the opposite? **Pediatric Diabetes**. . ISSN 13995448. 20:1 (2019) 5–9. doi: 10.1111/pedi.12787.

MARQUES, Cláudia *et al.* - High-fat diet-induced obesity Rat model: a comparison between Wistar and Sprague-Dawley Rat. **Adipocyte**. 5:1 (2016) 11–21. doi: 10.1080/21623945.2015.1061723.

MARTINEAU, Louis C. *et al.* - Anti-diabetic properties of the Canadian lowbush blueberry Vaccinium angustifolium Ait. **Phytomedicine : international journal of phytotherapy and phytopharmacology**. Germany. . ISSN 0944-7113 (Print). 13:9–10 (2006) 612–623. doi: 10.1016/j.phymed.2006.08.005.

MATIAS, Amanda Martins *et al.* - Differential Effects of High Sugar, High Lard or a Combination of Both on Nutritional, Hormonal and Cardiovascular Metabolic Profiles of Rodents. **Nutrients**. . ISSN 2072-6643. 10:8 (2018). doi: 10.3390/nu10081071.

MITTAL BALRAJ - Subcutaneous adipose tissue & visceral adipose tissue. **Indian Journal of Medical Research**. . ISSN 1930-7837. 149:5 (2019) 571–573. doi: 10.4103/ijmr.IJMR_1910_18.

MOLAN, A. L.; LILA, M. A.; MAWSON, J. - Satiety in rats following blueberry extract consumption induced by appetite-suppressing mechanisms unrelated to in vitro or in vivo antioxidant capacity. **Food Chemistry**. . ISSN 03088146. 107:3 (2008) 1039–1044. doi: 10.1016/j.foodchem.2007.09.018.

MONTANARI, T.; POŠĆIĆ, N.; COLITTI, M. - Factors involved in white-to-brown adipose tissue conversion and in thermogenesis: a review. **Obesity Reviews**. . ISSN 1467789X. 18:5 (2017) 495–513. doi: 10.1111/obr.12520.

MORENO-INDIAS, Isabel; TINAHONES, Francisco José - Impaired adipose tissue expandability and lipogenic capacities as ones of the main causes of metabolic disorders. **Journal of Diabetes Research**. . ISSN 23146753. 2015:2015). doi: 10.1155/2015/970375.

MOURA E DIAS, Mariana DE *et al.* - Diet-induced obesity in animal models: points to consider and influence on metabolic markers. **Diabetology & Metabolic Syndrome**. . ISSN 1758-5996. 13:1 (2021) 32. doi: 10.1186/s13098-021-00647-2.

MOUSOVICH-NETO, Felippe *et al.* - Brown adipose tissue remodelling induced by corticosterone in male Wistar rats. **Experimental Physiology**. . ISSN 1469445X. 104:4 (2019) 514–528. doi: 10.1113/EP087332.

MUOIO, Deborah M.; NEWGARD, Christopher B. - Mechanisms of disease: Molecular and metabolic mechanisms of insulin resistance and β-cell failure in type 2 diabetes. **Nature Reviews Molecular Cell Biology**. . ISSN 14710072. 9:3 (2008) 193–205. doi: 10.1038/nrm2327.

NETO, Catherine C. - Cranberry and blueberry: Evidence for protective effects against

cancer and vascular diseases. **Molecular Nutrition and Food Research**. . ISSN 16134125. 51:6 (2007) 652–664. doi: 10.1002/mnfr.200600279.

NGUYEN, P. *et al.* - Liver lipid metabolism. **Journal of Animal Physiology and Animal Nutrition**. . ISSN 09312439. 92:3 (2008) 272–283. doi: 10.1111/j.1439-0396.2007.00752.x.

NTZANI, Evangelia E.; KAVVOURA, Fotini K. - Genetic risk factors for type 2 diabetes: insights from the emerging genomic evidence. **Current vascular pharmacology**. United Arab Emirates. . ISSN 1875-6212 (Electronic). 10:2 (2012) 147–155. doi: 10.2174/157016112799305030.

NUNES S, SOARES, PEREIRA F, Reis F. - The role of inflammation in diabetic cardiomyopathy. **International Journal of Interferon, Cytokine and Mediator Research**. 4:2012) 59–73. doi: https://doi.org/10.2147/IJICMR.S21679.

NUNES, Sara *et al.* - Early cardiac changes in a rat model of prediabetes: brain natriuretic peptide overexpression seems to be the best marker. **Cardiovascular diabetology**. . ISSN 1475-2840 (Electronic). 12:2013) 44. doi: 10.1186/1475-2840-12-44.

NUNES, Sara *et al.* - Blueberry as an attractive functional fruit to prevent (Pre)diabetes progression. **Antioxidants**. . ISSN 20763921. 10:8 (2021) 1–23. doi: 10.3390/antiox10081162.

NUNES, Sara *et al.* - Blueberry counteracts prediabetes in a hypercaloric diet-induced rat model and rescues hepatic mitochondrial bioenergetics. **Nutrients**. . ISSN 20726643. 13:12 (2021). doi: 10.3390/nu13124192.

OHSUMI, Y. - Molecular dissection of autophagy: two ubiquitin-like systems. **Nature reviews. Molecular cell biology**. England. . ISSN 1471-0072 (Print). 2:3 (2001) 211–216. doi: 10.1038/35056522.

OLIVEIRA, Liliane Soares C. *et al.* - The inflammatory profile and liver damage of a sucrose-rich diet in mice. **The Journal of nutritional biochemistry**. United States. . ISSN 1873-4847 (Electronic). 25:2 (2014) 193–200. doi: 10.1016/j.jnutbio.2013.10.006.

OSEINI, Abdul M.; SANYAL, Arun J. - Therapies in non-alcoholic steatohepatitis (NASH). **Liver International**. . ISSN 14783231. 37:Suppl 1 (2017) 97–103. doi: 10.1111/liv.13302.

PAGLIASSOTTI, Michael J. - Endoplasmic reticulum stress in nonalcoholic fatty liver disease. **Annual Review of Nutrition**. . ISSN 01999885. 32:2012) 17–33. doi: 10.1146/annurev-nutr-071811-150644.

PARK, Anna - Distinction of white, beige and brown adipocytes derived from mesenchymal stem cells. **World Journal of Stem Cells**. . ISSN 1948-0210. 6:1 (2014) 33. doi: 10.4252/wjsc.v6.i1.33.

PARK, Jae Myung *et al.* - Prognostic impact of Beclin 1, p62/sequestosome 1 and LC3 protein expression in colon carcinomas from patients receiving 5-fluorouracil as adjuvant chemotherapy. **Cancer Biology and Therapy**. . ISSN 15384047. 14:2 (2013) 100–107. doi: 10.4161/cbt.22954.

PAULY, Marion *et al.* - High intensity aerobic exercise training improves chronic intermittent hypoxia-induced insulin resistance without basal autophagy modulation. **Scientific Reports**. . ISSN 20452322. 7:January (2017) 1–12. doi: 10.1038/srep43663.

PELLIZZON, Michael A.; RICCI, Matthew R. - The common use of improper control diets in diet-induced metabolic disease research confounds data interpretation: the fiber factor.

Nutrition & Metabolism. . ISSN 1743-7075. 15:1 (2018) 3. doi: 10.1186/s12986-018-0243-5.

PELLIZZON, Michael A.; RICCI, Matthew R. - Effects of Rodent Diet Choice and Fiber Type on Data Interpretation of Gut Microbiome and Metabolic Disease Research. **Current protocols in toxicology**. United States. . ISSN 1934-9262 (Electronic). 77:1 (2018) e55. doi: 10.1002/cptx.55.

PELLIZZON, Michael A.; RICCI, Matthew R. - Choice of Laboratory Rodent Diet May Confound Data Interpretation and Reproducibility. **Current Developments in Nutrition**. . ISSN 2475-2991. 4:4 (2020) nzaa031. doi: 10.1093/cdn/nzaa031.

PIACENTINI, Mauro *et al.* - Non-alcoholic fatty liver disease severity is modulated by transglutaminase type 2. **Cell Death & Disease**. . ISSN 2041-4889. 9:3 (2018) 257. doi: 10.1038/s41419-018-0292-8.

PIZZINO, Gabriele *et al.* - Oxidative Stress: Harms and Benefits for Human Health. **Oxidative Medicine and Cellular Longevity**. . ISSN 19420994. 2017:2017). doi: 10.1155/2017/8416763.

PRATO, S. DEL - Role of glucotoxicity and lipotoxicity in the pathophysiology of Type 2 diabetes mellitus and emerging treatment strategies. **Diabetic Medicine**. . ISSN 07423071. 26:12 (2009) 1185–1192. doi: 10.1111/j.1464-5491.2009.02847.x.

PRATO, Stefano Del; TIENGO, Antonio - The importance of first-phase insulin secretion: Implications for the therapy of type 2 diabetes mellitus. **Diabetes/Metabolism Research and Reviews**. . ISSN 15207552. 17:3 (2001) 164–174. doi: 10.1002/dmrr.198.

PREGUIÇA, Inês *et al.* - Diet-induced rodent models of obesity-related metabolic disorders—A guide to a translational perspective. **Obesity Reviews**. . ISSN 1467789X. 21:12 (2020) 1–29. doi: 10.1111/obr.13081.

PRIOR, Ronald L. *et al.* - Purified blueberry anthocyanins and blueberry juice alter development of obesity in mice fed an obesogenic high-fat diet. **Journal of agricultural and food chemistry**. United States. . ISSN 1520-5118 (Electronic). 58:7 (2010) 3970–3976. doi: 10.1021/jf902852d.

RADA, Patricia *et al.* - Understanding lipotoxicity in NAFLD pathogenesis: is CD36 a key driver? **Cell Death & Disease**. . ISSN 2041-4889. 11:9 (2020) 802. doi: 10.1038/s41419-020-03003-w.

RAPOSO, João Filipe - Diabetes : Factos e Números betes – Prevalência betes – Prevalência. **Revista Portuguesa de Diabetes**. 15:1 (2020) 19–27.

RAVIKUMAR, Brinda *et al.* - Mammalian macroautophagy at a glance. **Journal of Cell Science**. . ISSN 00219533. 122:11 (2009) 1707–1711. doi: 10.1242/jcs.031773.

REN, Tingting *et al.* - Protection of hepatocyte mitochondrial function by blueberry juice and probiotics via SIRT1 regulation in non-alcoholic fatty liver disease. **Food & function**. England. . ISSN 2042-650X (Electronic). 10:3 (2019) 1540–1551. doi: 10.1039/c8fo02298d.

RIIHINEN, Kaisu *et al.* - Organ-specific distribution of phenolic compounds in bilberry (Vaccinium myrtillus) and «northblue» blueberry (Vaccinium corymbosum x V. angustifolium). **Food chemistry**. England. . ISSN 0308-8146 (Print). 110:1 (2008) 156–160. doi: 10.1016/j.foodchem.2008.01.057.

RINELLA, Mary E. - Nonalcoholic fatty liver disease a systematic review. **JAMA - Journal of the American Medical Association**. . ISSN 15383598. 313:22 (2015) 2263–2273.

doi: 10.1001/jama.2015.5370.

ROBERTSON, R. Paul *et al.* - Glucose toxicity in beta-cells: type 2 diabetes, good radicals gone bad, and the glutathione connection. **Diabetes**. United States. . ISSN 0012-1797 (Print). 52:3 (2003) 581–587. doi: 10.2337/diabetes.52.3.581.

ROCHA, Milagros *et al.* - Mitochondria and T2D: Role of Autophagy, ER Stress, and Inflammasome. **Trends in Endocrinology and Metabolism**. . ISSN 18793061. 31:10 (2020) 725–741. doi: 10.1016/j.tem.2020.03.004.

ROMESTAING, Caroline *et al.* - Long term highly saturated fat diet does not induce NASH in Wistar rats. **Nutrition & Metabolism**. . ISSN 1743-7075. 4:1 (2007) 4. doi: 10.1186/1743-7075-4-4.

ROMESTAING, Caroline *et al.* - Long term highly saturated fat diet does not induce NASH in Wistar rats. **Nutrition and Metabolism**. . ISSN 17437075. 4:2007) 1–14. doi: 10.1186/1743-7075-4-4.

ROOPCHAND, Diana E. *et al.* - Blueberry polyphenol-enriched soybean flour reduces hyperglycemia, body weight gain and serum cholesterol in mice. **Pharmacological research**. . ISSN 1096-1186 (Electronic). 68:1 (2013) 59–67. doi: 10.1016/j.phrs.2012.11.008.

ROSENSTENGEL, Stephan *et al.* - Type of steatosis influences microcirculation and fibrogenesis in different rat strains. **Journal of investigative surgery : the official journal of the Academy of Surgical Research**. United States. . ISSN 1521-0553 (Electronic). 24:6 (2011) 273–282. doi: 10.3109/08941939.2011.586094.

ROSSI, Marta *et al.* - Epidemiology Behind Fruit and Vegetable Consumption and Cancer Risk with Focus on Flavonoids. **Plant Phenolics and Human Health: Biochemistry, Nutrition, and Pharmacology**. 2009) 471–487. doi: 10.1002/9780470531792.ch20.

RUTKOWSKI, D. Thomas *et al.* - UPR pathways combine to prevent hepatic steatosis caused by ER stress-mediated suppression of transcriptional master regulators. **Developmental cell**. . ISSN 1878-1551 (Electronic). 15:6 (2008) 829–840. doi: 10.1016/j.devcel.2008.10.015.

SAITO, Masayuki - Brown adipose tissue as a regulator of energy expenditure and body fat in humans. **Diabetes & metabolism journal**. . ISSN 2233-6079 (Print). 37:1 (2013) 22–29. doi: 10.4093/dmj.2013.37.1.22.

SANCHEZ-GURMACHES, Joan; HUNG, Chien Min; GUERTIN, David A. - Emerging Complexities in Adipocyte Origins and Identity. **Trends in Cell Biology**. . ISSN 18793088. 26:5 (2016) 313–326. doi: 10.1016/j.tcb.2016.01.004.

SARAVANAN, Natarajan *et al.* - Dietary ginger improves glucose dysregulation in a long-term high-fat high-fructose fed prediabetic rat model. **Indian journal of experimental biology**. India. . ISSN 0019-5189 (Print). 55:3 (2017) 142–150.

SEALE, P. - Transcriptional control of brown adipocyte development and thermogenesis. **International Journal of Obesity**. . ISSN 14765497. 34:S1 (2010) S17–S22. doi: 10.1038/ijo.2010.178.

SENFT, Daniela; RONAI, Ze'ev A. - UPR, autophagy, and mitochondria crosstalk underlies the ER stress response. **Trends in Biochemical Sciences**. . ISSN 13624326. 40:3 (2015) 141–148. doi: 10.1016/j.tibs.2015.01.002.

SETHUNATH, Deepak *et al.* - Automated assessment of steatosis in murine fatty liver.

PLoS ONE. . ISSN 19326203. 13:5 (2018) 1–16. doi: 10.1371/journal.pone.0197242.

SEYMOUR, E. Mitchell *et al.* - Blueberry intake alters skeletal muscle and adipose tissue peroxisome proliferator-activated receptor activity and reduces insulin resistance in obese rats. **Journal of medicinal food**. United States. . ISSN 1557-7600 (Electronic). 14:12 (2011) 1511–1518. doi: 10.1089/jmf.2010.0292.

SHI, Min *et al.* - Blueberry as a source of bioactive compounds for the treatment of obesity, type 2 diabetes and chronic inflammation. **Journal of Functional Foods**. . ISSN 17564646. 30:2017) 16–29. doi: 10.1016/j.jff.2016.12.036.

SHINDE, Abhijit Babaji; SONG, Anying; WANG, Qiong A. - Brown Adipose Tissue Heterogeneity, Energy Metabolism, and Beyond. **Frontiers in Endocrinology**. . ISSN 16642392. 12:April (2021) 1–13. doi: 10.3389/fendo.2021.651763.

SHULMAN, Gerald I. - Ectopic fat in insulin resistance, dyslipidemia, and cardiometabolic disease. **The New England journal of medicine**. United States. . ISSN 1533-4406 (Electronic). 371:12 (2014) 1131–1141. doi: 10.1056/NEJMra1011035.

SILVA, Sara *et al.* - Health promoting properties of blueberries: a review. **Critical Reviews in Food Science and Nutrition**. . ISSN 15497852. 60:2 (2020) 181–200. doi: 10.1080/10408398.2018.1518895.

SMITH, Briohny W.; ADAMS, Leon A. - Nonalcoholic fatty liver disease and diabetes mellitus: pathogenesis and treatment. **Nature reviews. Endocrinology**. England. . ISSN 1759-5037 (Electronic). 7:8 (2011) 456–465. doi: 10.1038/nrendo.2011.72.

SMITH, Ulf *et al.* - Insulin signaling and action in fat cells: Associations with insulin resistance and Type 2 diabetes. **Annals of the New York Academy of Sciences**. . ISSN 00778923. 892:1999) 119–126. doi: 10.1111/j.1749-6632.1999.tb07790.x.

SOKOLOWSKA, Emilia; BLACHNIO-ZABIELSKA, Agnieszka - The Role of Ceramides in Insulin Resistance. **Frontiers in Endocrinology**. . ISSN 16642392. 10:August (2019) 1–13. doi: 10.3389/fendo.2019.00577.

STANHOPE, K. L. *et al.* - Pathways and mechanisms linking dietary components to cardiometabolic disease: thinking beyond calories. **Obesity reviews : an official journal of the International Association for the Study of Obesity**. . ISSN 1467-789X (Electronic). 19:9 (2018) 1205–1235. doi: 10.1111/obr.12699.

STULL, April J. *et al.* - Bioactives in blueberries improve insulin sensitivity in obese, insulin-resistant men and women. **The Journal of nutrition**. . ISSN 1541-6100 (Electronic). 140:10 (2010) 1764–1768. doi: 10.3945/jn.110.125336.

STUMVOLL, Michael; GOLDSTEIN, Barry J.; HAEFTEN, Timon W. Van - Haeften_Pathogenesis of type 2 diabetes.pdf. **The Lancet**. 365:2005) 1333–1346.

SUGANAMI, Takayoshi; OGAWA, Yoshihiro - Adipose tissue macrophages: their role in adipose tissue remodeling. **Journal of Leukocyte Biology**. . ISSN 1938-3673. 88:1 (2010) 33–39. doi: 10.1189/jlb.0210072.

SZAJDEK, Agnieszka; BOROWSKA, E. J. - Bioactive compounds and health-promoting properties of berry fruits: a review. **Plant foods for human nutrition (Dordrecht, Netherlands)**. Netherlands. . ISSN 0921-9668 (Print). 63:4 (2008) 147–156. doi: 10.1007/s11130-008-0097-5.

TABÁK, Adam G. *et al.* - Prediabetes: A high-risk state for developing diabetes. **The Lancet**. . ISSN 1474547X. 379:9833 (2012) 2279–2290. doi: 10.1016/S0140-

6736(12)60283-9.Prediabetes.

TAKIKAWA, Masahito *et al.* - Dietary anthocyanin-rich bilberry extract ameliorates hyperglycemia and insulin sensitivity via activation of AMP-activated protein kinase in diabetic mice. **The Journal of nutrition**. United States. . ISSN 1541-6100 (Electronic). 140:3 (2010) 527–533. doi: 10.3945/jn.109.118216.

TANDRA, Sweta *et al.* - Presence and significance of microvesicular steatosis in nonalcoholic fatty liver disease. **Journal of Hepatology**. . ISSN 01688278. 55:3 (2011) 654–659. doi: 10.1016/j.jhep.2010.11.021.

TANDRA, Sweta *et al.* - Presence and significance of microvesicular steatosis in nonalcoholic fatty liver disease. **Journal of hepatology**. . ISSN 1600-0641 (Electronic). 55:3 (2011) 654–659. doi: 10.1016/j.jhep.2010.11.021.

TEKIRDAG, Kumsal; CUERVO, Ana Maria - Chaperone-mediated autophagy and endosomal microautophagy: Joint by a chaperone. **Journal of Biological Chemistry**. . ISSN 1083351X. 293:15 (2018) 5414–5424. doi: 10.1074/jbc.R117.818237.

TONG, Jingjing; YAN, Xianghua; YU, Li - The late stage of autophagy: Cellular events and molecular regulation. **Protein and Cell**. . ISSN 16748018. 1:10 (2010) 907–915. doi: 10.1007/s13238-010-0121-z.

TORRES, Daniel J. *et al.* - Diet-Induced Obesity and Leptin Resistance. 2019).

TSALAMANDRIS, Sotirios *et al.* - Risk Factors and Cardiovascular Disease Prevention The Role of Inflammation in Diabetes : Current Concepts and Future Perspectives. **European Cardiology Review**. 14:1 (2019) 50–59.

VEEN, Jelske N. VAN DER *et al.* - The critical role of phosphatidylcholine and phosphatidylethanolamine metabolism in health and disease. **Biochimica et Biophysica Acta - Biomembranes**. . ISSN 18792642. 1859:9 (2017) 1558–1572. doi: 10.1016/j.bbamem.2017.04.006.

VELICKOVIC, Ksenija D. *et al.* - Effects of long-term sucrose overfeeding on rat brown adipose tissue: A structural and immunohistochemical study. **Journal of Experimental Biology**. . ISSN 00220949. 221:9 (2018). doi: 10.1242/jeb.166538.

VUONG, Tri *et al.* - Fermented Canadian lowbush blueberry juice stimulates glucose uptake and AMP-activated protein kinase in insulin-sensitive cultured muscle cells and adipocytes. **Canadian journal of physiology and pharmacology**. Canada. . ISSN 0008-4212 (Print). 85:9 (2007) 956–965. doi: 10.1139/Y07-090.

WANG, Dong *et al.* - Pterostilbene, An Active Constituent of Blueberries, Suppresses Proliferation Potential of Human Cholangiocarcinoma via Enhancing the Autophagic Flux . **Frontiers in Pharmacology** . 10:2019).

WANG, Dong; WEI, Yuren; PAGLIASSOTTI, Michael J. - Saturated fatty acids promote endoplasmic reticulum stress and liver injury in rats with hepatic steatosis. **Endocrinology**. United States. . ISSN 0013-7227 (Print). 147:2 (2006) 943–951. doi: 10.1210/en.2005-0570.

WANG, Miao; KAUFMAN, Randal J. - The impact of the endoplasmic reticulum protein-folding environment on cancer development. **Nature Reviews Cancer**. . ISSN 1474-1768. 14:9 (2014) 581–597. doi: 10.1038/nrc3800.

WANG, Shiyu *et al.* - IRE1α-XBP1s induces PDI expression to increase MTP activity for hepatic VLDL assembly and lipid homeostasis. **Cell metabolism**. . ISSN 1932-7420

(Electronic). 16:4 (2012) 473–486. doi: 10.1016/j.cmet.2012.09.003.

WANG, Yu-Ping *et al.* - Effects of blueberry on hepatic fibrosis and transcription factor Nrf2 in rats. **World journal of gastroenterology**. . ISSN 2219-2840 (Electronic). 16:21 (2010) 2657–2663. doi: 10.3748/wjg.v16.i21.2657.

WANG, Yuping *et al.* - Dietary Supplementation of Blueberry Juice Enhances Hepatic Expression of Metallothionein and Attenuates Liver Fibrosis in Rats. **PLoS ONE**. . ISSN 19326203. 8:3 (2013) 2–9. doi: 10.1371/journal.pone.0058659.

WANG, Zhen *et al.* - Analysis of Inflammatory Mediators in Prediabetes and Newly Diagnosed Type 2 Diabetes Patients. **Journal of Diabetes Research**. . ISSN 23146753. 2016:2016). doi: 10.1155/2016/7965317.

WEI, Yongjie *et al.* - JNK1-mediated phosphorylation of Bcl-2 regulates starvation-induced autophagy. **Molecular cell**. . ISSN 1097-4164 (Electronic). 30:6 (2008) 678–688. doi: 10.1016/j.molcel.2008.06.001.

WICKRAMASINGHE, Manoj; WEAVER, Jolanta U. - Chapter 10 - Lipid Disorders in Obesity. Em WEAVER, JOLANTA URSZULA (Ed.) - **Practical Guide to Obesity Medicine** [Em linha]. [S.l.] : Elsevier, 2018 Disponível em WWW:<URL:https://www.sciencedirect.com/science/article/pii/B9780323485593000105>. ISBN 978-0-323-48559-3. p. 99–108.

WITZIG, Thomas E. *et al.* - The mTORC1 inhibitor everolimus has antitumor activity in vitro and produces tumor responses in patients with relapsed T-cell lymphoma. **Blood**. . ISSN 15280020. 126:3 (2015) 328–335. doi: 10.1182/blood-2015-02-629543.

WOOD DOS SANTOS, Tanila *et al.* - Effects of Polyphenols on Thermogenesis and Mitochondrial Biogenesis. **International journal of molecular sciences**. . ISSN 1422-0067 (Electronic). 19:9 (2018). doi: 10.3390/ijms19092757.

WORLD HEALTH ORGANIZATION - **Obesity and Overweight** [Em linha], atual. 2021. Disponível em WWW:<URL:https://www.who.int/news-room/fact-sheets/detail/obesity-and-overweight>.

WU, Hao *et al.* - The Gut Microbiota in Prediabetes and Diabetes: A Population-Based Cross-Sectional Study. **Cell Metabolism**. . ISSN 19327420. 32:3 (2020) 379-390.e3. doi: 10.1016/j.cmet.2020.06.011.

WU, Lingyan *et al.* - AMP-Activated Protein Kinase (AMPK) Regulates Energy Metabolism through Modulating Thermogenesis in Adipose Tissue. **Frontiers in physiology**. . ISSN 1664-042X (Print). 9:2018) 122. doi: 10.3389/fphys.2018.00122.

WU, Tong *et al.* - Circulating mesencephalic astrocyte-derived neurotrophic factor is increased in newly diagnosed prediabetic and diabetic patients, and is associated with insulin resistance. **Endocrine Journal**. . ISSN 13484540. 64:4 (2017) 403–410. doi: 10.1507/endocrj.EJ16-0472.

YAMAMOTO, Asako *et al.* - Imaging spectrum of abnormal subcutaneous and visceral fat distribution. **Insights into Imaging**. . ISSN 18694101. 11:1 (2020). doi: 10.1186/s13244-019-0833-4.

YOUNOSSI, Zobair M. - Non-alcoholic fatty liver disease – A global public health perspective. **Journal of Hepatology**. . ISSN 16000641. 70:3 (2019) 531–544. doi: 10.1016/j.jhep.2018.10.033.

ZARGHANI, Sara Shojaei *et al.* - Comparison of three different diet-induced non alcoholic

fatty liver disease protocols in rats: A pilot study. **Pharmaceutical Sciences**. . ISSN 2383-2886. 22:1 (2016) 9–15. doi: 10.15171/PS.2016.03.

ZHANG, Fang *et al.* - An Adipose Tissue Atlas: An Image-Guided Identification of Human-like BAT and Beige Depots in Rodents. **Cell Metabolism**. . ISSN 1550-4131. 27:1 (2018) 252-262.e3. doi: https://doi.org/10.1016/j.cmet.2017.12.004.

ZHANG, Li *et al.* - Extracts from Salvia-Nelumbinis naturalis alleviate hepatosteatosis via improving hepatic insulin sensitivity. **Journal of Translational Medicine**. . ISSN 1479-5876. 12:1 (2014) 236. doi: 10.1186/s12967-014-0236-8.

ZHANG, Xue Qun *et al.* - Role of endoplasmic reticulum stress in the pathogenesis of nonalcoholic fatty liver disease. **World Journal of Gastroenterology**. . ISSN 22192840. 20:7 (2014) 1768–1776. doi: 10.3748/wjg.v20.i7.1768.

ZHAO, Y. - **Berry fruit: Value-added products for health promotion**

ZHUGE, Qun *et al.* - Blueberry polyphenols play a preventive effect on alcoholic fatty liver disease C57BL/6 J mice by promoting autophagy to accelerate lipolysis to eliminate excessive TG accumulation in hepatocytes. **Annals of Cardiothoracic Surgery**. . ISSN 23041021. 9:3 (2020) 1045–1054. doi: 10.21037/apm.2020.03.38.

ZHUGE, Qun *et al.* - Blueberry polyphenols play a preventive effect on alcoholic fatty liver disease C57BL/6 J mice by promoting autophagy to accelerate lipolysis to eliminate excessive TG accumulation in hepatocytes. **Annals of palliative medicine**. China. . ISSN 2224-5839 (Electronic). 9:3 (2020) 1045–1054. doi: 10.21037/apm.2020.03.38.

Annexes

Annex I

Analysis of liver steatosis in histological sections using ImageJ software

To assess hepatic steatosis, each H&E-stained liver histology image was uploaded individually into the ImageJ software (Supplementary Figure 1A). Using FIJI (ImageJ v2) plugin Cell Counter, we first manually selected each visible nucleus with the Type 1 color marker (blue) to count the total number of hepatocytes. After counting all hepatocytes, microsteatotic hepatocytes were selected using the Type 2 color marker (cyan blue), and macrosteatotic hepatocytes were selected using the Type 3 color marker (green) (Supplementary Figure 1B). The final *Cell Counter* data was then used for data representation (Supplementary Figure 1C).

A

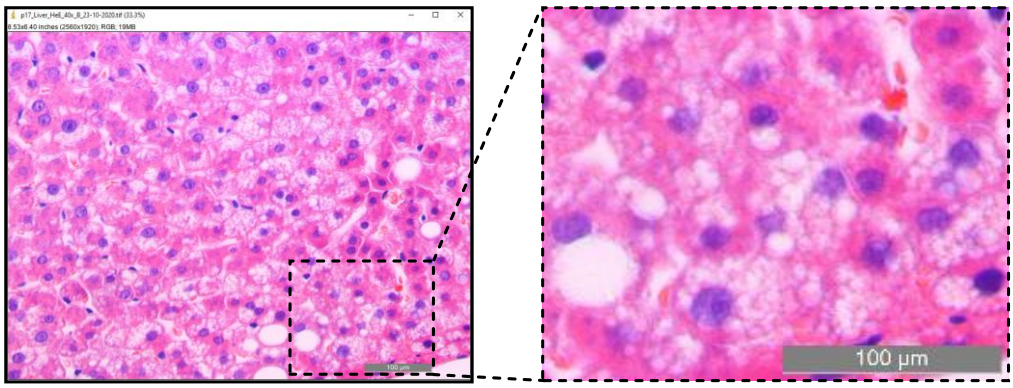

B

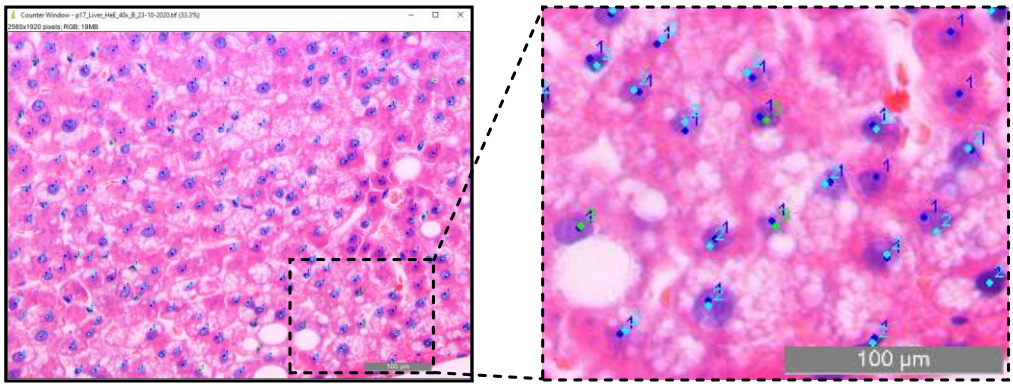

C

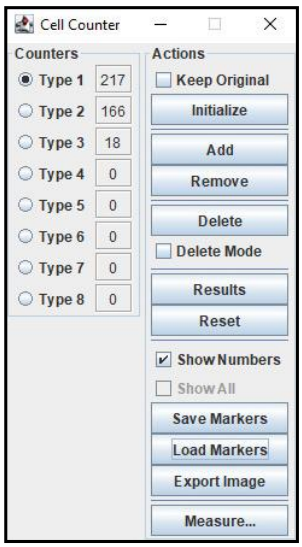

Supplementary Figure 30 – Sequence of image analysis operations performed with Cell Counter plugin in liver sections. (**A**) Initial Image. (**B**) Type 1 (blue), Type 2 (cyan blue) and Type 3 (green) markers, indicating non-steatotic, microsteatotic and macrosteatotic hepatocytes, respectively. (**C**) Cell Counter data panel.

Annex II

Semi-automated analysis of eWAT and iBAT histological sections using ImageJ software

To quantify the size and number of adipocytes in white adipose tissue (eWAT) and the size and number of lipid droplets in brown adipose tissue (iBAT), each H&E-stained histology image was uploaded individually into the ImageJ software. The semi-automated image analysis procedure is shown in Supplementary Figure 2. Briefly, each eWAT and iBAT input image (Supplementary Figure 2A) was split into its three-color channels (red, green, blue). The green channel of each image was saved (Supplementary Figure 2B) and analyzed using FIJI (ImageJ v2) plugin Adiposoft. Adipocyte (in eWAT) and lipid droplet (in iBAT) numbers, areas and diameters were measured (Supplementary Figure 2C). Based on multiple optimization experiments, diameter thresholds were defined for white adipocytes and brown adipocyte lipid droplets. Incomplete adipocytes/lipid droplets touching the image borders, as well as with diameters below the predefined thresholds, were automatically excluded and removed from the output data datasheet. Finally, each image was visually inspected to ensure maximum accuracy is achieved.

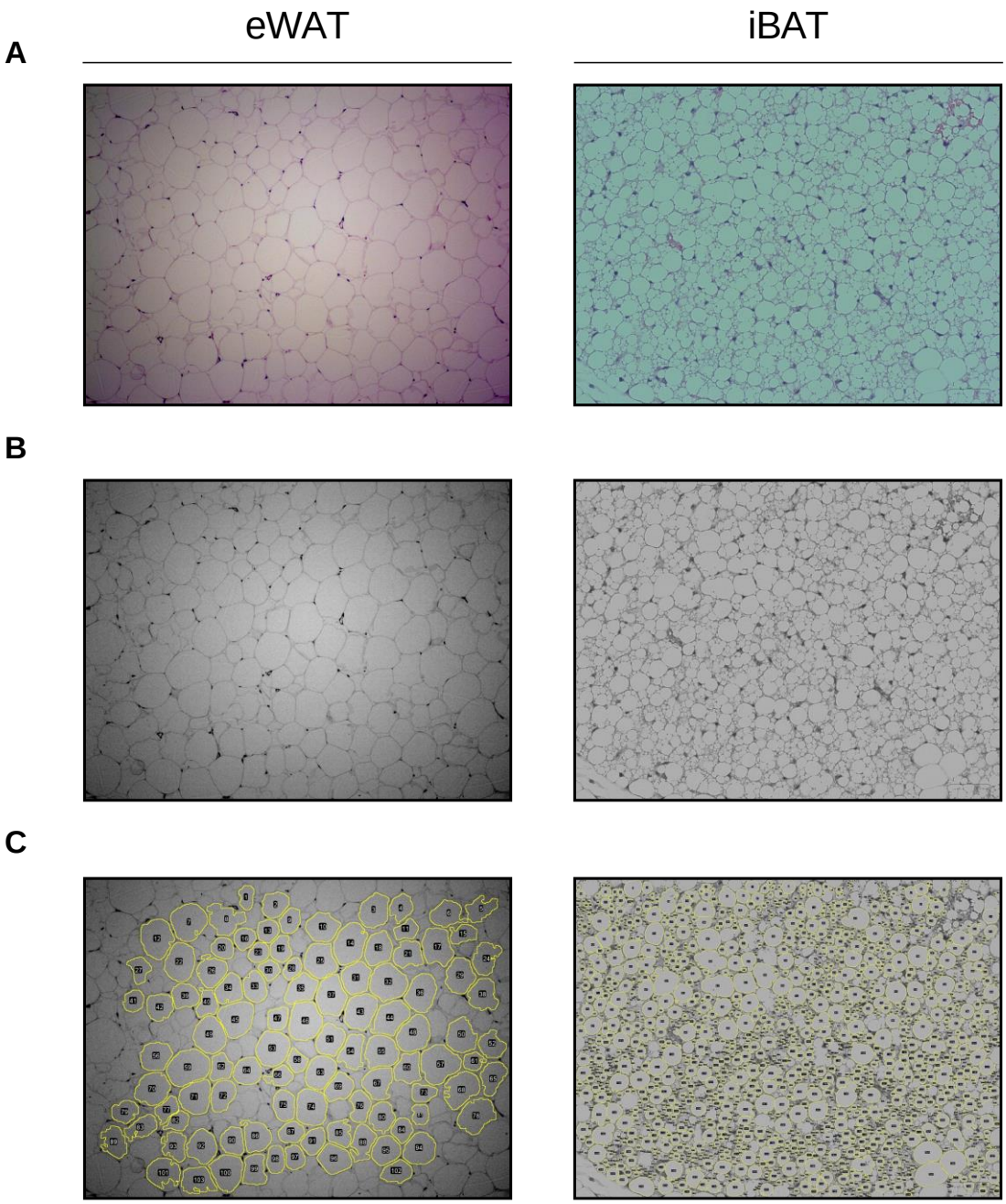

Supplementary Figure 31 – Sequence of image analysis operations performed with Adiposoft plugin in eWAT and iBAT sections. (**A**) Initial image. (**B**) Green-channel. (**C**) Final measured image. The yellow circles represent the delimitations of the identified and quantified adipocytes and lipid droplets.

Annex III

Antibody validation - Selectivity and specificity of antibodies

Antibody validation consists in the demonstration of antibody reproducibility, specificity and selectivity in the context for which they are used. An antibody is considered validated if it produces a band or bands of the expected molecular weight(s) for its target protein. Bands at incorrect molecular weight or the presence of multiple bands could represent the breakdown products of the target protein, spliced variants, or different post-translational modification status, which should raise caution in the use of this antibody.

To characterize the antibodies in terms of specificity and selectivity, liver and adipose tissue samples were separated by SDS-PAGE, transferred to PVDF membranes, blocked, and cut vertically into strips. Each strip was incubated with a different primary antibody and the corresponding secondary antibody, as detailed in Table 3 (Supplementary Figures 3 and 4). Although few antibodies produced multiple bands, the majority demonstrated specificity and selectivity for its target protein, as shown by the presence of a single band at the predicted molecular weight (Supplementary Figures 3 and 4). Only bands displayed at the predicted molecular weight were quantified and used for analysis.

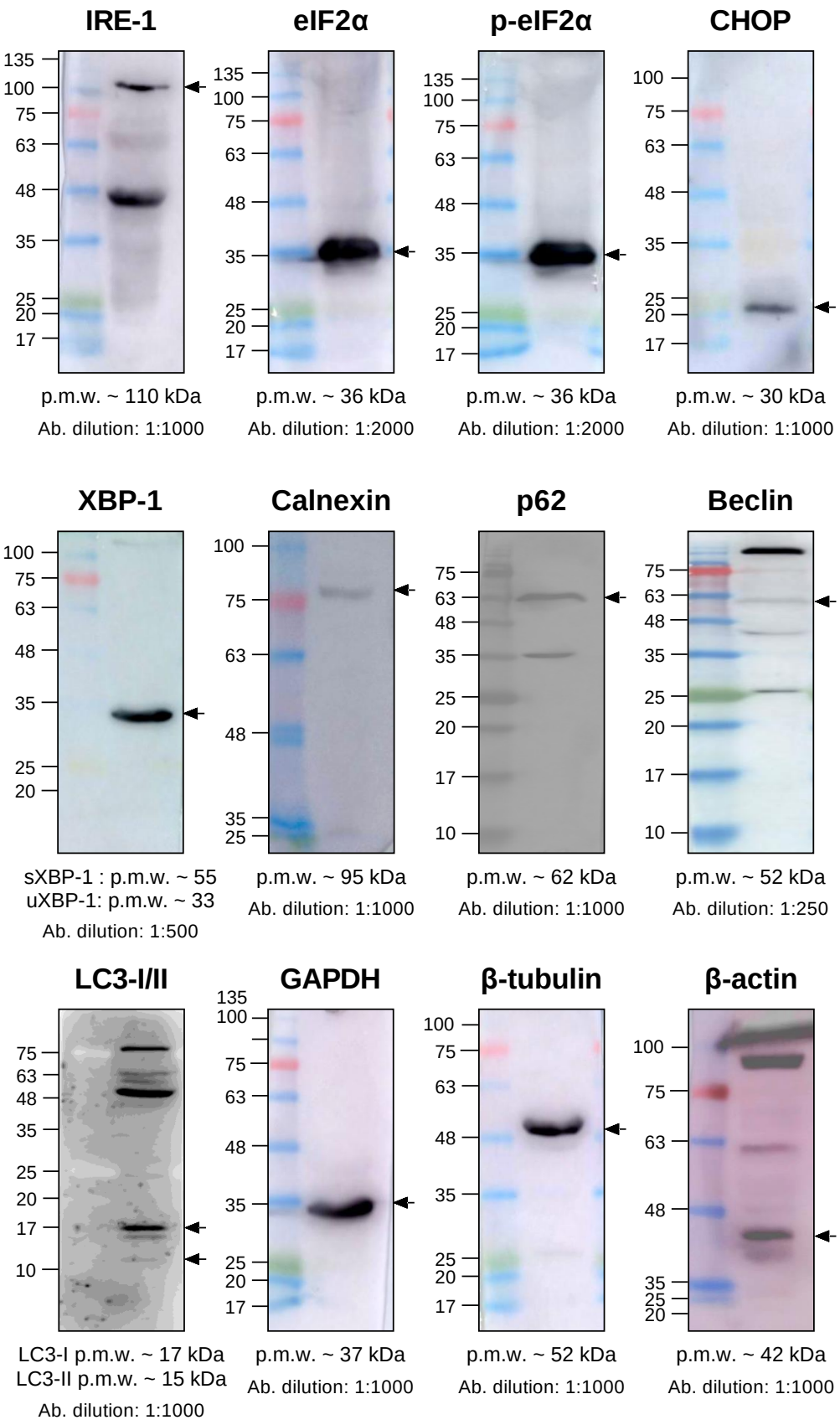

Supplementary Figure 32 – Validation of primary antibodies in rat liver lysates by Western blot. A volume of liver tissue lysate corresponding to 30 μg of protein was loaded in each lane. Ab. - Antibody; p.m.w. - predicted molecular weight.

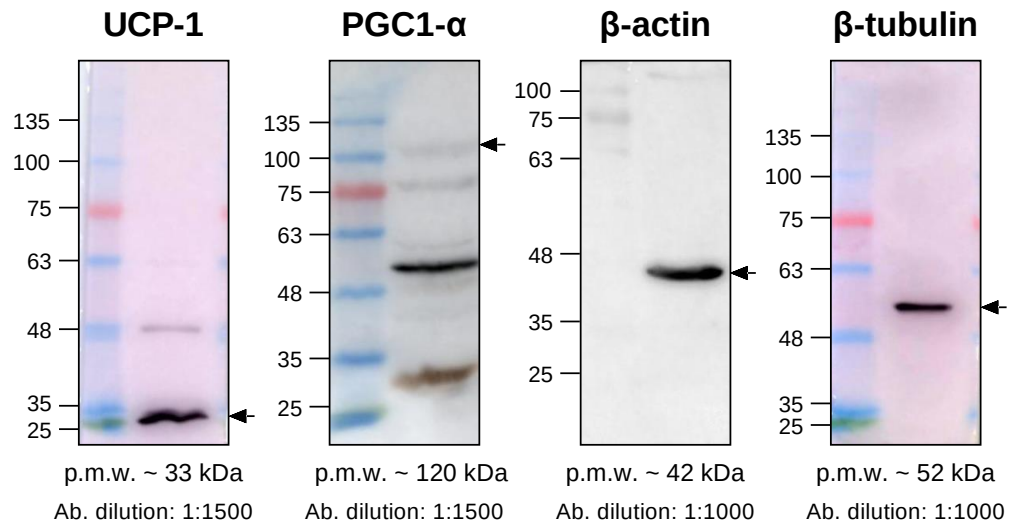

Supplementary Figure 33 – Validation of primary antibodies in rat interscapular brown adipose tissue (iBAT) lysates by Western blot. A volume of brown adipose tissue lysate corresponding to 10 μg of protein was loaded in each lane. Ab. - Antibody; p.m.w. - predicted molecular weight.

Antibody validation - Linear dynamic range

The linearity between protein amounts and signal intensities is imperative for quantitative use of Western blot. To obtain an accurate quantification, the linear dynamic range (LDR) for each target protein has to be determined. This enables the determination of the optimal quantity of protein to be loaded (avoiding weak signals and membrane saturation) and the selection of an appropriate loading control.

To determine the LDR of target proteins, we performed Western blot using a serial dilutions of tissue samples, which allowed us to define the relationship between sample loading and band intensity. Since Western blot sensitivity is also dependent on the optimal primary antibody dilution, some primary antibodies dilutions were used to optimize linearity (Supplementary Figures 5 and 6).

Overall, most antibodies demonstrated linearity, although for higher protein loading eIF2α, p-eIF2α and GAPDH antibodies did not. The dilution to half of GAPDH antibody enable better linearity for higher protein concentrations. The amount of protein loaded for analysis was within the LDR for all target proteins in each tissue (10 μg in iBAT and 30 μg in liver).

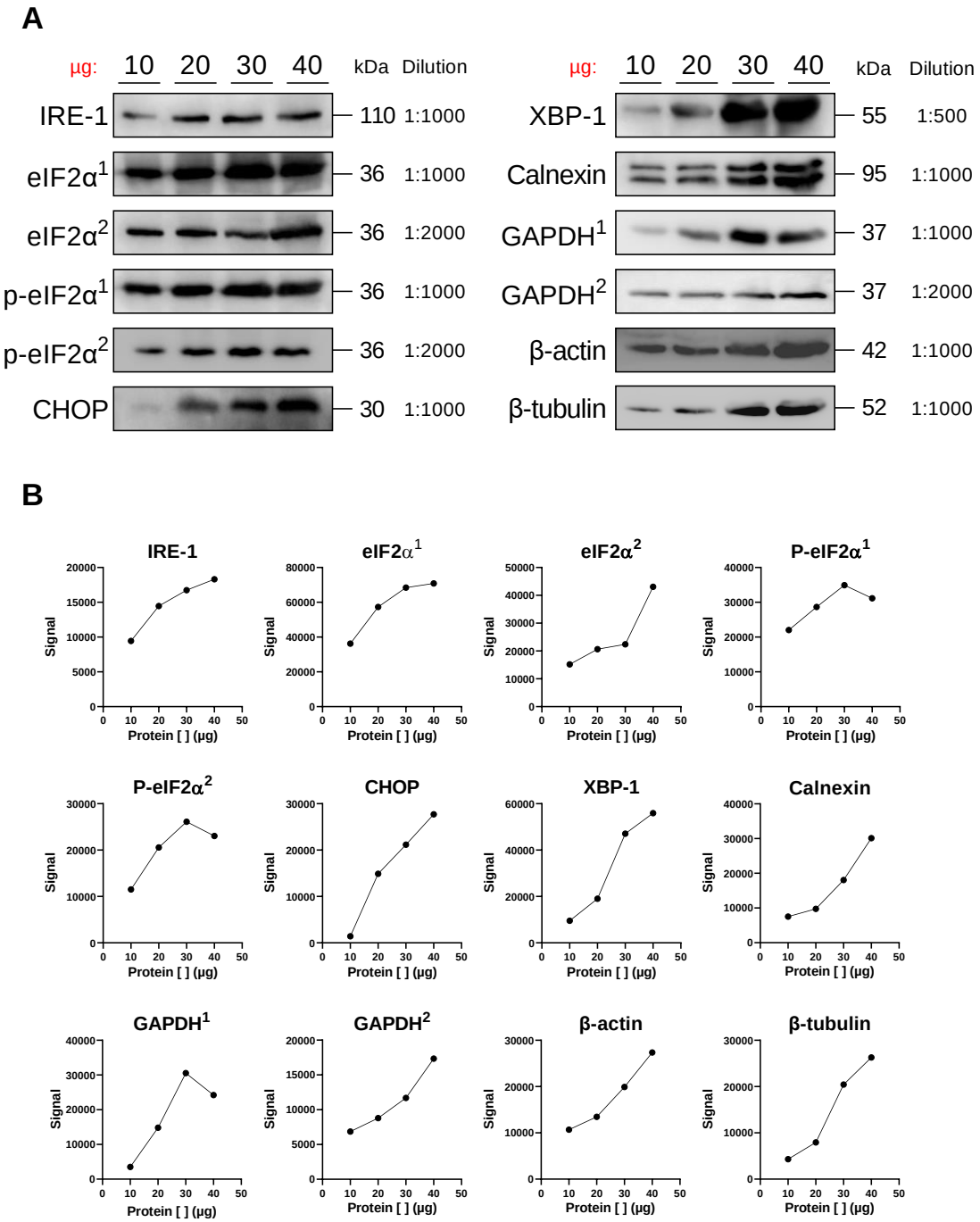

Supplementary Figure 34 – Linear dynamic range (LDR) assessment of a variety of proteins and different antibodies dilutions in liver lysates from male Wistar rats. (**A**) Immunoblotting of target proteins and loading controls. (**B**) Relationship between the band intensity signal expressed as arbitrary units and the amount of protein loaded (between 10 and 40 µg). The LDR of eIF2a, p-eIF2a and GAPDH were also assessed in two distinct antibody dilutions.

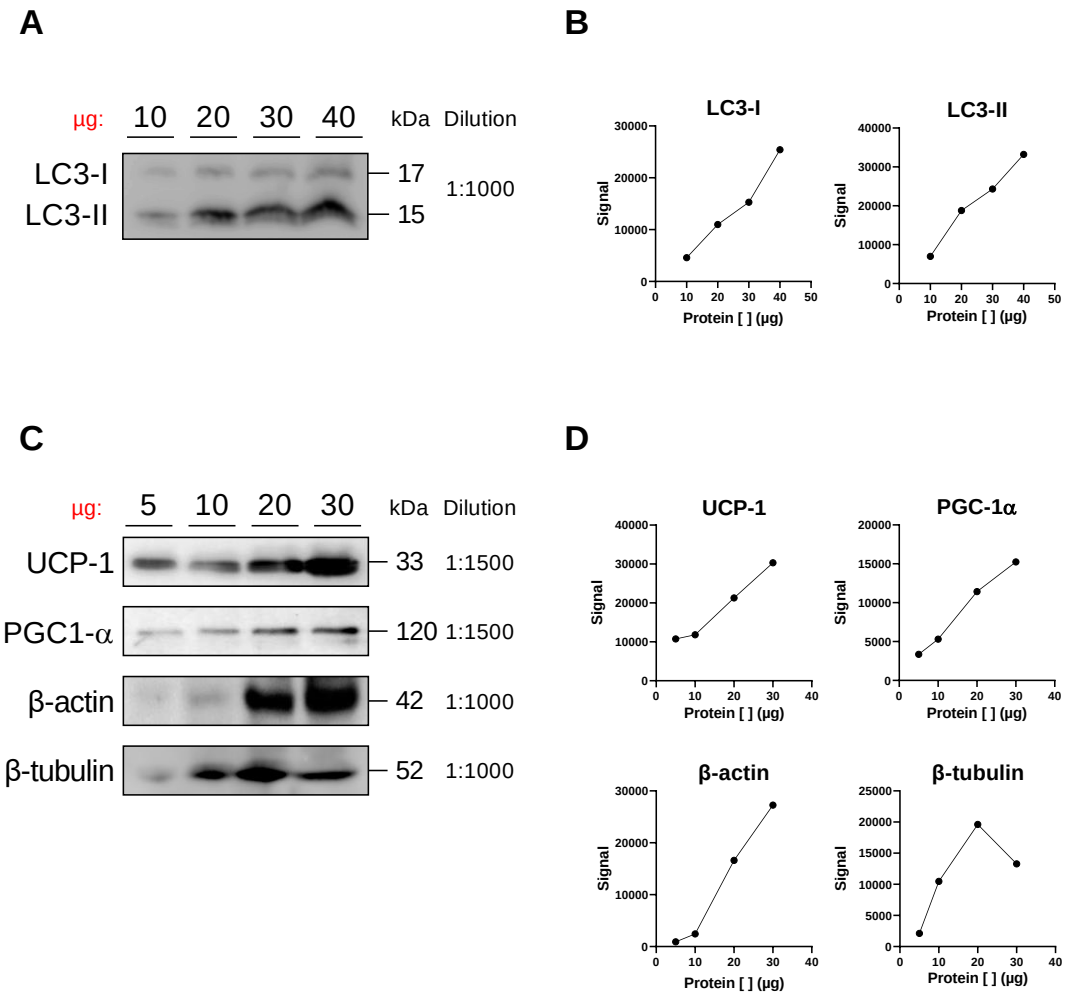

Supplementary Figure 35 – Linear dynamic range (LDR) assessment of different proteins in liver and interscapular brown adipose tissue (iBAT) lysates from male Wistar rats. (**A**) Immunoblotting of LC3-1 and LC3-II in liver protein lysates and (**B**) their corresponding quantification. 10 to 40 µg of protein were loaded. (**C**) Immunoblotting of LDR assessed proteins in iBAT and (**D**) their corresponding quantification. 5 to 30 µg of protein were loaded.